Hydrogen Bonds in Peptides and Proteins: Studies of Proline-Containing Peptides and Proteins

by

Eric S. Eberhardt

A dissertation submitted in partial fulfillment

of the requirements for the degree of

Doctor of Philosophy

(Biochemistry)

at the

University of Wisconsin–Madison

1995

Dedication

To my parents

Abstract

To predict the three-dimensional structure of a protein from its amino acid sequence, the energetic principles of the rate-determining steps that govern protein folding pathways must be understood. Two areas of particular importance in the folding of proteins are *cis-trans* prolyl peptide bond isomerization and hydrogen bond formation. To assess the energetics of *cis-trans* prolyl peptide bond isomerization, ^{13}C-enriched peptides were synthesized and ^{13}C NMR inversion transfer experiments were used to determine the energetics of the *cis-trans* proline isomerization. The solvent effect on prolyl peptide bond isomerization was determined by using solvents that cover a range of dielectric constants. These studies observed that the barrier to isomerization is 1.2 kcal/mol lower in apolor than in polar solvent and that the uncatalyzed isomerization rates are governed by the relative strength of hydrogen bond formation to the carbonyl oxygen of the prolyl peptide bond.

Using the rate of proline isomerization as an assay of hydrogen bond strength, the relative strength of a variety of hydrogen bond donors have been determined. Secondary amides, traditional models of the peptide bond, were found to be poor hydrogen bond donors, whereas water and primary amides were found to be strong hydrogen bond donors. These results argue against the framework model of protein folding and imply that the formation of amide–amide hydrogen bonds does not driving protein folding.

The effect of hydrogen bonds to prolyl peptide bonds on the stability of bovine pancreatic ribonuclease A (RNase A) has been explored. Site-directed mutagenesis studies of RNase A have shown that Lys41 is an important catalytic residue. To insure that Lys41 is positioned properly to effect catalysis, RNase A provides a covalent and noncovalent scaffold that restricts the conformational freedom of the polypeptide backbone. The role of hydrogen bond donated by Tyr97 has been explored with the Phe, Ala, and Gly mutants of Tyr97 have been prepared by site-directed mutagenesis, and the thermostability and catalytic efficiency

of the resulting mutants have been determined. The three mutants were found to have significantly lowered melting temperatures, 36 °C, 29.1 °C and 30.4 °C, respectively, from that of wild-type RNase A (63.5 °C). Although no significant change was observed in the K_m for the mutant enzymes as compared to wild-type RNase A, significant changes were observed in the values of k_{cat} for the mutant enzymes. Overall, the catalytic efficiency (k_{cat}/K_m) of the mutant enzymes was found to be a 100-fold lower than that of wild-type RNase A. These results illustrate that the Try97 is important for both protein stability and the proper positioning of Lys41.

The structural and energetic consequences of placing electron-withdrawing groups on proline residues has been determined. The natural hydroxyl and fluoro isomers of proline have been synthesized and X-ray diffraction analysis, FTIR spectroscopy and ^{1}H, ^{13}C, and ^{19}F NMR spectroscopy have been used to examine the influence of the inductive effect. These studies demonstrated that the inductive effect can influence the properties of proline resides, including the rate of prolyl peptide bond isomerization. Further, these studies suggest that the gauche effect may participate in determining pyrrolidine ring pucker and may contribute to the stabilization of collagen, the most abundant protein in vertebrates.

Acknowledgments

I am deeply indebted to all the members of the Raines Lab for the support and fellowship. I want to thank past and present members of the Markley Lab, especially, Stewart Loh and Andy Hinck: Stewart, for his countless hours of assistance in working out the bugs of the NMR experiments and Andy for his synthetic expertise. I am also indebted to Nick Panasik for his work on the crystal structures of the proline derivatives and Art Edison for his *ab initio* calculations on these structures. In addition, I want to thank the entire NMRFAM staff for the years of patiently answering all my questions. I am grateful to Dr. Raines for his support over these years, editing and otherwise. I am especially grateful to him for deferring the next generation of collagen experiments so that I was able undertake the work on RNase A and develop an array of new skills during my last year. Again, I thank my parents for their understanding and unwavering support. I also thank the NHL for postponing its 1995 season which allowed me to focus completely on this work.

Table of Contents

List of Figures

List of Tables

Chapter 1

Introduction

1.1 Overview

This thesis examines the role of hydrogen bonds in the folding and stability of proteins and the covalent and noncovalent interactions that affect the energetics of prolyl peptide bond isomerization. Although *cis-trans* prolyl peptide bond isomerization has been clearly identified as the slow kinetic phase in many protein folding pathways (Figure 1.1),[1] the contribution of conventional hydrogen bonds to the formation and stability of biological macromolecules remains a subject of significant interest and controversy.[2] Taking advantage of synthetic, spectroscopic, and recombinant DNA techniques, model peptides and site-directed mutants of bovine pancreatic ribonuclease A [RNase A; E.C. 3.1.27.5] were prepared in order to address the contribution of hydrogen bonding to prolyl peptide bonds towards protein stability. The ensuing introduction (Chapter 1) provides a brief discussion of RNase A as a model system and introduces the protein folding problem where studies of model systems and RNase A have been used to illustrate the issues relevant to the protein folding problem. Chapter 2 examines the effects of solvent on the kinetics and thermodynamics of *cis-trans* prolyl peptide bond isomerization in model peptides. The role of water and amide hydrogen bonds in protein folding and stability are discussed in Chapter 3 where, specifically, the relative strengths of amide–amide amide–water hydrogen bonds have been determined. The energetics and mechanism of δ-valerolactam dimerization have been re-examined in Chapter 4. Chapter 5 addresses the contribution of the phenolic side-chain of tyrosine to catalytic efficiency and stability RNase A through site-directed mutagenesis studies. The influence of the inductive effect on the structure of proline residues is discussed in Chapter 6. In Chapter 7, the energetics of prolyl peptide bond isomerization have been explored and the implications for collagen folding and assembly are discussed.

1.2 RNase A as a model protein

RNase A (Figure 1.2) is a small, single domain protein of 124 amino acids (calculated molecular weight 13.7 kDa) that catalyzes the hydrolytic cleavage of P-$O^{5'}$ bond of single-stranded RNA after pyrimidine residues. Because of its availability and small size, RNase A has been subject of many benchmark studies in all areas of biochemistry including the enzymology, folding, stability, structure, and chemistry of proteins.[3,4] Early knowledge of RNase A's three-dimensional structure, determined by x-ray diffraction analysis,[5] contributed to the development of all areas of structural biology. In addition, RNase A and its subtilisin cleavage product, RNase S, were the first proteins to be completely chemically synthesized using Merrifield's solid phase synthetic methodology.[6] The large amount of phylogenetic information that has been accumulated on pancreatic ribonucleases nicely compliments the wealth of available chemical and structural information (Figure 1.3). Only recently, however, has recombinant DNA technology been developed for RNase A.[7] This development now allows for the characterization of structure-function relationships of the protein with molecular detail.

1.3 The protein folding problem

A fundamental question still facing structural biology is how the amino acid sequence of a protein determines its three-dimensional structure and its function. Nearly thirty years ago, C. B. Anfinsen demonstrated that all the information needed for a polypeptide to fold into its three-dimensional structure was contained within its primary sequence.[8] Since then, advances have been made by many methods to strengthen our understanding of protein folding pathways and the thermodynamic driving forces involved in protein folding. Given a unique polypeptide sequence, however, the three-dimensional structure of a protein cannot be predicted using the current understanding of the molecular forces that govern protein conformation. This inability to predict the three-dimensional structure of a protein has

become known as the protein folding problem.[9-11] With the rapid expansion of DNA sequence information, the ability to predict protein structure and function from a DNA sequence would be extraordinarily useful as well as a significant achievement.

Anfinsen's seminal experiments on RNase A provided the framework for the protein folding field. Using denatured and reduced RNase A, Anfinsen observed the spontaneous refolding of RNase A, *in vitro*, where the four native disulfide bonds and full enzymatic activity were restored.[8] This experiment demonstrated that the active, three-dimensional structure of RNase A is determined by its amino acid sequence. Since then, efforts to resolve the protein folding problem have proceeded largely along two tracks: 1) the determination of the thermodynamic driving force of protein folding; and, 2) the elucidation of protein folding pathways and characterization of protein folding intermediates. Anfinsen's work with RNase A led directly to the thermodynamic hypothesis of protein folding, which states that the native conformation of a protein is the conformation at which the global free energy is at a minimum.[12]

Because protein conformation is determined by the rotational barriers about covalent bonds of the polypeptide and, in general, these barriers to rotation are quite small, noncovalent interactions (such noncovalent interactions include van der Waals interactions, electrostatic interactions, hydrogen bonds and the hydrophobic effect) can readily influence the thermodynamically favored conformation.[13] Therefore, the ability to predict protein tertiary structure depends upon the accurate measure of the noncovalent interactions that govern rotations about covalent bonds. Proteins exhibit a surprisingly small difference in free energy between the unfolded, or denatured state, and the folded, or native, state, and all destablizing or stabilizing interactions must be considered. The challenge, then, is to dissect the thermodynamic forces that drive protein folding when the net difference in free energy between the unfolded and folded protein is small.

Hydrogen bonding and the hydrophobic effect. For one or more of the noncovalent interactions to act as a driving force in protein folding, a relative thermodynamic advantage must exist for the folded conformation over the unfolded conformation. In considering the process of protein folding, a significant amount of conformational entropy must be overcome because of the enormous number of polypeptide conformations available to the unfolded polypeptide chain. Both hydrogen bond formation and the hydrophobic effect have been proposed as the principal thermodynamic forces that are used to overcome this conformational entropy. Studies of model systems where specific interactions can be characterized and quantified have played a large role in shaping the debate over the relative contribution of both of these interactions. For example, simple amides or small peptides have been used to address the contribution of hydrogen bond formation towards protein folding and stability. Similarly, hydrocarbon transfer experiments have been used to determine the thermodynamic signature of the hydrophobic effect.[14] Nevertheless, these model systems have occasionally yielded conflicting interpretations that hamper the extrapolation of these studies to the protein folding problem. For example, contradictory conclusions are often drawn from studies which attempt to address the role of hydrogen bonding in protein folding and stability (see: Chapter 3 and Chapter 4). Hydrogen bond formation occurs when two electronegative atoms share a hydrogen atom. Conventional hydrogen bond strengths have been estimated to range from 1.0 – 5.0 kcal/mol, depending on the orientation of the interaction and the relative abilities of the participants to act as the hydrogen bond donor or acceptor.[15] In general, hydrogen bond formation is favored in hydrophobic environments, and it is associated with a large enthalpy of formation. Studies of the dimerization in CCl_4 of *N*-methylacetamide (NMA),[16] a mimic of the peptide backbone, and δ-valerolactam,[17] a *cis* amide, illustrate this point. For NMA and δ-valerolactam, dimerization is favored (ΔG°) by -0.9 kcal/mol and -3.0 kcal/mol at 25 °C, respectively.

These experiments also indicated that hydrogen bond formation is enthalpically driven in apolar environments.

In contrast, the dimerization of both NMA and δ-valerolactam in aqueous solution is extremely unfavorable. When dimerization does occur in aqueous solution, it occurs only at extremely high concentrations of amide, and the process appears to be entropically driven through the release of water molecules (See: Chapter 4). Yet, a widely cited study by Susi and coworkers reports a large enthalpy change, -5.5 ± 1 kcal/mol, for the dimerization of δ-valerolactam.[18] However, these studies in aqueous solution are complicated by a temperature dependent mechanism of dimerization and the tendency of these amides to aggregate rather than form dimers at high concentrations.[19] Regardless of these complications, both these studies and others[20] have clearly demonstrated that amide–amide hydrogen bond formation is more favorable in hydrophobic environments than in aqueous environments.

The hydrophobic effect is believed to act as a major driving force in protein folding. While many definitions exist, in this thesis, the hydrophobic effect refers to the thermodynamic consequences of the unfavorable interactions between hydrocarbons and water.[14] The hydrophobic effect, whereby the transfer of a nonpolar solute from an aqueous environment to its liquid[21] or vapor phase[22] is thermodynamically favored, and is characterized by a favorable change in heat capacity (ΔC_p) and a significant entropic component (ΔS°). The molecular picture of the thermodynamic contribution of the hydrophobic effect remains unresolved and often controversial. Still, most data are consistent with a picture in which hydrophobic solutes are surrounded, or caged, by ordered water molecules. Consequently, the favorable change in entropy observed during the transfer of hydrophobic solutes out of water is believed to be associated with the release of these water molecules to bulk solvent. Recent reviews on the role of the hydrophobic effect in protein folding, however, disagree significantly on the magnitude of its contribution.[9,10,23]

α-Helices as model systems. Model peptide systems have been extremely useful in the elucidation of the relative contributions of the thermodynamic forces that drive protein folding. An important secondary structural element of proteins is the α-helix, and the mechanism of α–helix formation has been studied extensively. In particular, the use of Zimm-Bragg theory has shaped much of the debate regarding the formation of helical conformations in aqueous solution.[24] Originally developed to allow for the prediction of helical structure in peptides, Zimm-Bragg theory requires the use of a two-state model (random coil ↔ complete helix) and the experimental determination of two parameters for each amino acid: 1) σ, the helix nucleation parameter, and 2) *s*, the helix propagation parameter. Given the sequence of a peptide, this statistical treatment of a peptide allowed for the first predictions of α-helix formation. The principal limitation of Zimm-Bragg methodology is that the value of *s* for each amino acid is independent of neighboring amino acids. This limitation is highlighted by the inability of this methodology to predict helical content in peptides containing fewer than 30 amino acid residues. In most proteins, helical regions tend to average 11 residues in length.[25] Furthermore, many peptide sequences from helical regions in proteins do not form helices independently in aqueous solution. For example, sequences from helical regions of myoglobin[26] and staphylococcal nuclease[27] do not exhibit any helix forming tendency in aqueous solution. The observation that the S-peptide (the 21 N-terminal residues of RNase A) and C-peptide (the 13 N-terminal residues of RNase A) form α-helices in aqueous solution allowed for the first systematic studies of specific sidechain interactions that can influence helix nucleation and propagation.[4]

The use of Zimm-Bragg formalisms and studies of S-peptide and C-peptide have culminated in the *de novo* design of α-helix forming peptides. Marqusee and Baldwin have design and studied alanine-based peptides that readily form α-helices in aqueous solution.[28] The principal advantage afforded by these *de novo* peptide systems is the ability to characterize sidechain sidechain interactions that can either facilitate formation or enhance

the stability of α-helices in aqueous solution. For example, one result of particular interest involves the relationship between Phe8 and His12 and C-peptide helix stability. An important catalytic residue in RNase A, His12 is believed to enhance C-peptide helix stability by stabilizing the helix dipole, and the presence of Phe8 enhances this stability further. When incorporated into alanine-based peptides in the preferred *i*, *i*+4 arrangement, Phe and His exhibit the same helix stabilizing effect observed in C-peptide.[29] The origin of this effect is believed to involve the potentially favorable aromatic edge-to-face orientation predicted for benzene molecules in the gas phase.[30] If Phe8, which is a conserved residue in pancreatic ribonucleases, participates in catalysis of RNA by properly orienting His12 within the active site of RNase A, site-directed mutagenesis of Phe8 might be of interest to the study both enzymology and protein stability.

The development of these alanine-based peptides have allowed for the systematic analysis of many important issues including the bases for helix initiation, helix termination, and N-capping. Unfortunately, these studies have not determined the energetic contribution, the change of enthalpy (ΔH°), of helix formation. The value of ΔH° has been estimated to be -1 kcal/mol residue.[31] The change in heat capacity (ΔC_p) for these model systems has been difficult to determine and appears to be small.[25] Consequently, the contribution of amide–amide hydrogen bond formation and the hydrophobic effect towards helix formation remains unclear. These systematic studies of α-helix forming peptides, however, have provided a general picture of helix formation. Helices, in general, are formed through a cooperative process where the formation of the first mainchain amide–amide hydrogen bond facilitates the formation of the next main-chain amide–amide hydrogen bond. Further, these studies have demonstrated that noncovalent sidechain–sidechain interactions can influence significantly helix formation and stability.

The prolyl peptide bond. The recent development of NMR exchange methodologies and stop-flow fluorescence experiments in combination with the protein engineering of small,

single-domain proteins like barnase, bovine pancreatic trypsin inhibitor (BPTI),[32] staphylococcal nuclease[33,34] T4 lysozyme,[35,36] λ repressor,[37]and RNase A have provided insight into the molecular forces that govern protein folding. Yet, the ability to predict the energetic consequences of a specific mutation remains elusive. As A. Fersht and K. Dill point out in a recent review, "how depressingly far we have yet to go to understand the forces that underlie mutational energetics".[13] For thermodynamic analysis, small proteins are usually treated within a simplified framework of the two state model (unfolded ↔ folded). This assumption reduces the protein folding problem to delineation of the folding energetics under specific conditions. By treating protein folding as any other chemical reaction, efforts have been made to identify and characterize the protein folding transition state[38] and other significant barriers that regulate the kinetics of folding.[39] A related approach has been to address the protein folding problem to delineation of the folding pathways. In particular, *cis-trans* prolyl peptide bond isomerization has been identified as a rate-limiting step in many protein folding pathways, including that of RNase A.

In 1975, Brants and Halverson suggested that *cis-trans* prolyl peptide bond isomerization may account for the slow kinetic phase observed in some protein folding pathways.[1] This proposal was based on several observations. First, the kinetics exhibited during the slow kinetic phase of the folding and unfolding of many small proteins was characteristic of amide bond isomerization. Specifically, an activation free energy of 20 kcal/mol was observed for the transition between the slow and fast kinetic phases of proteins that exhibited biphasic behavior. Second, the ratio of slow and fast phases were found to depend upon experimental conditions. Finally, this biphasic kinetic behavior was associated with proteins whose native crystalline structures that contained prolyl peptide bonds in the unusual *cis* conformation.

The last observation was particularly significant since the *trans* conformation is greatly preferred over the *cis* conformation in most peptide bonds. For proline-containing

peptides, however, the *trans* conformation is only slightly favored over the *cis* conformation with these peptides usually exhibiting a 4:1 *trans:cis* isomer ratio in aqueous solution. In general, the steric conflict between the δ-carbon of the pyrrolidine ring and α-carbon of the preceding residue is thought to be the origin of the unique energetics of the prolyl peptide bond. Table 1.1 illustrates the relationship between the preceding residue and the percent *cis* isomer. As the preceding residue becomes more bulky, from Gly to Tyr, the *cis* isomer becomes the preferred conformation. Nevertheless, as is discussed below and in Chapters 2 and 5, noncovalent interactions can also influence the prolyl peptide bond equilibrium constant ($K_{E/Z}$). Similarly, covalent interactions can alter prolyl peptide bond energetics. The studies described in Chapters 6 and 7 indicate that electron withdrawing substituents on the pyrrolidine ring can alter the barrier to prolyl peptide bond isomerization and that the gauche effect has a significant impact on pyrrolidine ring conformation and prolyl peptide bond energetics. Consequently, an understanding of the kinetic and thermodynamic barriers of prolyl peptide bond isomerization will provide a step toward achieving the overall goal of being able to predict the three-dimensional structure of a protein from its amino acid sequence.

1.4 Resonance and the Barrier to Amide Bond Rotation

The energetics of the prolyl peptide bond also affords a unique opportunity to explore resonance theory and further develop our understanding of the energetics of amide isomerization. The barrier to rotation about amide bonds, including prolyl peptide bonds, has been ascribed to the double-bond character of the C-N bond.[40] The amide C-N bond length of 1.33-1.37 Å reflects this double bond character by being intermediate to the typical C-N single bond length of 1.47 Å and the C=N double bond length of 1.30 Å. Amidic resonance in general (Figure 1.4), which is best illustrated as a hybrid of the two Lewis structures, occurs when the lone pair of electrons on nitrogen are conjugated with the π-electrons of the

carbonyl group. In addition to explaining the double bond character of the amide C-N bond, resonance theory illustrates many other features characteristic of the amide bond. First, resonance occurs when all atoms of the amide bond are coplanar, thereby allowing conjugation between the lone pair of electrons on nitrogen and the π-electrons of the carbonyl to take place. Second, the charge separation in resonance structure II suggests that there must be a dipole moment associated with the amide bond. Finally, these resonance structures suggest that the amide nitrogen hybridization state depends on the localization of electron density within the C-N bond. The resonance structures illustrate that when electron density is localized on the amide nitrogen, as in resonance structure I, the nitrogen should be sp^3 hybridized. Whereas, when the amide bond is fully conjugated, resonance structure II, the nitrogen should be sp^2 hybridized. Recent *ab initio* calculations of model amides have suggested, however, that electron density is not transferred to the oxygen of the amide when the amide atoms are coplanar.[41] These studies suggest that electron density may instead be localized on the carbon of the carbonyl group, in contrast to the traditional picture of amidic resonance.

Crystalline structures of amides and proline-containing peptides reveal these structural features of the amide bond. In addition, spectroscopic studies of anilides and toluamides have nicely illustrated the relationship between C-N and C=O bond order and the amide rotational barrier.[42] Isomerization around the amide bond involves changes in C=O and C-N bond lengths, pyramidalization of the nitrogen, and rotation of the carbonyl to a position which is orthogonal to the plane of the amide bond ground state. When the single-bond character of the amide bond predominates, as in resonance structure I, rotation occurs readily; whereas, when the amide bond contains significant double bond character, as in resonance structure II, rotation about the amide bond is less frequent. To elucidate the mechanism of amide and prolyl peptide bond isomerization, it is necessary to understand the distribution of the electron density within the amide C-N bond.

Solvent, inductive, and steric effects can influence either the ground state, transition state, or both, during the process of amide bond isomerization and may alter the barrier to isomerization ($\Delta G^{\ddagger}$). While the solvent effect isgenerally understood to mainifest itself on the ground state energy levels, the influence of solvent effect on the prolyl peptide bond at the transition state depends upon the structure of the transition state. *Ab initio* molecular orbital calculations of model amides can provide insight, though often contradictory, into of the nature amide isomerization transition state since many of the changes involved in rotation about the C-N bond are difficult to measure experimentally. For example, calculations of the barrier to isomerization of *N*, *N*-dimethylforamide suggest that the syn transition state is preferred by 0.49 kcal/mol over the anti transition state, but gas phase calculations of *N*, *N*-dimethylacetamide isomerization suggest that barrier to the anti transition state is 4.2 kcal/mol lower than that to the syn transition state (Figure 1.5). Both of these studies, however, find significant lengthening of the C-N bond, and a nominal increase in the C=O bond order at the amide transition state. This result is consistent with the traditional picture of amidic resonance. Recent calculations of formamide isomerization raises question about this traditional picture of amidic resonance by suggesting that pyrmidalization of the nitrogen accompanies rotation about the C-N bond, and that charge transfer at the chemical transition state does not occur from the nitrogen to the oxygen as suggested by classical resonance theory.[41] Our experiments on proline-containing peptides address this debate (Chapter 2).[43]

Figure 1.1 The *cis* (*E*) and *trans* (*Z*) prolyl peptide bond isomers.

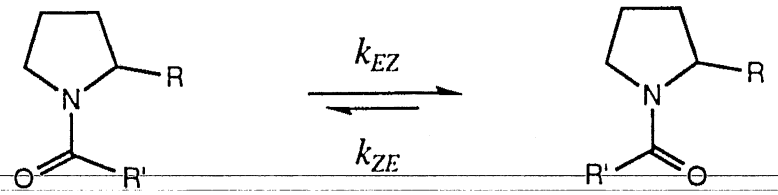

***cis* (*E*) isomer** ***trans* (Z) isomer**

Figure 1.2 Ribbon diagram of the structure of RNase A. Shown are the important catalytic residues: His12, His119, and Lys41. Shown as white circles are the location of residues relevant to this thesis: Pro42, Tyr97. Also shown are the 4 disulfide bonds.

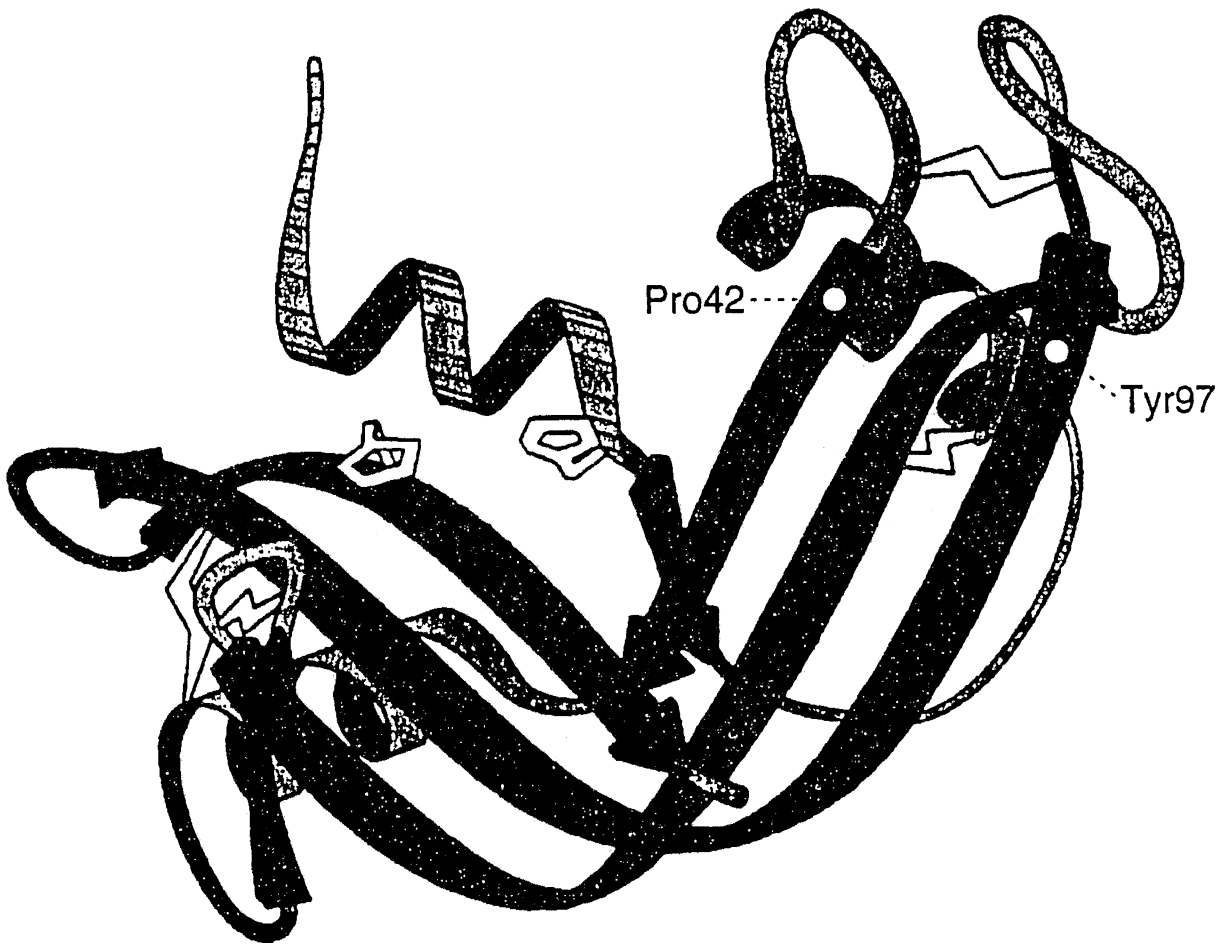
Pro42
Tyr97

Figure 1.3 Amino acid sequences of 41 pancreatic ribonucleases in the IUB one letter code (z = Glx; b = Asx). Only differences from the bovine pancreatic sequence are shown. Residues are numbered by homology with the bovine enzyme. Deletions in the sequences are indicated by –, and unidentified residues by x.[44,45]

OX 1
WATER BUFFALO, SWAMP TYPE 2
WATER BUFFALO, RIVER TYPE 3
ELAND 4
NILGAI 5
GNU 6
TOPI 7
IMPALA 8
THOMSON'S GAZELLE 9
GOAT 10
PRONGHORN 11
GIRAFFE 12
REINDEER 13
ROE DEER 14
MOOSE 15
RED DEER 16
FALLOW DEER 17
OX (FROM SEMINAL PLASMA) 18
DROMEDARY 19
BACTRIAN CAMEL 20
HIPPOPOTAMUS 21
PIG 22
LESSER RORQUAL 23
HORSE 24
RAT 25
HOUSE 26
HAMSTER 27
MUSKRAT 28
PORCUPINE 29
CAPYBARA 30
GUINAE PIG A 31
GUINAE PIG B 32
CUIS 33
CHINCHILLA 34
CASIRAGUA 35
COYPU 36
MAN 37
TWO-TOED SLOTH 38
THREE-TOED SLOTH 39
RED KANGAROO 40
WALLABY 41
SNAPPING TURTLE 42

Figure 1.4 The major resonance structures of the amide bond.

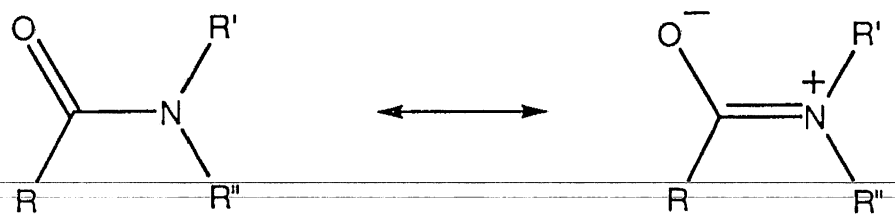

I II

Figure 1.5 Notional transition state structures for amide bond isomerization.

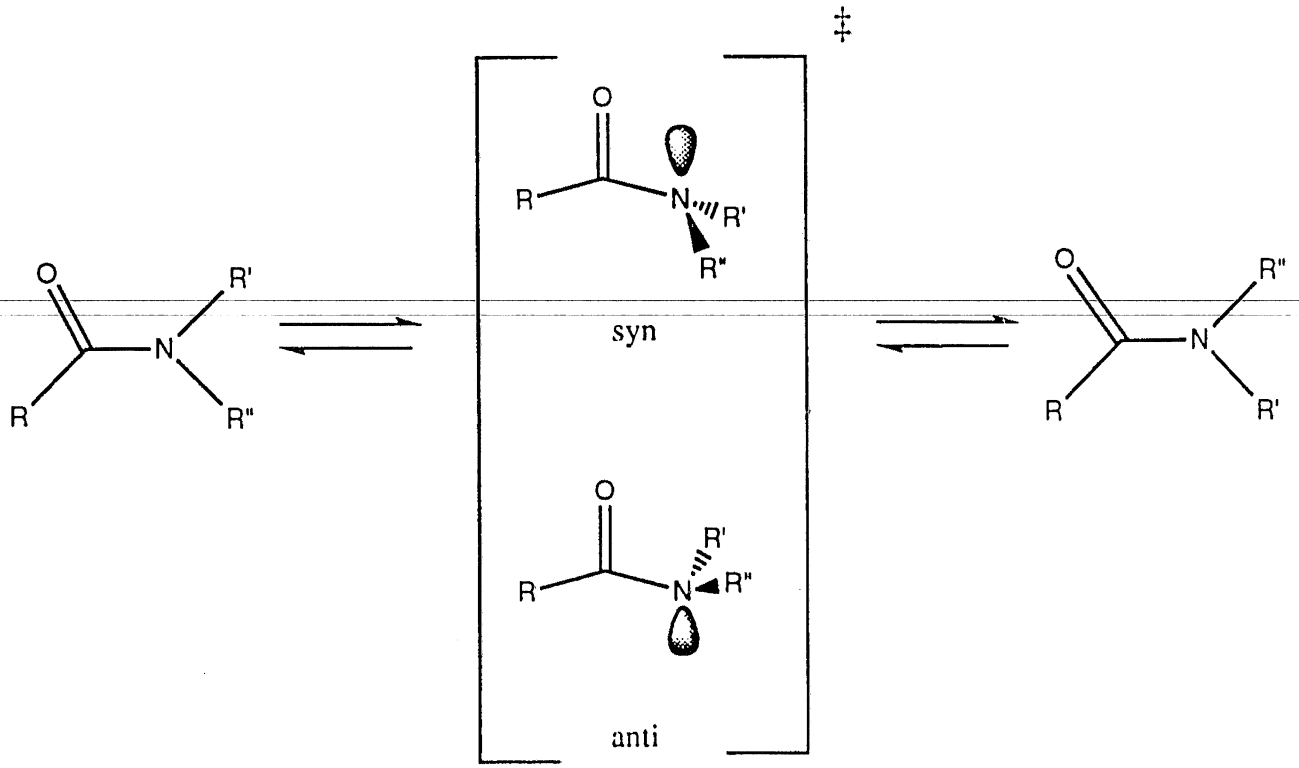
‡
O
R
N
R'
R"
syn
anti

Table 1.1 Influence of the Preceding Residue on Prolyl Peptide Bond Equilibrium[46]

Peptide	% cis
Gly-Pro	37
Ala-Pro	39
Phe-Pro	77
Tyr-Pro	79

Chapter 2

Solvent Effects on the Energetics of Prolyl Peptide Bond Isomerization

Previously published as:

Eberhardt, E. S., Loh, S. N., Hinck, A. P., Raines, R. T. Solvent Effects on the Energetics of Prolyl Peptide Bond Isomerization. *Journal of the American Chemical Society*. **1992**, *114*. 5437-5439.

Eberhardt, E. S., Loh, S. N., Raines, R. T. Thermodynamic Origin of Prolyl Peptide Bond Isomers. *Tetrahedron Letters*. **1993**, *34*, 3055-3056.

2.1 Introduction

The interconversion of *cis* (*E*) and *trans* (*Z*) isomers of peptide bonds that include the nitrogen of proline residues can give rise to a slow kinetic phase during protein folding (Figure 2.1).[1,11,47-54] This interconversion is catalyzed by PPIases.[55-58,59-62] Two of these enzymes, cyclophilin and FK-506 binding protein (FKBP), bind the immunosuppresants Cs-A and FK-506. These immunosuppressive agents are competitive inhibitors of *cis–trans* prolyl peptide bond isomerization, perhaps by acting as transition state inhibitors. At the initiation of our studies, the mechanism of PPIase catalysis had been studied extensively. First, isotope effect[63] studies of proline-containing peptides suggested that the prolyl peptide bond does not suffer nucleophilic attack during catalysis by cyclophilin. Second, systematic mutation of cysteine residues in cyclophilin indicated that an enzymic sulfur is unlikely to participate directly in catalysis.[64,65] Third, the results of calorimetry experiments showed that a large decrease in heat capacity accompanies the binding of FK-506 to FKBP.[66] Finally, structural studies of cyclophilin[67-71] and FKBP[72-75] revealed active sites composed of hydrophobic sidechains.[76] These results led to a proposed mechanism for PPIase catalysis, whereby desolvation of the prolyl peptide bond would be sufficient to effect catalysis of prolyl peptide bond isomerization.[77-79] We have determined the effect of solvent on the kinetics and thermodynamics of prolyl peptide bond isomerization in order to assess the contribution of desolvation to catalysis by the PPIases.

Experimental Design. To examine the solvent effect on prolyl peptide bond isomerization, the protected dipeptide *N*-acetyl-Gly-[β, γ-^{13}C] *D, L* -Pro-methyl ester (**2.1**) was synthesized (See: Chapter 8). In order to improve the precision of our ^{13}C experiments, peptides were prepared with ^{13}C enriched proline. Glycine was chosen to proceed proline in order to minimize any steric interactions that could alter the energetics of the prolyl peptide bond. A model of peptide **2.1**, *N*-acetyl-Pro-methyl ester (**2.2**) was used for FTIR

spectroscopic determination of the amide I vibrational mode. The structure and energetics of prolyl peptide bond isomerization of **2.2** are described in Chapters 6 and 7.

All peptides studied in this thesis were designed as protected peptides in order to avoid intramolecular hydrogen bonding and electrostatic interactions that can significantly alter the energetics of prolyl peptide bond. These intramolecular hydrogen bonds are readily formed in apolar solution[20,80,81] and have been observed in crystalline *N*-acetyl-proline[82] and *N*-acetyl-proline *N*-methyl amide[83,84] (Figure 2.2). While **2.1** has the opportunity to form an intramolecular hydrogen bond (Figure 2.2C), FTIR analysis of the amide I vibrational mode of **2.1** in toluene does not reveal any characteristics consistent with the formation of this intramolecular hydrogen bond, and the expected NOE's between the α–proton of glycine and the α–proton of proline are not observed.

In addition, protected peptides were used in these studies in order to avoid electrostatic interactions that can alter the equilibrium constant. For example, at pH 1.5, the $K_{E/Z}$ for the unprotected dipeptide, Gly-Pro, is 6.7; whereas at pH 6.5, the $K_{E/Z}$ is 2.7. In general, unprotected dipeptides exhibit different thermodynamic signatures from either longer or protected peptides. Shown in Figure 2.3 are the activation parameters ($\Delta H^{\ddagger}$, $\Delta S^{\ddagger}$) for several peptides (including peptides **2.1**, and **2.2**) that illustrate the thermodynamic differences between proline-containing peptides with the propensity to stabilize favorable intramolecular interactions and proline-containing oligopeptides that are not susceptible to intramolecular interactions. Clearly, the two classes of peptides can be differentiated, as illustrated the two slopes, by the distinct thermodynamic characteristics. Further, this analysis illustrates that peptides **2.1**, and **2.2** do not exhibit any unusual thermodynamic characteristics and that these peptides are reasonable models for the study of prolyl peptide bond isomerization.

Determination of *cis-trans* isomerization rates. NMR spectroscopy affords a unique opportunity to examine the energetics of prolyl peptide bond isomerization. A wide

variety of NMR experiments have been used in the determination of amide isomerization rates. These experiments have included line shape analysis, pD jump, and saturation transfer experiments.[46] We determined the rates of *cis-trans* isomerization of prolyl peptide bonds by using complementary inversion transfer experiments[85] The inversion transfer pulse sequence (1), where $\Delta\delta$ is the chemical shift difference between the *cis* and *trans* resonances and τ is the variable time delay that allows for exchange to occur, yields the spectra of a typical experiment shown in Figure 2.4.

$$(\pi/2)x - 1/2\Delta\delta - (\pi/2)x - \tau - (\pi/2)x - \text{acquire} \qquad (1)$$

The peak heights were determined from of the data illustrated in Figure 2.4 and a bi-exponential fit was performed to the magnetization decay curves illustrated in Figure 2.5 (For a detailed description of equations used to fit the magnetization decay curves and experimental conditions, see Chapter 8). The two advantages afforded by the inversion transfer experiment over other NMR methods are that problems of incomplete saturation are avoided and that the dynamic range available is larger, thereby increasing the amount and quality of data over that from saturation transfer experiments.

2.2 Results and Discussion

As described above, catalysis of prolyl peptide bond isomerization had been thought to proceed through a mechanism of desolvation. This proposal has its origin in NMR lineshape analyses of simple amides. These studies clearly demonstrate that the rate of amide bond isomerization does indeed depend on solvent.[86-89] Table 2.1 illustrates the effect of solvent on the barrier to amide isomerization. In general, desolvation of an amide lowers the barrier to isomerization by 1-2 kcal/mol. To explain this difference in activation energy, the electron distribution about the prolyl peptide bond must be considered in the ground state and

the transition state structures. If the amide group has greater charge separation when planar than when orthogonal, then its isomerization via an orthogonal transition state should be faster in less polar solvents.[47] Further, if the partial charge on oxygen is greater in planar than in orthogonal amides, then protic solvents should restrict isomerization by forming a hydrogen bond to oxygen.[90] Since no studies have characterized the solvent effect on proline containing peptides, the experiments below examine the contribution of desolvation in catalysis of proline isomerization by PPIases.

The isomerization rates for **2.1** were determined in different solvents. The temperature effects on the rate constant for the isomerization of **2.1** are shown as Arrhenius plots in Figure 2.6. The data in Figure 2.6 indicate qualitatively that protic solvents restrict isomerization of **2.1**. Similar to the results observed for DMF, the isomerization rate constants for **2.1** significantly increase in apolar solvent compared to polar solvent. Although the rate constants of isomerization for **2.1** are influenced by solvent dielectric constant, the ability of a solvent to donate a hydrogen bond provides a better correlation for the barrier to isomerization. The relationship between the free energy of activation for the isomerization of **2.1** and the frequency of its amide I absorption band is shown in Figure 2.7. The amide I vibrational mode, which is primarily a C=O stretch, absorbs at lower frequency with increasing strength of a hydrogen bond to the amide oxygen.[91-94] The data in Figure 2.7 therefore suggest that the barrier to isomerization ($\Delta G^{\ddagger}$) is proportional to the strength of hydrogen bonds formed to the amide oxygen (given by υ). These results are consistent with conventional pictures of amide resonance, which requires the transfer of charge between oxygen and nitrogen during isomerization.

The equilibrium constant, $K_{E/Z} = k_{EZ}/k_{ZE}$ about X-Pro peptide bonds is believed to be governed by steric interactions between the pyrrolidine ring of proline and the preceding residue. For example, the unprotected dipeptides Gly-Pro and Phe-Pro are observed to have 37 and 79 % *cis* isomer in aqueous solution, respectively.[46] Other covalent and noncovalent

interactions, like electrostatic or inductive effects (See: Chapter 7), can alter the value of $K_{E/Z}$. In contrast to the barrier to isomerization, the solvent effects on the $K_{E/Z}$ for **2.1** are small and consistent with the behavior of other amides.[58] The value of the equilibrium constant for all of the solvents was $K_{E/Z} = k_{EZ}/k_{ZE} = 4.3 \pm 0.9$ at 60 °C, as calculated by interpolating the Arrhenius plots of Figure 2.6. The absence of a solvent effect on $K_{E/Z}$ is also evident from the parallel lines in Figure 2.6.

The effect of temperature on the value of $K_{E/Z}$ for **2.1** in aqueous buffer and toluene is shown in Figure 2.8. Van't Hoff analysis of these results (assuming $\Delta C_p^\bullet = 0$) indicates that the difference in free energy ($\Delta G^\circ = -1.34 \pm 0.05$ kcal/mol in aqueous solution and $\Delta G^\circ = -1.48 \pm 0.08$ kcal/mol in toluene at 25 °C) for the X-Pro isomers of **2.1** originates almost entirely from enthalpic differences between these isomers. Further, the similarity of the enthalpies determined in aqueous buffer ($\Delta H^\circ = -1.27 \pm 0.04$ kcal/mol) and in toluene ($\Delta H^\circ = -1.27 \pm 0.06$ kcal/mol) suggests that the enthalpic forces that differentiate the *cis* and *trans* isomers of prolyl peptide bonds are similar in protic and aprotic environments. These results are similar to those of *ab initio* molecular orbital calculations, which predict that the *trans* isomer of NMA in the both the gas phase and water is favored by $\Delta H^\circ = 2.50$ kcal/mol at 25 °C.[95] Differences in entropy, though small, favors the *cis* isomer in both aqueous buffer and toluene. The entropic preference is less in aqueous buffer ($\Delta S^\circ = -0.25 \pm 0.06$ cal·mol/K) than in toluene ($\Delta S^\circ = -0.71 \pm 0.18$ cal·mol/K). This result is consistent with the amide carbonyl of *cis* isomer having lower solvent accessibility than in the *trans* isomer of **2.1**, which diminishes the ability of the amide carbonyl to restrict H_2O molecules through hydrogen bonding.

The solvent effect for the uncatalyzed *cis-trans* prolyl peptide bond isomerization is shown as a free energy profile in Figure 2.9. Desolvation of the prolyl peptide bond should lower the barrier of isomerization by increasing the relative contribution of uncharged resonance structure II. Since the calculated dipole moment is similar for both the *cis* and

trans prolyl peptide bond isomers, the solvent effect should be similar for each isomer.[96-98] Table 2.2 shows the activation energies for the isomerization of **2.1** in different solvents.[99] As with the other peptides[77], the barrier to isomerization is enthalpic in origin reflecting the change in bond order required for isomerization. Unfortunately, no obvious correlation between solvent and the entropies of activation is observed for the isomerization of **2.1**. While the solvent effect on the prolyl peptide bond transition state remains unclear, the observation that the entropy of activation is near zero suggests that solvent does not alter the transition state.[100]

2.3 Conclusion

These experiments clearly illustrate that the barrier to *cis-trans* prolyl peptide bond isomerization is significantly lower in aprotic solvent that in protic solvent. Further, these results indicate that the barrier to isomerization is governed by the relative strength of the hydrogen bond to the to the oxygen of the prolyl peptide bond. In contrast, the equilibrium constant about the prolyl peptide bond is not altered significantly by solvent. Similar medium effects may modulate the stability of planar peptide bonds during the folding,[1,52] function,[101-103] or lysis[42,104] of proteins.

Figure 2.1 The *cis* (*E*) and *trans* (*Z*) prolyl peptide bond isomers and the principle resonance structures for each isomer.

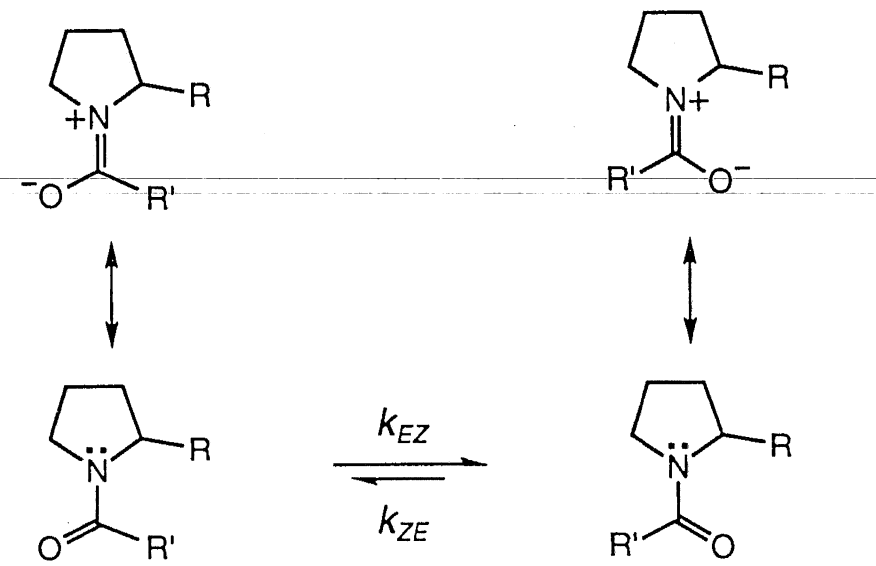

cis (*E*) isomer

trans (*Z*) isomer

Figure 2.2 Potential conformations for A) *N*-acetyl proline; B) *N*-acetyl proline methyl amide C) **2.1**.

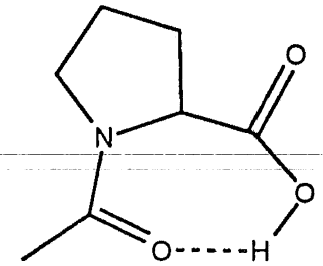

A

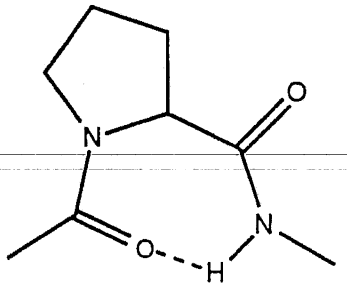

B

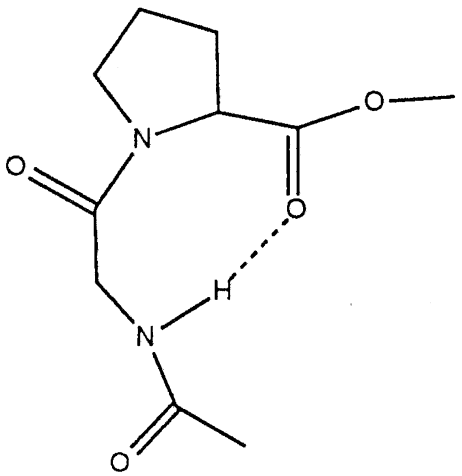

C

Figure 2.3 Enthalpy-entropy compensation for prolyl peptide bond isomerization for oligopeptide (▲), dipeptides (O), and Gly-Gly-Lys-Phe-Pro (Δ). Key to structures: 1, *N*-acetyl-Gly-[β, γ-^{13}C] *D, L* -Pro-methyl ester (**2.1**); 2, *N*-acetyl-[β, γ-^{13}C] *D, L* -Pro-methyl ester; 3, *N*-acetyl-Gly-[β, γ-^{13}C] *D, L* -Pro-dimethylamide; 4, Suc-Ala-Leu-Pro-Phe-pNA[100]; 5, Suc-Ala-Ala-Pro-Phe-pNA[100]; 6, Gly-Gly-Pro-Ala[74]; 7, *N, N*-dimethylacetamide[89]; 8, Suc-Ala-Trp-Pro-Phe-pNA[100]; 9, Suc-Ala-Gly-Pro-Phe-pNA[100]; 10, Gly-Pro[105]; 11, Ala-Pro[106]; 12, Val-Pro[106]; 13, His-Pro[107]; 14, Gly-Gly-Lys-Phe-Pro[108]. Linear regression analysis is shown for 1-9 (—) and 10-14 (---).

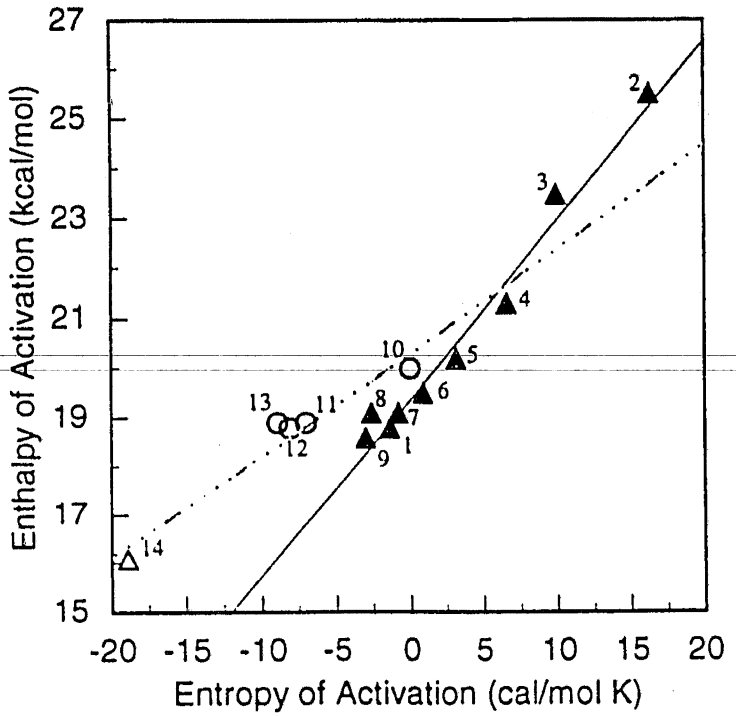
Enthalpy of Activation (kcal/mol)
27
25
23
21
19
17
15
-20
-15
-10
-5
0
5
10
15
20
Entropy of Activation (cal/mol K)
1
2
3
4
5
6
7
8
9
10
11
12
13
14

Figure 2.4 Shown are ^{13}C spectra of **2.1** in 20 % D_2O: 80% H_2O; 100 mM sodium phosphate buffer, pH 7.2, (348 K) at different τ (sec) delay times. **1**, 0.001 sec; **5**, 0.15 (sec); **10**, 0.40 (sec); **15**, 0.80 (sec); **20**, 2.0 (sec); **25**, 4.0 (sec).

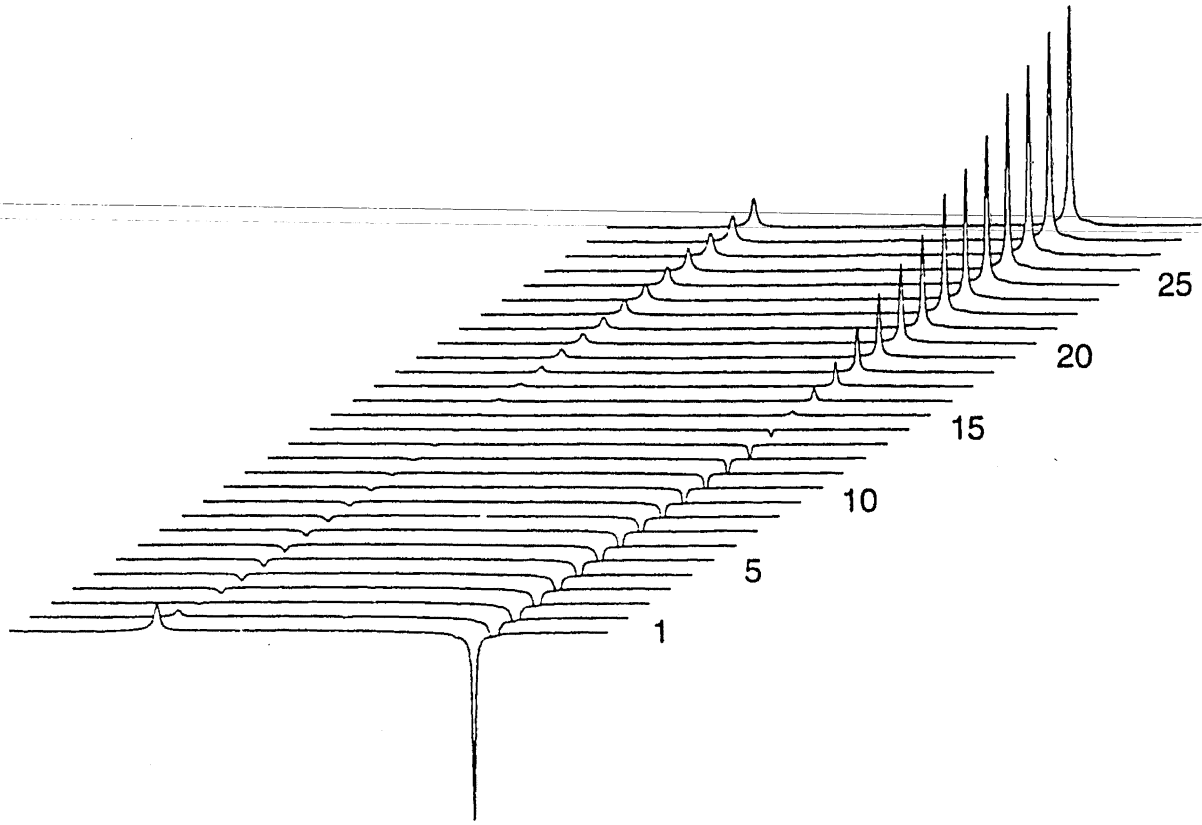
25
20
15
10
5
1

Figure 2.5 Magnetization transfer curves of **2.1** in 20 % D_2O: 80% H_2O 100 mM sodium phosphate buffer, pH 7.2, (348 K). The *cis* (▲) and *trans* (●) resonances of a typical experiment where individual peak heights are plotted against τ (sec) delay times.

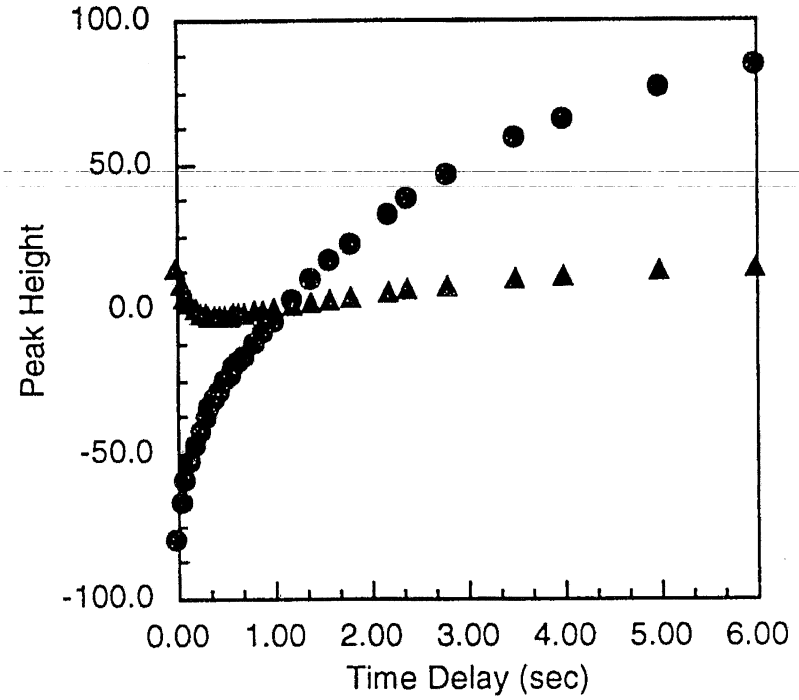
100.0
50.0
0.0
-50.0
-100.0
Peak Height
0.00
1.00
2.00
3.00
4.00
5.00
6.00
Time Delay (sec)

Figure 2.6 Arrhenius plots for isomerization of **2.1** in different solvents. Solvents (dielectric constant at 25°C) were ◇, dioxane (2.21); ○, benzene (2.27); ▽, toluene (2.38); ●, isopropanol (19.92); ■, ethanol (24.55); ◆, trifluoroethanol (26.14); □, acetonitrile (35.94); △, *N*,*N*-dimethylformamide (36.71); and ⊠, water (78.30). Linear regression analysis is shown for each protic solvent (—) and all aprotic solvents (---). (A) *cis* to *trans*. (B) *trans* to *cis*.

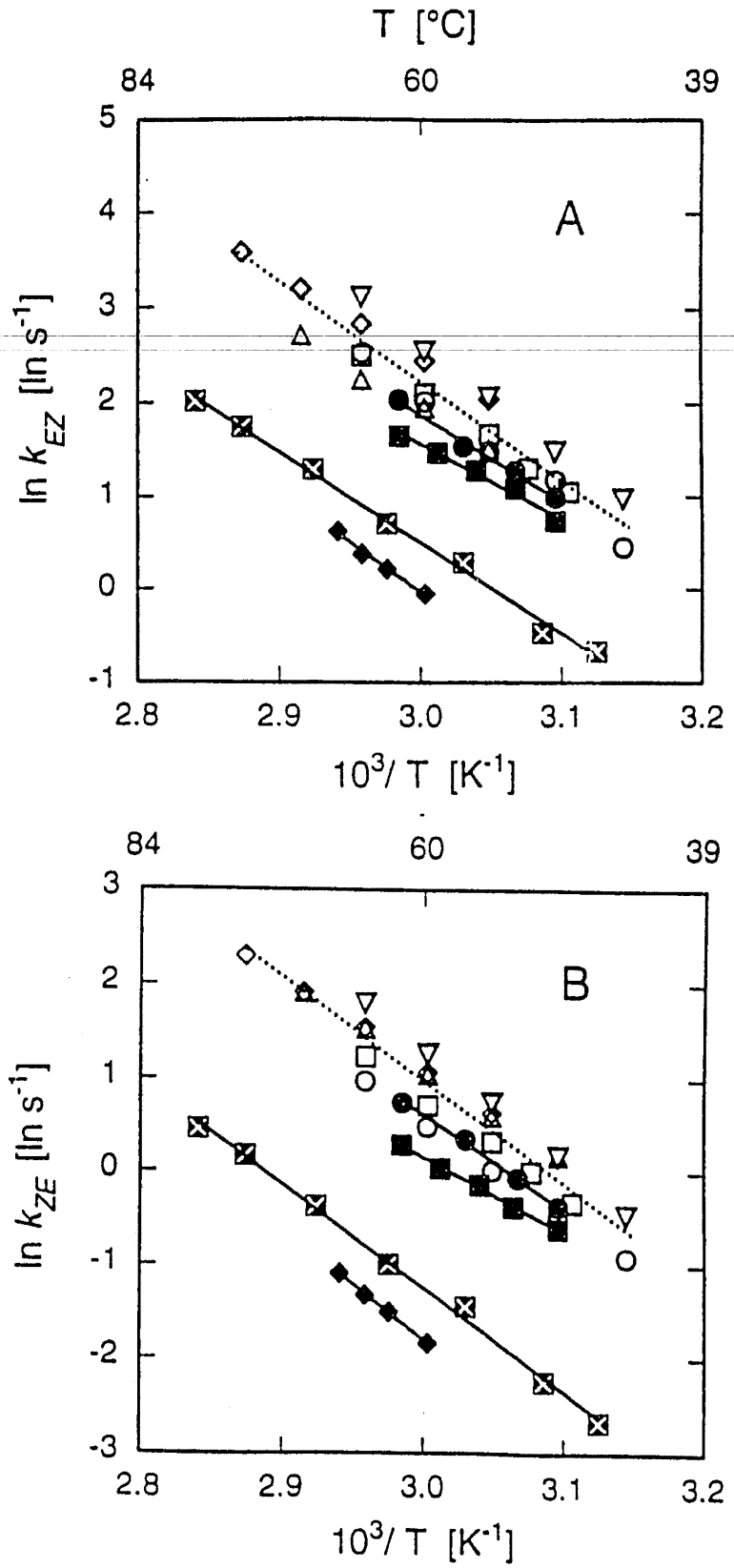
T [°C]
84
60
39
A
ln k_{EZ} [ln s^{-1}]
5
4
3
2
1
0
-1
2.8
2.9
3.0
3.1
3.2
10^3/ T [K^{-1}]
84
60
39
B
ln k_{ZE} [ln s^{-1}]
3
2
1
0
-1
-2
-3
2.8
2.9
3.0
3.1
3.2
10^3/ T [K^{-1}]

Figure 2.7 Plots of $\Delta G^{\ddagger}$ for isomerization of **2.1** vs υ of amide I vibrational mode of Ac–Pro–OMe in different solvents. Symbols are as in Figure 2.6. Values of $\Delta G^{\ddagger}$ were calculated by interpolating the Arrhenius plots of Figure 2.6 at 60°C. Weighted linear regression analysis is shown for *cis* to *trans* [—, slope = –0.025 ± 0.003 kcal·cm/mol] and *trans* to *cis* [---, slope = –0.029 ± 0.002 kcal·cm/mol]. $\Delta G^{\ddagger}_{\text{aprotic}} - \Delta G^{\ddagger}_{\text{water}} = 1.3 \pm 0.2$ kcal/mol.

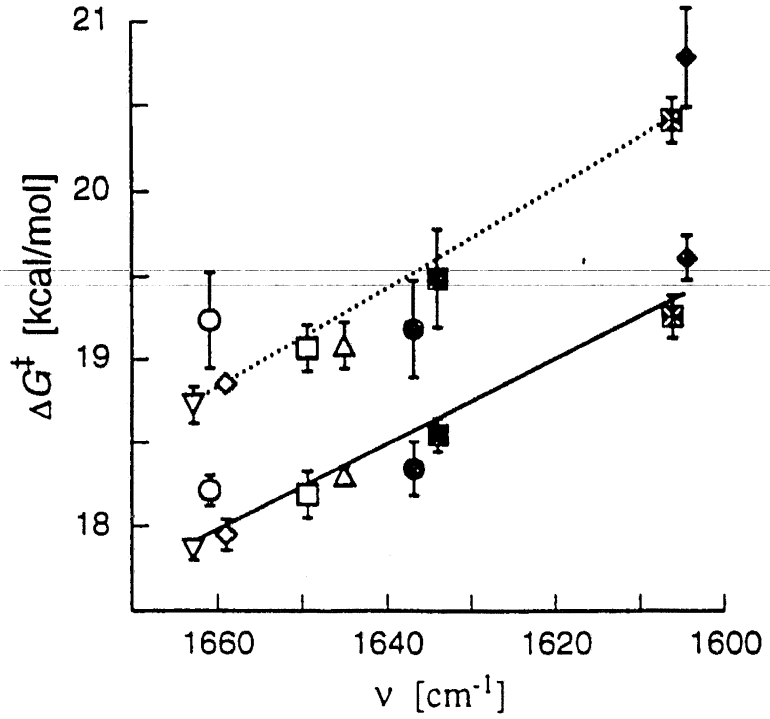
21
20
19
18
$\Delta G^{\ddagger}$ [kcal/mol]
1660
1640
1620
1600
ν [cm^{-1}]

Figure 2.8 Van't Hoff plot for the *cis* to *trans* isomerization of **2.1** in toluene, ○, and water, ●.

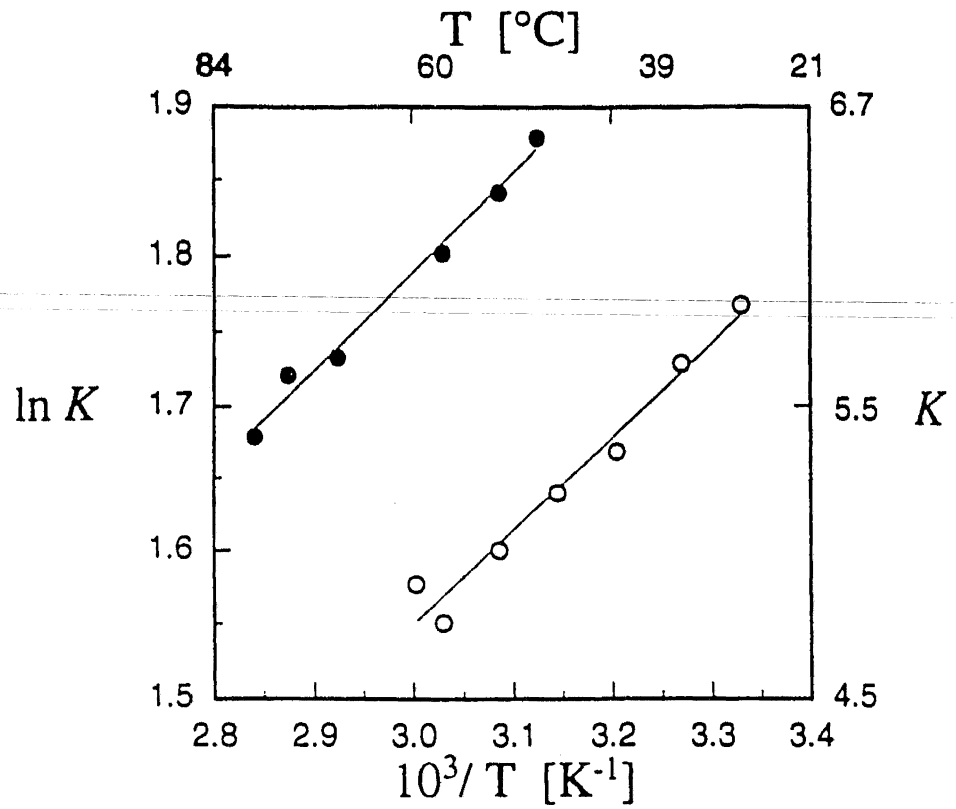
T [°C]
84
60
39
21
1.9
1.8
1.7
1.6
1.5
6.7
5.5
4.5
ln K
K
2.8
2.9
3.0
3.1
3.2
3.3
3.4
10³/ T [K⁻¹]

Figure 2.9 The solvent effect on prolyl peptide bond isomerization is shown as a free energy profile. The solid line (—) represents the barrier under in protic solvent. The dash line (---) represents the barrier to isomerization under aprotic conditions. Also shown are the ground state structures as well as the putative transition state for prolyl peptide bond isomerization.

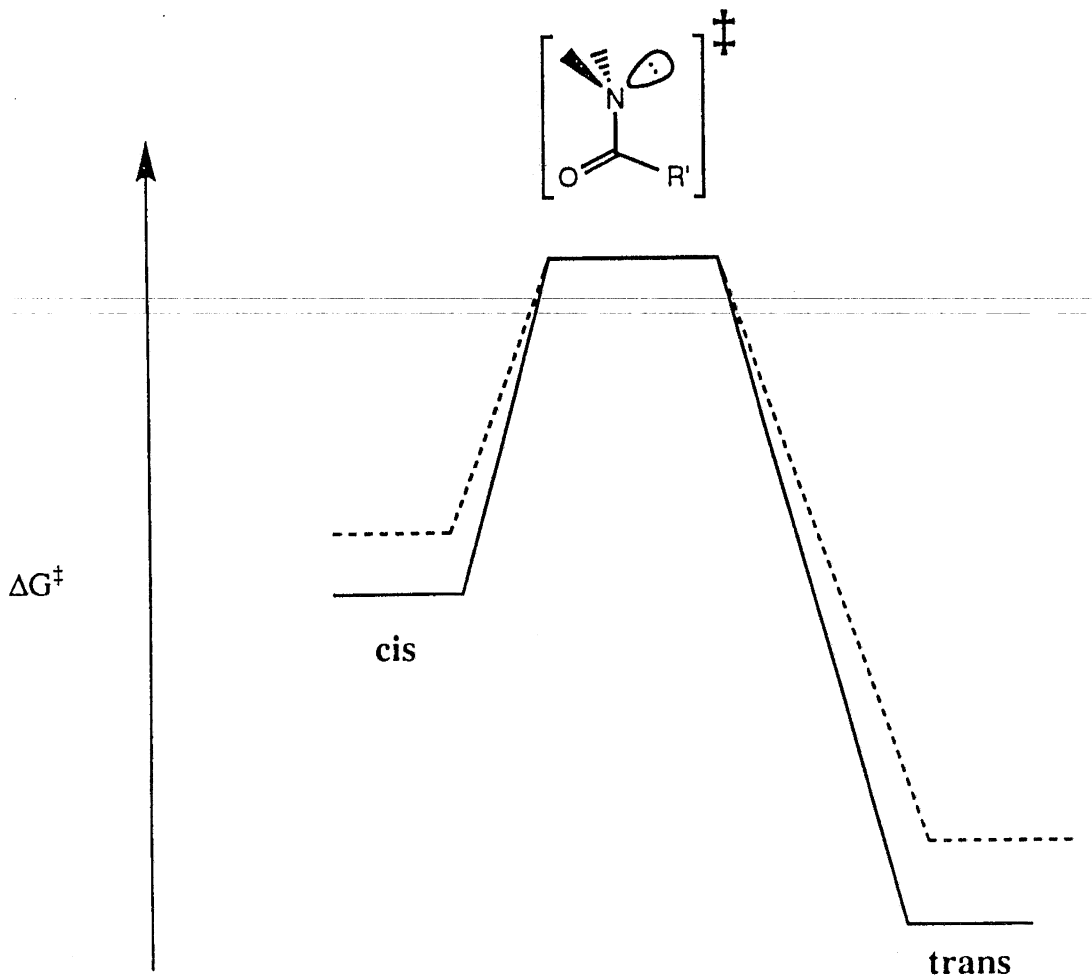

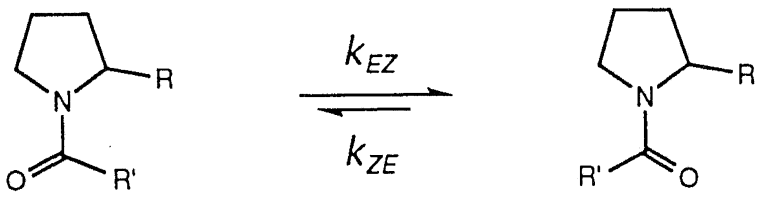

cis (*E*) isomer *trans* (*Z*) isomer

Table 2.1 Solvent Effect on Amide Activation Energies[99]

Amide	Solvent	$\Delta G^{\ddagger}$ (kcal/mol)
DMF	neat	20.8-22.4
	CCl_4	20.5
	TFA (0.3 M)	20.7
DMA	neat	21.0
	H_2O	19.0-20.0

Table 2.2 Solvent Effects on Activation Parameters for Isomerization of **2.1**[43]

Solvent	Rate constant	$\Delta H^{\ddagger}$ (kcal/mol)	$\Delta S^{\ddagger}$ (cal/mol K)
acetonitrile	k_{EZ}	19.25 ± 0.14	3.18 ± 0.43
	k_{ZE}	19.97 ± 0.14	2.71 ± 0.43
benzene	k_{EZ}	20.79 ± 0.29	7.74 ± 0.87
	k_{ZE}	19.46 ± 0.09	0.66 ± 0.27
DMF	k_{EZ}	17.55 ± 0.14	-2.29 ± 0.41
	k_{ZE}	18.62 ± 0.05	-0.73 ± 0.15
dioxane	k_{EZ}	16.67 ± 0.03	-3.84 ± 0.08
	k_{ZE}	18.30 ± 0.09	-1.85 ± 0.26
ethanol	k_{EZ}	15.35 ± 0.29	-9.61 ± 0.88
	k_{ZE}	14.96 ± 0.16	-13.56 ± 0.32
isopropanol	k_{EZ}	17.68 ± 0.29	-2.01 ± 0.67
	k_{ZE}	19.42 ± 0.16	0.69 ± 1.14
toluene	k_{EZ}	22.28 ± 0.11	12.95 ± 0.34
	k_{ZE}	23.35 ± 0.06	13.89 ± 0.20
trifluoroethanol	k_{EZ}	20.60 ± 0.29	2.97 ± 0.86
	k_{ZE}	23.08 ± 0.13	6.89 ± 0.40
water	k_{EZ}	18.78 ± 0.13	-1.42 ± 0.39
	k_{ZE}	21.21 ± 0.13	2.29 ± 0.38

All experiments were performed in the solvents indicated with 100 mM of **2.1.** Activation parameters were calulated by a plot of the slope and y-intercept of $\log(k_{EZ}/T)$ vs 1/T K.

Chapter 3

Amide–Amide and Amide–Water Hydrogen Bonds: Implications for Protein Folding and Stability

Previously published as:

Eberhardt, E. S. and Raines, R. T. Amide–Amide and Amide–Water Hydrogen Bonds: Implications for Protein Folding and Stability. *Journal of the American Chemical Society*. **1994**, *116*, 2149-2150.

3.1 Introduction

As a protein folds, many of its mainchain amide groups exchange hydrogen bonds with water for hydrogen bonds with other mainchain amides. The energetic contribution of this exchange to the folding and stability of proteins is unclear.[2,9,10,25,31,109] Theoretical,[19,110-113] calorimetric,[114,115] and spectroscopic[16,17,20,92,116,117] studies indicate that amide–amide hydrogen bonds form readily in nonpolar media. In contrast, amide–amide hydrogen bonds form only at extremely high amide concentrations in water.[18,118] Extensive efforts[119-121] to evaluate the contribution of amide–amide hydrogen bonds to the aqueous stability of a particular receptor–ligand complex ultimately failed to exclude contributions to binding from other forces.[122] To assess the importance of amide–amide hydrogen bonds in protein folding and stability, we have determined the relative strength of amide–amide and amide–water hydrogen bonds.

3.2 Results and Discussion

Our analyses were performed on the simple peptide Ac–Gly–[β,δ-^{13}C]Pro–OMe (**3.1**) and the related amide [^{13}C=O]Ac–Pro–OMe (**3.2**) (Figure 3.1). Racemic **3.1** and **3.2** were synthesized as described Chapter 8 using standard methods.[123] In a previous study, the kinetic barrier to prolyl peptide bond isomerization of **3.1** was shown to depend on the ability of the solvent to donate a hydrogen bond to the amidic carbonyl group (See: Chapter 2).[43] Here, the effects of amide solvents and water on this same kinetic barrier were determined using inversion transfer ^{13}C NMR spectroscopy (See: Chapter 8).[85,124] Solvent effects on the amide I vibrational mode of **3.2** were determined using IR spectroscopy. The amide solvents studied mimic amide groups found in proteins.

The relationship between the free energy of activation for the isomerization of **3.1** and the frequency of the amide I absorption band of **3.2** is shown in Figure 3.2. The amide I vibrational mode absorbs at lower frequencies with increasing strength of a hydrogen bond to

the amide oxygen.[94] Also, the rate of prolyl peptide bond isomerization is related inversely to the strength of hydrogen bonds formed to the amide oxygen. The axes in Figure 3.2 report independent measures of the ability of a solvent to donate a hydrogen bond to an amide oxygen. Further support for this interpretation of Figure 3.2 comes from the solvent dependence for the eight solvents studied here (Figure 3.3) of the frequency of the ester carbonyl stretching vibration of **3.2**, which is related to that of the amide I vibrational mode by the following equation (1):

$$\upsilon_{\text{ester C=O}} = (0.36 \pm 0.07)\upsilon_{\text{amide I}} + (1.2 \pm 0.1)\text{x}10^3 \qquad (1)$$

The data in Figure 3.2 show that water donates a strong hydrogen bond to an amidic carbonyl group. The analogous ability of secondary amide solvents, which resemble the mainchain of proteins, to donate a hydrogen bond is dramatically less. The concentration of each solvent studied here was >10 *M*, which is likely to exceed the effective concentration of peptide bonds to one another, at least during the early stages of protein folding.[125] These results suggest that amide–amide hydrogen bond formation alone is unlikely to drive protein folding. This study, however, does not explicitly address any entropic contribution to protein folding and stability that may arise from the release of water molecules upon formation of amide–amide hydrogen bonds. Since the released water molecules form hydrogen bonds with bulk water, this entropic contribution is likely to be small.

The data in Figure 3.2 also show that formamide, which mimics the primary amide in the sidechains of asparagine and glutamine residues, is a significantly better hydrogen bond donor than is any of the secondary amides studied, and is almost as good as water. This result suggests that sidechain–mainchain hydrogen bonds can contribute more to protein stability than can mainchain–mainchain hydrogen bonds. This idea is consistent with asparagine, glutamine, and glycine being preferred residues at the *C*-terminus of α-

helices.[126,127] There, an amide side chain can donate a hydrogen bond to a mainchain carbonyl group, and a glycine residue can maximize the exposure of a mainchain carbonyl group to solvent water.[10,128,129]

What is the origin of the dramatic difference observed between the hydrogen bond donating abilities of secondary amides and formamide? An important contribution may arise from the effective concentration of donors, since an additional potential donor is always proximal to every hydrogen bond donated by formamide. Alternatively, the observed difference may result largely from steric constraints that restrict the number or geometry of hydrogen bonds donated by secondary amides, as has been proposed for large alcohols.[92,130,131] Regardless of its origin, the observed differences in hydrogen bond donating abilities are likely to be manifested during protein folding and in folded proteins.

3.3 Conclusion

Approximately $^3/_4$ of the mainchain amides in globular proteins form hydrogen bonds with other mainchain amides.[125] Although the formation of such intramolecular amide–amide hydrogen bonds in water can be exothermic,[132] the results presented here and elsewhere[114,115] indicate that amides form stronger intermolecular hydrogen bonds with water than with other amides. We conclude that mainchain–mainchain hydrogen bonds can form only in a cooperative process, which is likely to be facilitated by the hydrophobic collapse of the unfolded protein and the consequent shedding of water molecules from mainchain amides.[10] We also suggest that the desolvation of individual mainchain amides diminishes the stability of folded proteins.[133,134]

Figure 3.1 Structure of proline derivatives: Ac–Gly–[β,δ-^{13}C]Pro–OMe (**3.1**), and the related amide [^{13}C=O]Ac–Pro–OMe (**3.2**).

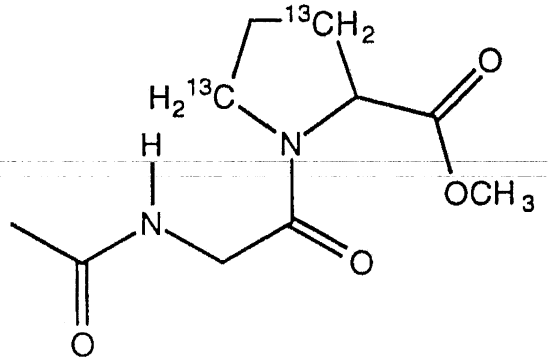

3.1

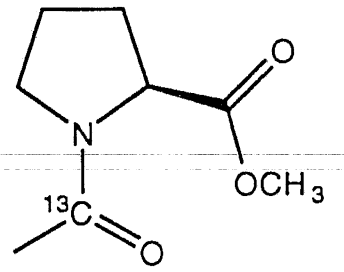

3.2

Figure 3.2 Plots of $\Delta G^{\ddagger}$ for isomerization of **3.1** vs. υ of amide I vibrational mode of **3.2** in different solvents. The solvents (neat concentration, M; pK_a in Me_2SO, if known[135]) were as follows: A, dioxane (11.7); Δ, *N*,*N*-dimethylformamide (13.0); ■, *N*-methylpropionamide (10.7); ▲, *N*-ethylacetamide (10.8; 26.1); ▼, *N*-methylacetamide (13.1; 25.9); ●, *N*-methylformamide (17.1); ●, formamide (25.2; 23.45); ⊠, water (55.5; 32). A, *cis* to *trans*. B, *trans* to *cis*. Unweighted linear regression analysis gives slopes –0.022 ± 0.003 (A) and –0.030 ± 0.006 (B).

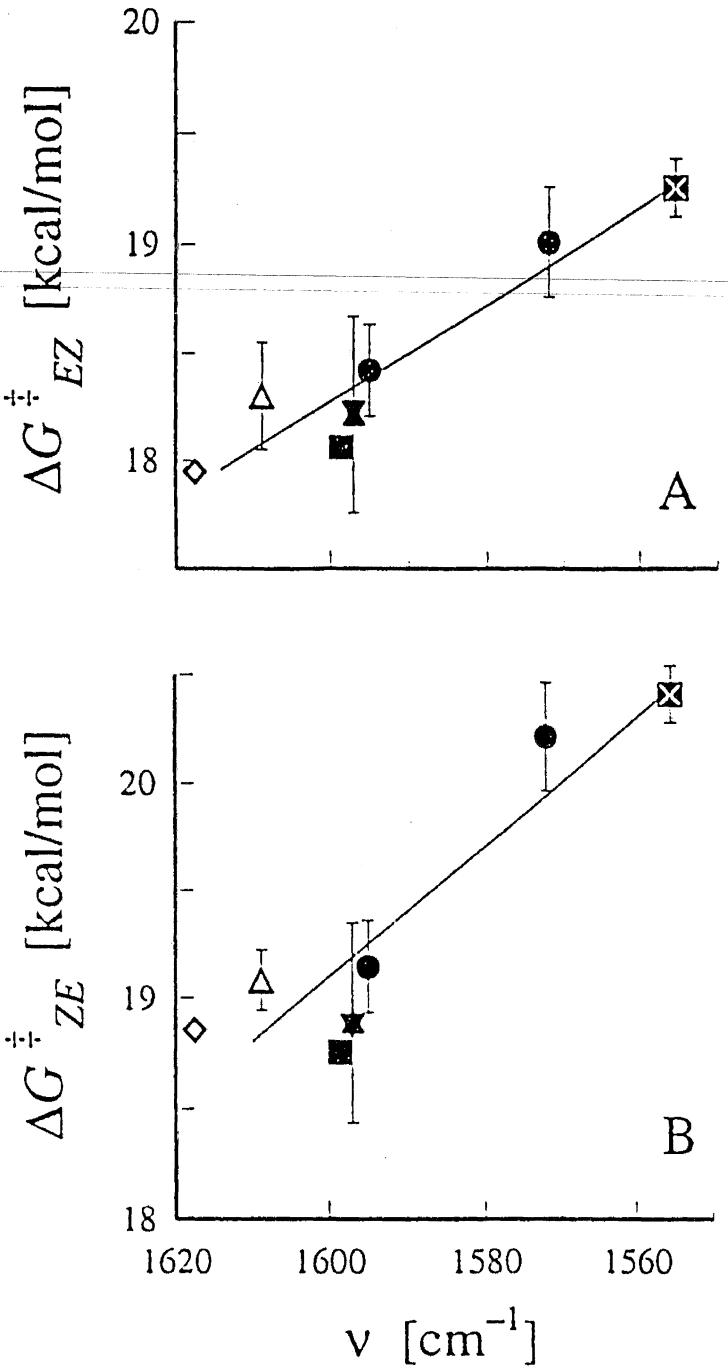
20
19
18
$\Delta G^{\ddagger}_{EZ}$ [kcal/mol]
A
20
19
18
$\Delta G^{\ddagger}_{ZE}$ [kcal/mol]
B
1620
1600
1580
1560
ν [cm^{-1}]

Figure 3.3 Plot of the amide I vibrational mode **3.2** vs. the ester carbonyl stretch region of **3.2** in different solvents. Solvents are as in Figure 3.1.

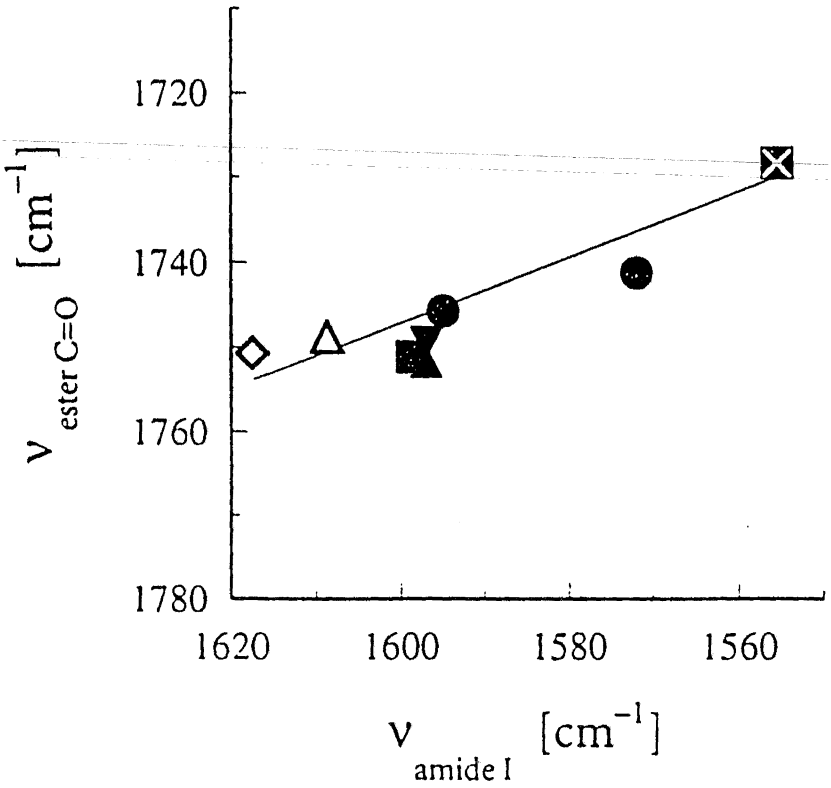
1720
1740
1760
1780
1620
1600
1580
1560
ν ester C=O [cm⁻¹]
ν amide I [cm⁻¹]

Chapter 4

Mechanism and Thermodynamics of Amide Hydrogen Bond Formation in Aqueous and Organic Solvents: Dimerization of δ-Valerolactam

This work was undertaken as a collaboration with: Loh, S. N., Eberhardt, E. S., Edison, A. S., Weinhold, F., Raines, R. T. & Markley, J. L.

4.1 Introduction

Since amide–amide hydrogen bonds are the most prevalent hydrogen bonds observed within proteins, an understanding of the energetic contributions of such hydrogen bonds is essential for the accurate prediction of a three dimensional protein structure from its amino acid sequence. Due to the complexity of the protein folding problem, studies of model amides have been used to dissect the contribution of amide–amide hydrogen bonds in aqueous solution. In apolar solvents, amide-amide hydrogen bond formation is associated with a large enthalpic component, and the bonds are readily formed at dilute amide concentrations. In contrast, amide-amide hydrogen bond formation in aqueous solution occurs at only extremely high amide concentrations. The thermodynamic driving force is, however, unclear. Studies of *N*-methyl acetamide,[16] diketopiperadine,[136] urea,[118] and δ-valerolactam[18] in aqueous solution reveal that a significant enthalpic contribution is associated with amide–amide hydrogen bond formation. Of these studies, δ-valerolactam was observed to have the largest enthalpy change upon association (-5.5 ± 1 kcal/mol). Using nuclear magnetic resonance spectroscopy and infrared spectroscopy, the association of δ-valerolactam in CCl_4 and H_2O has been re-examined.

4.2 Results and Discussion

The dimerization of δ-valerolactam was determined from its amide ^1H chemical shift as a function δ-valerolactam concentration in CCl_4 and H_2O (Figure 4.1). The changes in chemical shift reflect the formation of a hydrogen bonded lactam dimer, since ^{13}C T_1 and ^1H-^{13}C heteronuclear measurements (data not shown) indicate that large aggregates are not being formed at high lactam concentrations. The IR data of δ-valerolactam in CCl_4 (Figure 4.2) shows that hydrogen bonding at 100 mM concentrations of lactam (Figure 4.2A) and an absence of H-bonded NH frequencies in the NH region of 1 mM lactam (Figure 4.2B). The absence of hydrogen bonding in the NH region of the 1 mM lactam sample indicates that the

non-hydrogen bonded monomer is the predominate species in solution under these conditions. At 100 mM lactam in CCl_4, both the NH and amide I vibrational modes become red-shifted (3416 and 1675 cm^{-1} at 1 mM to 3205 and 1672 cm^{-1}, respectively) indicating dimerization of the δ-valerolactam molecules. The appearance of additional frequencies (near 3804 and 3142 cm^{-1}) and the shoulder in the amide I region indicate that other hydrogen bonded species exist at high δ-valerolactam concentrations, though the identity of these minor species remains unknown. The IR and NMR data in CCl_4 are consistent with a simple mechanism of lactam dimerization with no participation of solvent (Figure 4.4A).

While the dimerization of δ-valerolactam occurs over five orders of magnitude of lactam concentration in organic solvent, the transition in water was much steeper (Figure 4.1). The observed difference is reconciled by invoking different binding mechanisms in aqueous solution and organic solvent. In aqueous solution, dimerization in water is accompanied by the release of water molecules; whereas, in CCl_4, solvent does not enter into the reaction. The amide I vibrational mode of δ-valerolactam in H_2O supports the involvement of solvent in lactam dimerization since the lactam molecules are always participating in a hydrogen bond with either another lactam molecule or, one or two water molecules (Figure 4.3). As the mole fraction solute (δ-valerolactam) decreases, spectra 1-5, the contribution of δ-valerolactam dimer (1663 cm^{-1}) to the amide I vibrational mode decreases, while the contribution of the fully hydrated monomeric species (MW_2) increases (1625 cm^{-1}). The emergence of an intermediate species, centered around 1635 cm^{-1} as illustrated in Figure 4.3, is believed to be a lactam molecule hydrated by one water molecule, the MW_1 species. This intermediate species is similar to the behavior observed for acetone and mixtures of apolar and protic solvents and appearance of this δ-valerolactam intermediate species is consistent with a single water molecule being bound to each lactam molecule.[137]

To extract the binding parameters for the dimerization reaction of δ-valerolactam in aqueous solution, the following equilibrium (1) must be considered:

$$2M \overset{K_a}{\rightleftharpoons} D + xH_2O \quad (1)$$

where K_a is the association constant and M and D represent the monomer and dimer respectively. Given that [T], the total lactam concentration, is equal to [M] + 2[D], the expression (2) that describes the equilibrium in (1) can be solved for [M]:

$$[M] = \frac{-[H_2O]^x + \sqrt{[H_2O]^{2x} + 8K_a[T][H_2O]^x}}{4K_a} \quad (2)$$

K_a and x, the stoichiometery of solvent molecules involved, can then be extracted from a nonlinear least-squares fit of the form

$$\delta_{obs} = \frac{[M]}{[T]}\delta_M + \frac{[T]-[M]}{[T]}\delta_D \quad (3)$$

where δ_{obs} is the observed NMR parameter while δ_M and δ_D are the baseline spectral values of the lactam monomer and dimer, respectively. Table 4.1 illustrates the dimerization parameters for δ-valerolactam in CCl_4 and H_2O. The most significant result is that the dimerization of δ-valerolactam in CCl_4 can be readily modeled by using the mechanism illustrated in Figure 4.4A. From a standard van't Hoff analysis, the dimerization of δ-valerolactam CCl_4 is found to be enthalpically driven (ΔH° = -7.9 ± 0.05; ΔS° = -16.6 ± 0.09). In water, however, x shows a significant temperature dependency change from 2.5 at 2.5 °C to 1.8 at 61 °C. The change in x indicates that the mechanism of dimerization is temperature dependent. Therefore, a straight forward van't Hoff analysis cannot be used to extract the energetics of δ-valerolactam dimerization in aqueous solution. These results suggests that the mechanism of dimerization changes with increasing temperature. Figure 4.4C illustrates mechanism of δ-valerolactam dimerization in aqueous solution at low temperatures. As temperature increases, the mechanism shifts from Figure 4.4C to Figure 4.4B to Figure 4.4A. Preliminary *ab initio* calculations of the dimerization of MW_1

and MW_2 species, *in vaccuo*, is slightly opposed enthalpically but driven entropically by the release of water. This conclusion is consistent with the calculated driving forces for the binding of β-lactam inhibitors.[121,138] Although the *in vaccuo* nature of these calculations does not permit a quantitative thermodynamic analysis, these results imply that after the hydrophobic collapse of a protein during folding, the formation of buried amide hydrogen bonds can be entropically driven by the release of water molecules. This mechanism for amide–amide hydrogen bond formation may only be applicable, however, for the formation of amide–amide hydrogen bonds that are shielded from bulk solvent.

4.3 Conclusion

As model system for amide–amide hydrogen bond formation, the dimerization of δ-valerolactam has illustrated the challenges in determining the mechanism and thermodynamic driving forces which govern amide–amide hydrogen bond formation in aqueous solution. These experiments demonstrate that the mechanism for amide–amide hydrogen bond formation is temperature dependent, and suggest that amide–amide hydrogen bond formation can be entropically driven by the release of water molecules if the amides are shielded from bulk solvent. Finally, these experiments caution against the use of a standard van't Hoff analysis in determining the thermodynamics of amide–amide hydrogen bond formation in aqueous solution.

Figure 4.1 Plot of the amide proton chemical shift as a function of δ-valerolactam concentration in CCl_4(▼) and H_2O(●). All measurements were made at 22 °C. Solid line represents the best fit of eq 3 to the data. Theoretical curves for dimerization in CCl_4 was obtained with the solvent parameter x set to zero.

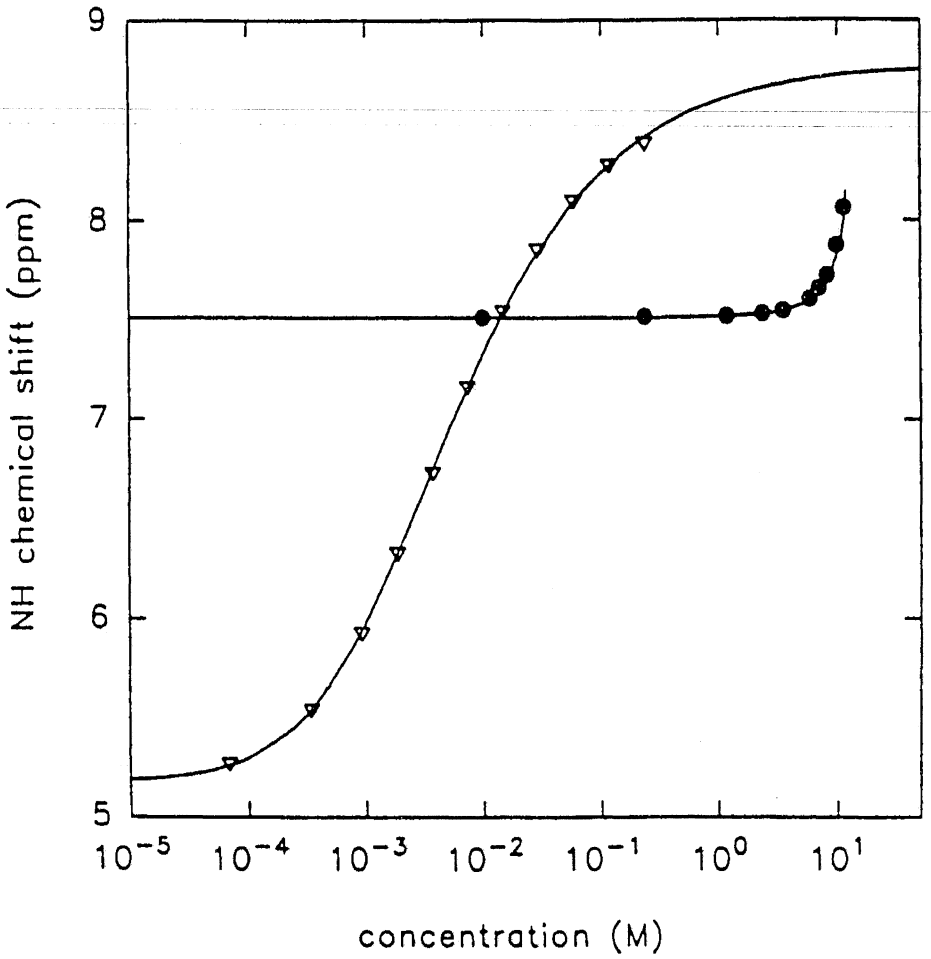
9
8
7
6
5
NH chemical shift (ppm)
10^{-5} 10^{-4} 10^{-3} 10^{-2} 10^{-1} 10^{0} 10^{1}
concentration (M)

Figure 4.2 IR spectra of δ-valerolactam in CCl_4 showing the NH stretch region from 3500 to 3000 cm^{-1}, and the amide I vibrational mode from 1750 to 1550 cm^{-1}. In A) a δ-valerolactam concentration of 1.0 M; B) a δ-valerolactam concentration of 0.001 M at 22 °C. M and D are monomer and dimer respectively.

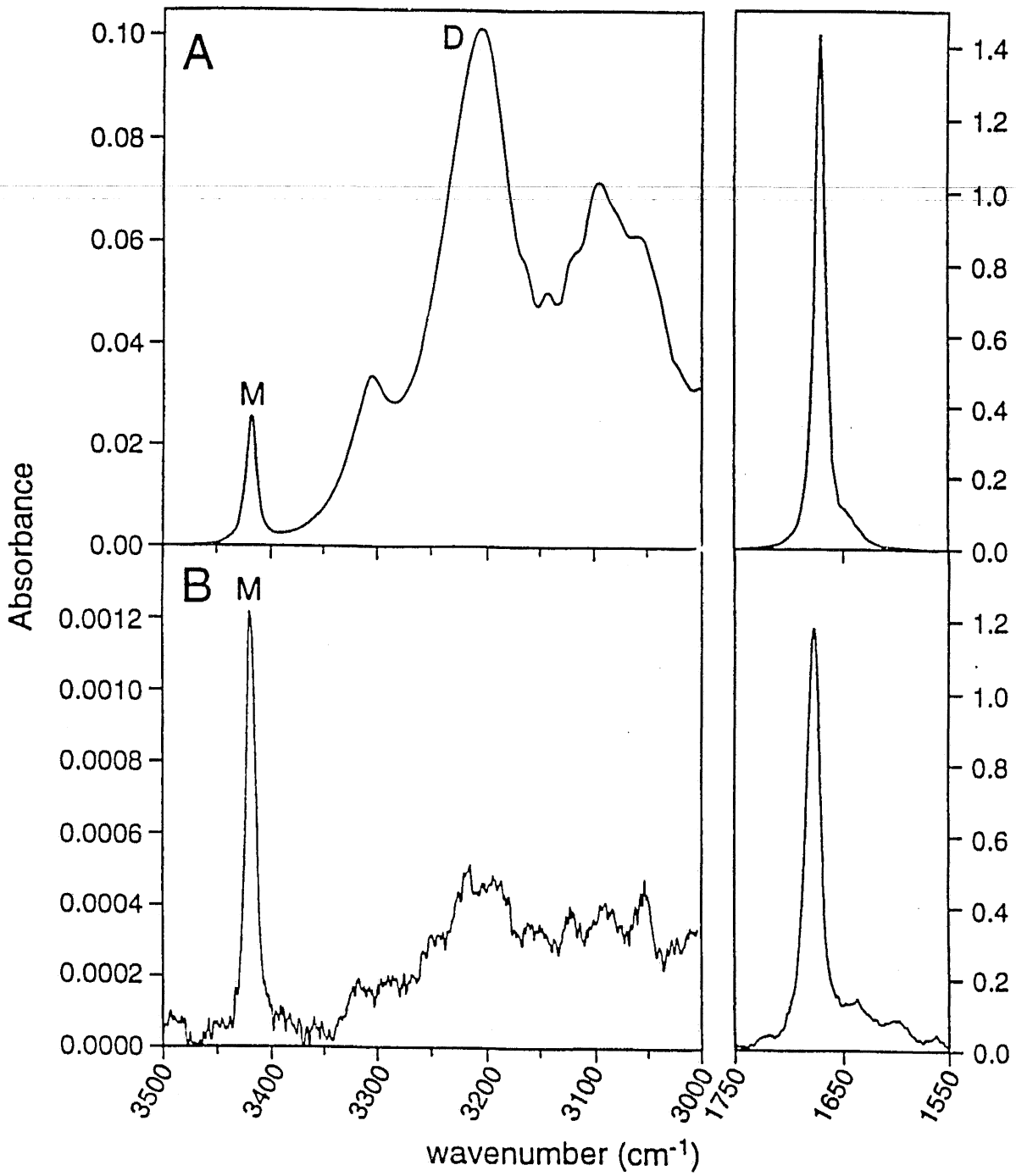
A
D
M
B
M
Absorbance
0.10
0.08
0.06
0.04
0.02
0.00
0.0012
0.0010
0.0008
0.0006
0.0004
0.0002
0.0000
1.4
1.2
1.0
0.8
0.6
0.4
0.2
0.0
3500
3400
3300
3200
3100
3000
1750
1650
1550
wavenumber (cm-1)

Figure 4.3 IR spectra of δ-valerolactam in H_2O, recorded at 22 °C showing the amide I vibrational mode. Concentrations of δ-valerolactam were: 1, 11.3 M; 2, 9.87 M; 3, 8.23 M; 4, 7.05 M; 5, 5.88 M. Each spectrum was resolution-enhanced and normalized. The y-axis represents arbitrary absorbance units.

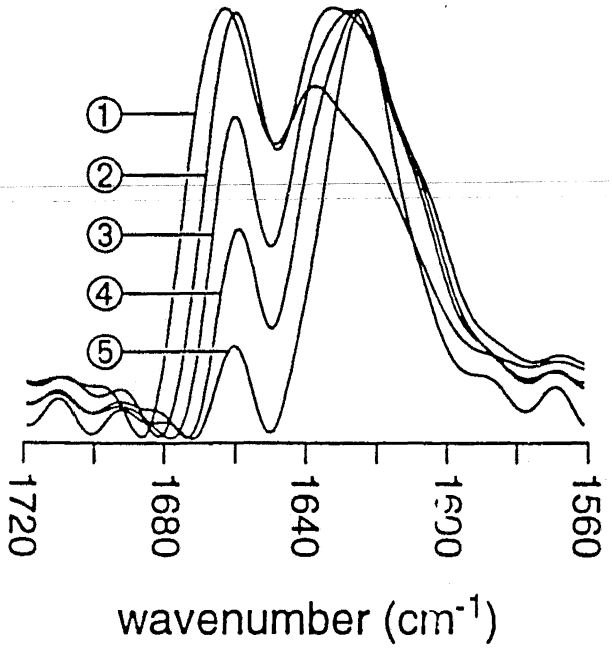
①
②
③
④
⑤
1720
1680
1640
1600
1560
wavenumber (cm-1)

Figure 4.4 Putative dimerization mechanisms of δ-valerolactam. A) Dimerization mechanism in CCl_4. B) Dimerization mechanism in H_20. C) Dimerization mechanism in H_20 at low temperature.

(A)

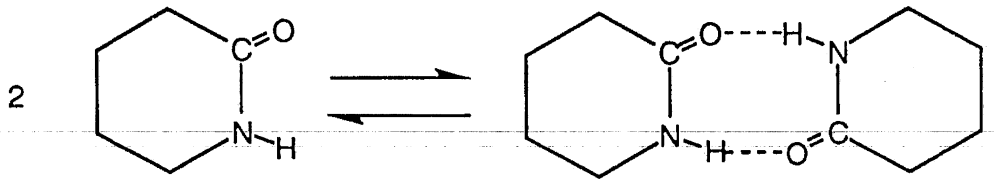

M D

(B)

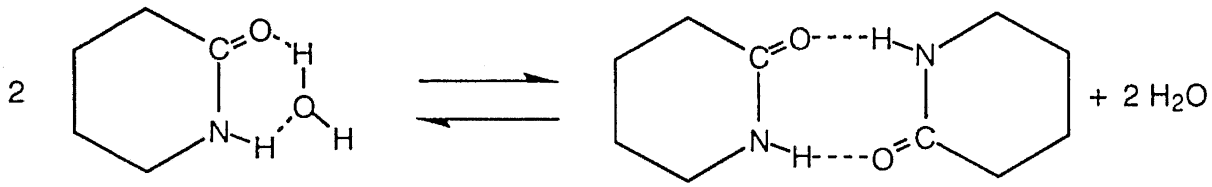

MW_1 D

(C)

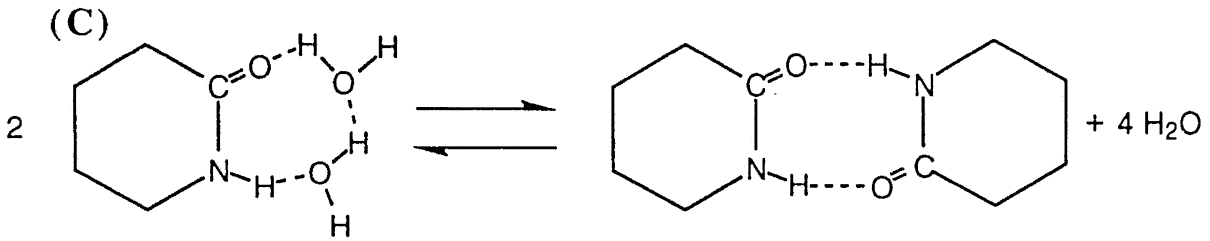

MW_2 D

Table 4.1 Binding Parameters for δ-Valerolactam Dimerization in Aqueous and Organic Solution

T (°C)	H_2O x	H_2O $K_{a,obs}$[b]	CCl_4 K_a (M^{-1})
6.7	2.45 ± 0.10	95.5 ± 30	340 ± 30
19.3	2.24 ± 0.10	45.9 ± 13	186 ± 15
29.9	2.23 ± 0.10	42.7 ± 9.8	
38.3	2.00 ± 0.10	18.3 ± 8.1	83.5 ± 5.5
45.6	1.80 ± 0.10	9.37 ± 3.2	
54.1	1.84 ± 0.10	9.78 ± 2.8	
61.4	1.77 ± 0.10	7.36 ± 2.5	37.0 ± 2.0

[a] Errors indicate 95% confidence limits. [b] Units of $K_{a,obs}$ vary.

Chapter 5

Contribution of a Phenolic Hydrogen Bond to Ribonuclease A Stability and Catalysis

Prepared as a Publication for *Protein Science.*

5.1 Introduction

The contribution of hydrogen bonds and hydrophobic forces to protein stability remains an unresolved question in biochemistry. The ability to generate mutant proteins with single amino acid substitutions has greatly enhanced our understanding of the molecular basis for protein stability. Recent studies on T4 lysozyme,[36,139,140] λ repressor,[37,141] and RNase T1[109,142] have attempted to determine the contributions of both hydrogen bonds and the hydrophobic forces in conferring protein stability. Evolution has refined the architecture of proteins such that the orientation of catalytic residues is modulated by noncovalent interactions distant from the active site. Still, a full understanding of these noncovalent interactions remains a significant challenge for protein engineers and in the *de novo* design of proteins. This study explores the noncovalent architecture of RNase A by examining the contribution of a hydrogen bond donated by the sidechain of Tyr97 to the stability of RNase A and explores the role of Tyr97 in properly positioning Lys41 within the active site of RNase A.

The structure of RNase A complexed with uridine 2',3'-cyclic vanadate (U>v) has provided invaluable insight into the catalytic mechanism of RNase A (Figure 5.1).[143] U>v is thought to be a putative transition state analog, since RNase A catalyzed reactions are thought to proceed through a transition state that contain significant pentavalent character. In the active site, the sidechains of His12 and His119 are proximal to the vanadyl group of U>v, and the N_ε of the Lys41 sidechain is 2.76 and 3.65 Å from the $O_{2'}$ and O_{1v} oxygens, respectively, of U>v. Also shown in Figure 5.1 are 2 other amino acid residues that interact intimately with the vanadyl group. The sidechain nitrogen of Gln11 forms a hydrogen bond with the nonbridging oxygen, O_{1v} ($N_{\delta 2} - O_{1v}$ distance = 2.56 Å), and the mainchain nitrogen of Phe120 forms a hydrogen bond with the nonbridging oxygen, O_{3v} ($N - O_{3v}$ distance = 2.88 Å).

Despite extensive study, the precise role of each active-site residue in catalysis by RNase A is uncertain. RNase A catalyzes the cleavage of the P–$O_{5'}$ bond of RNA specifically after pyrimidine residues. Figure 5.2 depicts a mechanism of catalysis that is consistent with all known data. In this mechanism, His12 acts as a general base that abstracts a proton from the 2'-hydroxyl of a substrate molecule thereby facilitating attack on the phosphorus atom.[144] This attack proceeds in-line to displace the nucleoside.[145] His119 acts as a general acid that protonates the 5'-oxygen to facilitate its displacement with both products being released to solvent.[146] The slow hydrolysis of the 2',3'-cyclic phosphate occurs separately and resembles the reverse of transphosphorylation.[146,147]

The picture for the role of Lys41 in the cleavage of RNA has been developed over the last thirty years.[148] In the mechanism in Figure 5.2, the reaction apparently passes through a transition state that has a pentavalent phosphorus atom. Lys41 is believed to assist catalysis by stabilizing this transition state through donation of a hydrogen bond or Coulombic interactions.[149] The sidechain of Lys41 was originally identified as an important residue in catalysis through chemical modification studies with dinitrophenol.[150] Since then, studies have postulated that the sidechain of Lys41 selectively stabilizes the chemical transition state for RNA cleavage.[151-154] Molecular dynamics simulations support this role by suggesting that the sidechain of Lys41 interacts with the phosphoryl oxygen of the phosphate group in the transition state.[154] Only recently, however, has recombinant DNA technology been developed for RNase A that allows for the characterization of structure-function relationships of the protein by site-directed mutagensis.[7] Mutants of Lys41 have been shown to have a deleterious effect on the ability of RNase A to catalyze the cleavage of RNA.[149,155] In addition, studies of semisynthetic RNase A, where the K41C enzyme was prepared and specifically alkylated with various functional groups, suggest that the geometry and relative strength of the hydrogen bond donated by the sidechain of Lys41 is related to the catalytic efficiency of the enzyme.[155]

In wild-type RNase A, a covalent and nonconvalent network is employed to lower the conformational freedom of the polypeptide backbone, and that may help to position Lys41 properly within the active site. Figure 5.3 illustrates the protein architecture that is involved in the positioning Lys41. On the *N*-terminal side of Lys41, the sidechains of Cys40 and Cys95 participate in a disulfide bond that covalently fastens together the first and third strands of the anti-parallel β-sheet. Similarly, the phenolic sidechain of Tyr97 donates a hydrogen bond from the third β-strand to the mainchain oxygen of Lys41, which participates in the prolyl peptide bond of Pro42, in the first β-strand. This hydrogen bond ($C{=}O_{41}$-$O\eta_{97}$ distance=2.36 Å) is completely buried within the interior of the protein with the entire Tyr97 sidechain being inaccessible to solvent. Spectroscopic studies of RNase A indicate that Tyr97 is found not to ionize up to pH 11.0.[156] Further, phylogenetic analysis of pancreatic ribonucleases from over 40 different species indicate that Tyr97 is a conserved residue thereby implying an important role for this residue.[44] Here, the Phe, Ala, and Gly mutants of Tyr97 have been prepared by site-directed mutagensis in order to measure the contribution of a phenolic hydrogen bond to the thermostability and catalytic efficiency of RNase A.

5.2 Results

The thermal denaturation curves for the Tyr97 mutants and wild-type RNase A are illustrated in Figure 5.4. All three mutants were significantly less stable than wild-type RNase A. Removal of a hydroxyl group from the sidechain at position 97, as in the Y97F RNase A, lowered the T_m by 27.5 °C. The additional removal of the phenol sidechain, as in Y97A RNase A, further lowered the T_m by an additional 6 °C. Yet, a subtle increase in stability of 1.3 °C was observed for the Y97G mutant over the Y97A. Table 5.1 highlights the difference in stability, $\Delta(\Delta G)$, for the mutant proteins as compared to wild type. Of the mutants, Y97A showed the largest decrease in stability while Y97F exhibited the smallest change.

Table 5.2 illustrates the influence that Tyr97 has on the steady-state kinetic parameters, k_{cat}, K_m, and k_{cat}/K_m, for the cleavage of poly(C). Overall, the K_m values for all Tyr97 mutant proteins increased by less than 3.5-fold. Although all Tyr97 mutant proteins exhibited small effects on the K_m, a 10-fold increase in the K_m was observed when the sidechain of Lys41 is removed, as in K41A RNase A. In contrast, a significant change was observed for the Tyr97 mutants on the value of k_{cat}. The turnover for these mutant enzymes were two orders of magnitude slower than wild-type RNase A. Overall, a significant reduction was observed in the catalytic efficiency (k_{cat}/K_m) of the mutant enzyme as compared with that of wild-type RNase A. A 70-fold reduction in k_{cat}/K_m was observed for the Y97F enzyme; whereas, Y97A and Y97G were found to be nearly 200-fold lower in catalytic efficiency.

5.3 Discussion

Contribution of the hydroxyl group of Tyr97 to protein stability. Removal of the hydrogen bond between hydroxyl group of Tyr97 and the mainchain oxygen of Lys41 is extremely deleterious towards the thermal stability of RNase A. As shown in Table 5.1, the difference in stability, $\Delta(\Delta G)$, for Y97F from wild type RNase A was determined to be -9.7 kcal/mol. This change in stability is significantly larger than would be anticipated for the mutation of a residue from tyrosine to phenylalanine. Earlier studies of RNase T1[109] have examined the effect of a tyrosine (Tyr68) to phenylalanine mutation on protein stability. In RNase T1, the sidechain of Tyr68 is completely inaccessible to solvent where the hydroxyl group donates a hydrogen bond to the mainchain oxygen of Gly71. The T_m of this particular mutant of RNase T1 is found to be lowered by only 4 °C, or, with a $\Delta(\Delta G)$ of -1.35 kcal/mol. Consequently, the 9.7 kcal/mol difference in protein stability cannot be attributed to the removal of a hydrogen bond alone.

Without structural information about Y97F RNase A and Y68F RNase T1, a quantitative analysis that accurately accounts for the -8.35 kcal/mol difference for similar mutant types is extremely difficult. However, since the Tyr sidechains of both enzymes are completely solvent inaccessible, the origin for this difference may be the nature of the hydrogen bond acceptors. In wild-type RNase A, the Tyr97 hydroxyl group donates a hydrogen to oxygen of Lys41, or rather, the prolyl peptide bond of Pro42. Whereas, in wild-type RNase T1, Tyr68 donates a hydrogen bond to the oxygen of Gly71, which is part of a typical peptide bond with Ser72. The relative decrease in protein stability for both Y97F RNase A and Y68F RNase T1 that results from the unfavorable proximity of the benzyl sidechain of phenylalanine and the unsatisfied carbonyl of the peptide bond should be equivalent. Yet, the difference in prolyl peptide bond energetics for wild-type and Y97F RNase A may be significant. During the refolding of RNase A, the prolyl peptide bond of Pro42 has been identified as being responsible for a slow kinetic phase in protein folding.[51,157] Previous work on model peptides has indicated that the removal of a strong hydrogen bond donor can lower the barrier to prolyl peptide bond isomerization by 1.2 kcal/mol.[43] The energetics of peptide bonds that precede proline residues differ significantly from the energetics of typical peptide bonds, and the formation of a strong hydrogen bond to the oxygen of the prolyl peptide bond helps compensate to for this shift in peptide bond *cis/trans* energetics by raising the barrier to isomerization. Consequently, one role for the Tyr97 hydrogen bond may be to stabilize the energetically preferred *trans* isomer. Folding studies of P42A RNase A were shown to eliminate a slow kinetic phase in the folding of RNase A.[158] However, the role of Tyr97 in the affecting the folding pathways of RNase A remains unknown. Therefore, structural studies that determine the orientation of the Pro42 in the folded RNase A and refolding studies are necessary to assess accurately these roles for Tyr97.

Contribution of the benzyl sidechain to protein stability. Complete removal of the phenolic sidechain of Tyr97 further lowers the melting temperature of RNase A. As illustrated in Table 5.1, the difference in $\Delta(\Delta G)$ of -12.1 and -11.6 kcal/mol is calculated for Y97A and Y97G RNase A, respectively. With -9.7 kcal/mol being associated with the removal of the hydroxyl group, the difference in stability from Y97F for Y97A and Y97G RNase A is -2.7 and -1.9 kcal/mol respectively. These changes in stability can be attributed to the removal of hydrophobic surface area. Estimates of the hydrophobic contribution from octanol phase transfer studies (ΔG_{tr}) indicate that the contribution of a benzyl group towards protein stability can range from 1 – 3 kcal/mol.[109] Similarly, estimates of the hydrophobic effect for the elimination of a methylene group can range from 0.4 – 1.1 kcal/mol.[159] Surprisingly, Y97G RNase A was found to be 0.5 kcal/mol more stable than the Y97A enzyme. The response of protein structure to cavity-creating mutations has been well studied.[140,141] These studies indicate that the hydrophobic core is flexible and that core sidechains can reorganize in response to cavity-forming mutations to lead to the recovery of protein stability.[160] This type of organization may account for the unexpected stability of the Y97G RNase A.

Conformational advantages of the hydrogen bond donated by Tyr97. RNase A employs a covalent and nonconvalent network of interactions that appear to lower the conformational freedom of the polypeptide backbone and thereby position Lys41 properly within the active site. The hydrogen bond formed by Tyr97 tethers the first and third β-strands. Although such a hydrogen bond may lower the conformational entropy of this region, the neighboring disulfide bond between Cys40 and Cys95 should be the primary structural feature that reduces the conformational entropy of the region. Pro42, a conserved residue, eliminates a possible rotomer about the dihedral angle, ϕ, from the polypeptide backbone of RNase A. However, as described above, the energetic cost of eliminating a degree of freedom is offset by an increased preference for the *cis* isomer about the prolyl

peptide bond. Apparently, a significant role for the phenolic sidechain of Tyr97 is the formation of a hydrogen bond that raises the barrier to prolyl peptide bond isomerization.

The influence of the hydrogen bond donated by Tyr97 on the cleavage of RNA. The changes in the kinetic parameters listed in Table 5.2 are consistent with Tyr97 affecting the active-site residue Lys41. The observed change in K_m for the Tyr97 mutants are minimal. This result is not surprising since Lys41 is not believed to play a significant role in ground state binding of the substrate poly(C). Lys41 participates in the cleavage of RNA by stabilizing the chemical transition state and mutant enzymes that alter the position of Lys41 within the active site of RNase A should influence k_{cat}. The activity of all Tyr97 mutant enzymes are lowered by nearly two orders of magnitude implying that Lys41 is not in optimal position within the active site. Thus, the hydrogen bond donated by Tyr97 is important for optimal catalytic activity of RNase A.

5.4 Conclusion

The phenolic sidechain of Tyr97 contributes to RNase A stability through both the donation of a hydrogen bond and the hydrophobic effect. Removal of the hydrogen bond donated by Tyr97 manifests itself by a reduction in the catalytic activity of RNase A, and the lower activity mirrors the thermal stability of the mutant enzymes. This reduction in activity is likely to be consequence of increased conformational freedom of the polypeptide backbone around Lys41 and the culminates in the repositioning the Lys41 N_ε within the active site of RNaseA.

Figure 5.1 Structure of the complex of RNase A with uridine 2',3'-cyclic vanidate, a putative transition state analog. Shown are the catalytic residues of RNase A including His12, His 119, Lys41 and Gln11.

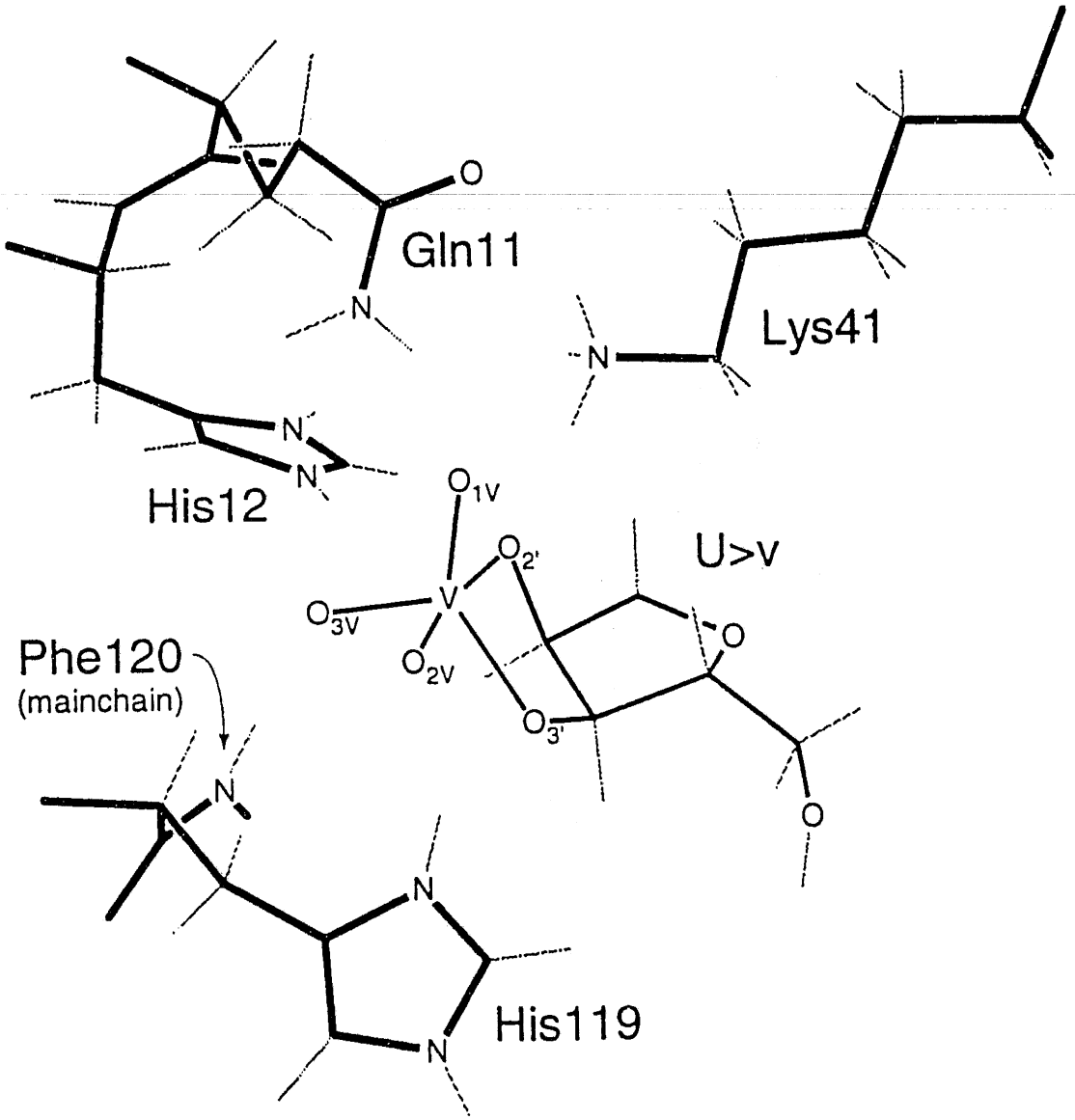
Gln11
Lys41
His12
U>v
Phe120
(mainchain)
His119

Figure 5.2 Mechanism of transphosphorylation and hydrolysis reactions catalyzed by RNase A. B: represents His12; $^{+}$A-H represents His119.[45]

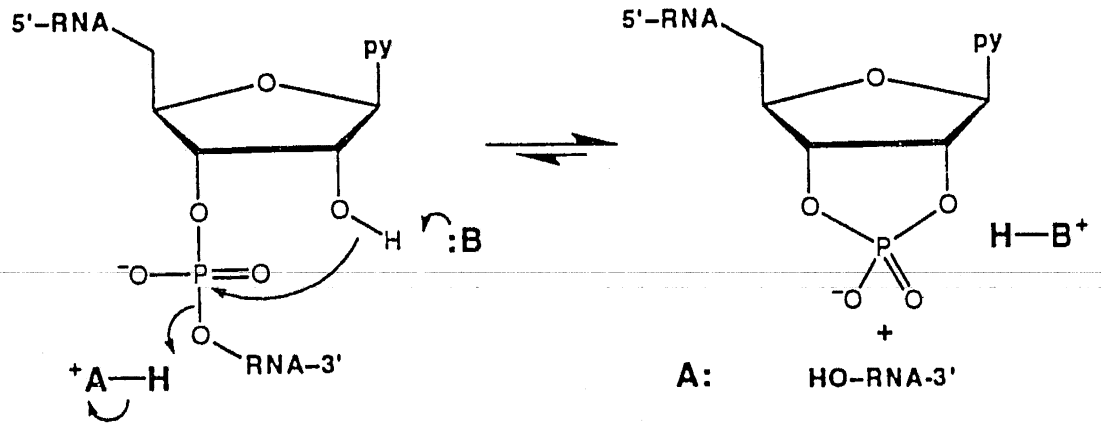

Transphosphorylation

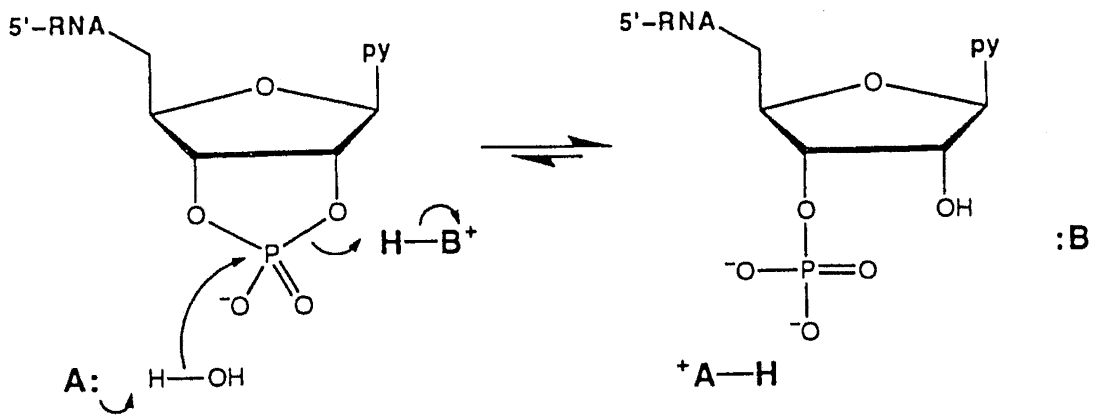

Hydrolysis

Figure 5.3 Hydrogen bond formed between the sidechain of Tyr97 and polypeptide backbone oxygen of Lys41. Shown are residues that lower the conformational degrees of freedom of the polypeptide backbone, including Tyr97 (yellow), Pro42 (yellow), Lys41 (red), and the disulfide bond formed between Cys95 and Cys40 (green).

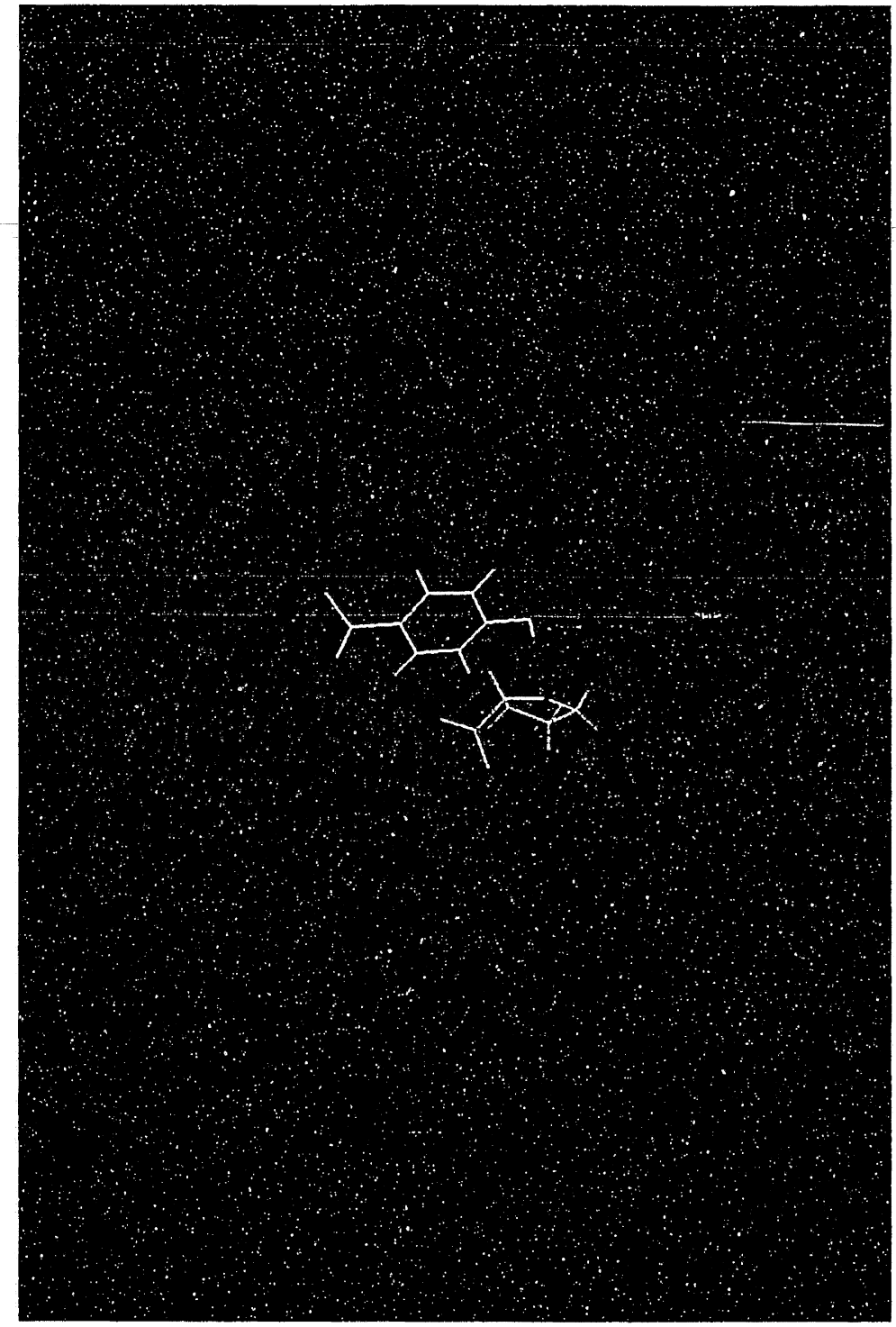

Figure 5.4 Thermal denaturation curve for wild-type, o, Y97F, ▼, Y97A, ▼, and Y97G, ●, RNase A. Shown is the fraction unfolded(f_u), percent unfolded/total protein, for wildtype and the mutant proteins vs. temperature (°C).

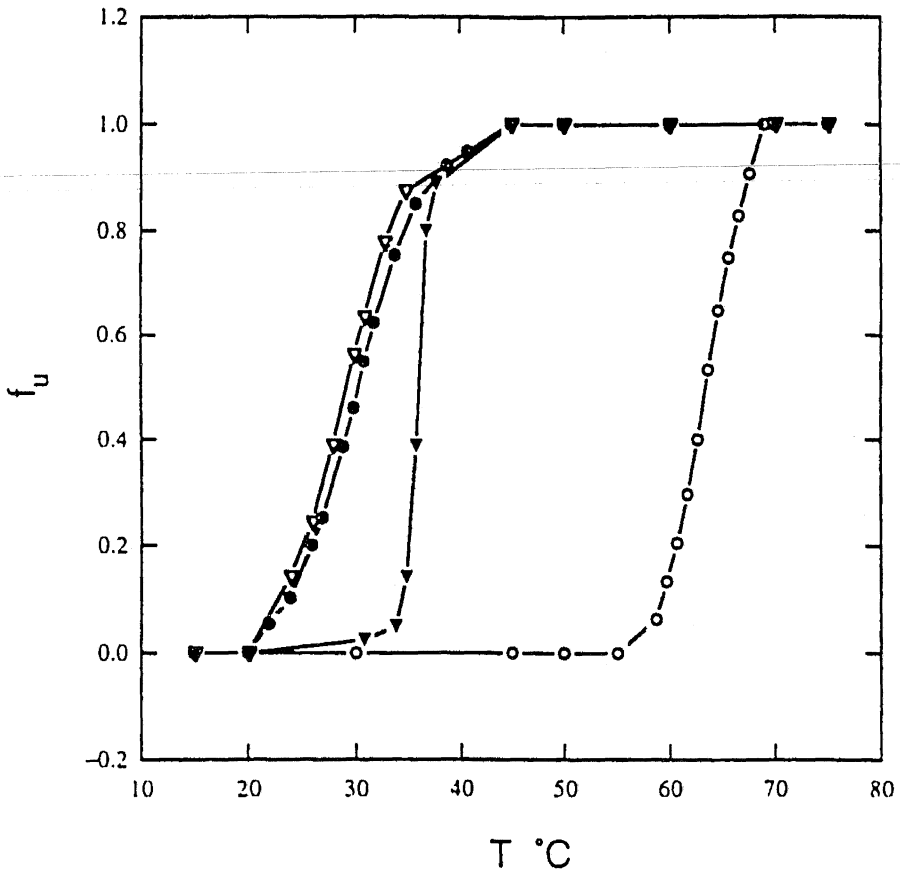
1.2
1.0
0.8
0.6
0.4
0.2
0.0
−0.2
f_u
10
20
30
40
50
60
70
80
T °C

Table 5.1 Differences in Mutant RNase A Stability

RNase A	T_m (°C)[a]	$\Delta(T_m)$ (°C)[b]	$\Delta(\Delta G)$[c,d] kcal/mol
WT	63.5	-	-
Y97F	36.0	27.5	9.7
Y97A	29.1	34.4	12.1
Y97G	30.4	33.2	11.6

[a] T_m was determined at the midpoint of the thermal denaturation curve.
[b] ΔT_m = wt(T_m) -mutant(T_m).
[c] 95 % confidence error was determined to be ± 0.4 kcal/mol for all mutant proteins studied.
[d] $\Delta(\Delta G) = [\Delta(T_m)] \times \Delta S_m$, where ΔS_m is the value of wild-type protein.[161]

Table 5.2 Steady-State Kinetic Parameters for the Cleavage of Poly(C) by Wild-Type, K41A, Y97F, Y97A, Y97G RNase A

RNase A	k_{cat} [s^{-1}]	K_m [mM][c]	k_{cat}/K_m[10^6 $s^{-1}M^{-1}$]
WT[a]	510 ± 10	0.034 ± 0.002	15 ± 1
K41A[b]	0.036 ± 0.0004	0.39 ± 0.04	0.000092 ± 0.000008
Y97F	5.02 ± 0.15	0.023 ± 0.002	0.22 ± 0.02
Y97A	9.23 ± 0.20	0.120 ± 0.009	0.077± 0.008
Y97G	8.53 ± 0.30	0.108 ± 0.013	0.079 ± 0.03

[a] see[45].
[b] see [149].
[c] Based on monomeric phosphate units of poly C.

Chapter 6

Inductive Effects on the Structure of Proline Residues

Previously published as:

Panasik, N. Jr., Eberhardt, E. S., Edison A. S., Powell, D. R., Raines, R. T. Inductive Effects on the Structure of Proline Residues. *International Journal of Peptide and Protein Research. 1994, 44,* 262-269.

6.1 Introduction

Collagen is the most abundant protein in vertebrates.[162-164] Each polypeptide chain of collagen is composed of approximately three hundred repeats of the sequence: X–Y–Gly, where X is often a proline (Pro) residue and Y is often a 4(*S*)-hydroxyproline (Hyp) residue. In connective tissue, collagen chains form triple-helical arrays in which all of the peptide bonds are in the *trans (Z)* conformation. These arrays are then organized into fibrils of great tensile strength.[165]

The role of the hydroxyl group of Hyp residues in collagen structure and function is uncertain. The hydroxylation of proline residues occurs after collagen biosynthesis, but before the chains begin to form a triple helix. The effect of prolyl hydroxylation on the rate of triple helix formation is not known. Hydroxylation is known, however, to increase the thermal stability of triple-helical collagen,[166,167]but the molecular basis for this increased stability is not clear. Models based on the structure[168] of triple-helical collagen and conformational energy calculations suggest that no hydrogen bonds can be formed between the hydroxyl group of Hyp residues and any backbone groups of the same triple helix.[169] Several other models have been proposed, however, in which a water molecule forms a bridge between the hydroxyl group and a mainchain carbonyl group.[164]

The electronegative oxygen atom of a hydroxyl group is effective at withdrawing electron density by through-bond and through-space interactions. This inductive effect is apparent in the acid dissociation constants of appropriate derivatives. For example, the pK_a of the secondary ammonium group of Pro is 10.64, while that of Hyp is 9.66; and the pK_a of the carboxylic acid group of Pro is 1.95, while that of Hyp is 1.82.[170] These differences in acidity are consistent with the manifestation of an inductive effect that draws electron density toward the hydroxyl group of Hyp.

Any inductive effect from the hydroxyl group of Hyp residues should be apparent in the structure of these residues. To determine the effect of electron withdrawal on the

structures of proline residues, *N*-acetyl-proline methylester (**6.1**), *N*-acetyl-4(*S*)-hydroxyproline methylester (**6.2**), and *N*-acetyl-4(*S*)-fluoroproline methylester (**6.3**) were synthesized. The methylester was used to minimize intramolecular hydrogen bonding, as has been observed in *N*-acetyl-proline[82] and *N*-acetyl-proline *N*'-methylamide.[83,84] Compound **6.3** was studied because the fluoro group is a small substituent that extends the range of inductive effects. Inductive effects that arise either through bonds or through space have been described by many empirical parameters.[171] For example, the acid dissociation constants of 4-substituted quinuclidines are related by the parameter σ_I, where $\sigma_I = \frac{pK_a^H - pK_a^X}{5.15}$.[172] Hydrogen, hydroxyl, and fluoro groups have σ_I values of 0.00, 0.27, and 0.51, respectively.

The structures of **6.1** – **6.3** were determined by x-ray diffraction analysis, and were also studied by *ab initio* molecular orbital calculations at the RHF/3-21G level of theory. The results of this work provide a high-resolution picture of the inductive effect on the structure of analogous proline residues.

6.2 Results and Discussion

Approximately ten percent of the residues in most forms of collagen are Hyp residues.[162-164] The presence of the hydroxyl group on the C$^\gamma$ atom of proline residues is known to increase the stability of collagen triple helices.[166,167] Here, we show that the inductive effect of the hydroxyl group affects the structure of the proline residue itself.

The crystalline structures of **6.1** – **6.3** were determined by x-ray diffraction analysis. The crystallographic parameters for **6.1** – **6.3** are given in Table 6.1. Atomic coordinates and equivalent isotropic displacement coefficients for **6.1** – **6.3** are given in Tables 6.2 – 6.4. The molecular packing in crystals of **6.1** – **6.3** is shown in Figure 6.1. Crystals of **6.1** contained one distinct molecule in each unit cell. In contrast, crystals of either **6.2** or **6.3** contained two distinct molecules (labeled A and B) in each unit cell. In crystals of **6.2**, the hydroxyl group

of molecule **6.2A** donated a hydrogen bond to the amide carbonyl group of molecule **6.2B**. The closest non-bonded distance from atom $H_1{}^{\delta 2}$(A) to O_2(B) was 1.680Å. In molecule **6.2B**, the $C_0 - N_1$ bond was (0.023±0.007)Å shorter and the $C_0 - O_0$ bond was (0.007±0.007)Å longer than were these bonds in molecule **6.2A**. In crystals of **6.3**, the corresponding bond lengths in molecules **6.3A** and **6.3B** did not differ significantly.

Perspective drawings of the crystalline structures of **6.1** – **6.3** are given in Figure 6.2. References to atoms follow the recommendations of the IUPAC-IUB Commission on Biochemical Nomenclature,[173] as indicated in Figure 6.2. The x-ray diffraction analyses indicated that **6.2** and **6.3** crystallized with a *trans (Z)* amide bond. In contrast, **6.1** crystallized with a *cis (E)* amide bond. This conformation was observed in crystals from two independent preparations (second data set not shown). The *trans* isomer of **6.1** is known to be about 4-fold more abundant than the *cis* isomer in a variety of solvents.[174] Although the *cis* isomer of **6.1** is disfavored, the difference in energy between the *cis* and *trans* isomers is small. The crystallization of **6.1** in the *cis* conformation is not unusual, as 10–30% of prolyl amide bonds are in the *cis* conformation in small peptides of known crystalline structure.[175]

The pyrrolidine rings in crystalline **6.1** – **6.3** were puckered in one of two distinct conformations, as shown in Figure 6.3. The pyrrolidine ring of crystalline **6.1** was puckered in the C$^{\gamma}$-endo conformation. (In the C$^{\gamma}$-endo conformation, the $C_1{}^{\gamma}$ atom lies above the plane of the peptide bond, in the orientation drawn in Figure 6.1.) This conformation is the one found most often in proline residues with *cis* peptide bonds.[176] The pyrrolidine rings of both molecules **A** and **B** of crystalline **6.2** and **6.3** were puckered in the C$^{\gamma}$-exo conformation. This conformation is the one found most often in proline residues with *trans* peptide bonds.[176] In **6.2** and **6.3**, the C$^{\gamma}$-exo conformation places the hydroxyl or fluoro group in an axial position, which is also the preferred orientation of these groups in the 2' position of ribose.[177]

An electron withdrawing substituent on the $C_1\gamma$ atom decreased the $C_1\delta 2 - C_1\gamma$, $C_1\gamma - C_1\beta$, and $C_1\beta - C_1\alpha$ bond lengths. The largest effect on bond length was a shortening of the $C_1\gamma - C_1\beta$ bond. Any substituent effect on bond length beyond $C_1\delta 2$ or C_1 was too small to be resolved by the x-ray diffraction analysis. A plot of the $C_1\delta 2 - C_1\gamma$, $C_1\gamma - C_1\beta$, and $C_1\beta - C_1\alpha$ bond lengths determined from the crystalline structures versus the same bond lengths obtained from *ab initio* calculations is shown in Figure 6.4. The proximity of the data to the dashed line in Figure 6.4 indicates that the observed and calculated bond lengths largely agree. The $C_1\delta 2 - C_1\gamma$, $C_1\gamma - C_1\beta$, and $C_1\beta - C_1\alpha$ bond lengths in **6.1** and **6.2** did not differ significantly from those of other proline residues and 4-hydroxyproline residues, respectively, in the Cambridge Crystallographic Data Bank. (The Data Bank does not contain the structure of any 4-fluoroproline residues.)

The presence of an electron withdrawing substituent increased the pyramidylization of the nitrogen atom in crystalline **6.2** and **6.3**. The pyramidylization of the nitrogen atom of an amide bond can be expressed by the parameter δ_1, which here refers to the angle that the N_1–C_0 bond makes with the plane defined by the N_1, $C_1\alpha$, and $C_1\delta$ atoms of the pyrrolidine ring.[178] If $\delta_1 = 0°$, then the atoms bound to N_1 are planar. If $|\delta_1| = 54.74°$ (that is, $|\delta_1| = \frac{1}{2}\cos^{-1}\left(-\frac{1}{3}\right)$), then the atoms bound to N_1 are tetrahedral. The value of δ_1 tends to be somewhat greater than 0° ($-5° < \delta_1 < 10°$) for prolyl peptide bonds in the *cis* conformation, and somewhat less than 0° ($-10° < \delta_1 < 5°$) for bonds in the *trans* conformation. In crystalline **6.1**, $\delta_1 = 1.05°$, indicating that C_0 atom lies only slightly above the plane of the N_1, $C_1\alpha$, and $C_1\delta$ atoms, in the orientation that is drawn in Figure 6.2. In contrast, the values of δ_1 in crystalline **6.2** and **6.3** are –9.24° (**6.2A**), –1.52° (**6.2B**), –16.31° (**6.3A**), and –3.54° (**6.3B**). The deviation from planarity of the amide bonds of **6.2A** and **6.3A** is significantly larger than that of most prolyl peptide bonds.[26] The trend in the pyramidylization at nitrogen (**6.3>6.2>6.1**) is consistent with the inductive effects[14] of the fluoro, hydroxyl, and hydrogen groups (**6.3>6.2>6.1**). These results can be interpreted as indicating an increase in the sp^3

character of the prolyl nitrogen atom with increasing electron withdrawal by a substituent in the 4-position of a proline residue.

The observed changes in nitrogen pyramidylization suggest that the inductive effects of substituents in the 4-position of proline residues can alter the distribution of electrons in a prolyl peptide bond. This alteration is likely to affect the kinetics of the *cis–trans* isomerization of peptide bonds that include the nitrogen atom of 4-substituted proline residues. The inductive effect on the energetics of prolyl peptide bond isomerization is now being determined with the analytical methods that we have described previously.[43,98]

Figure 6.1 Packing of crystalline **6.1**, **6.2**, and **6.3**.

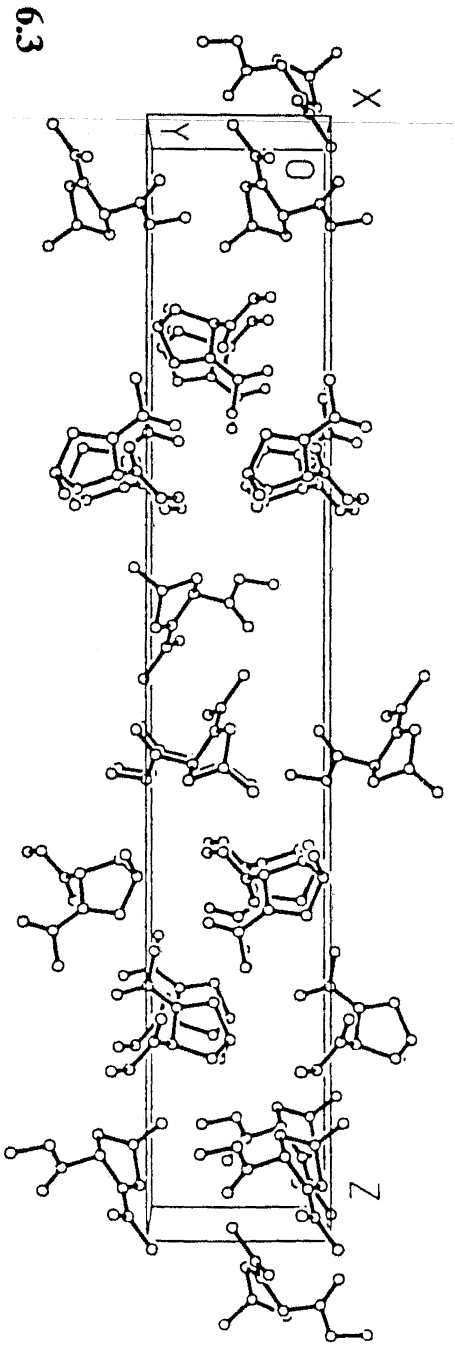
6.3
X
Y
O
Z

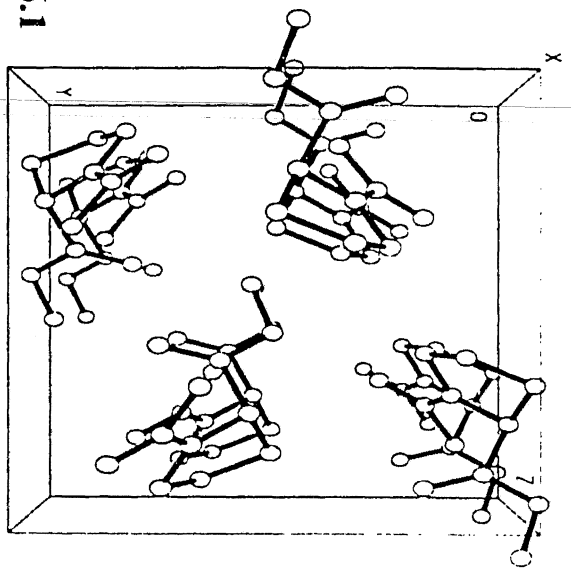
6.1
X
Y
O
Z

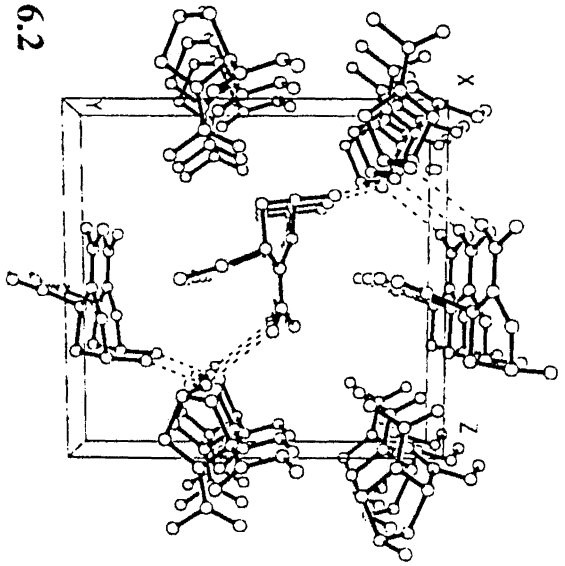
6.2
X
Y
O
Z

Figure 6.2 Labeling of nonhydrogen atoms in **6.1** (X = H), **6.2** (X = OH), and **6.3** (X = F); and view showing amide bond conformation in crystalline **6.1**, **6.2** (molecules A and B), and **6.3** (molecules A and B).

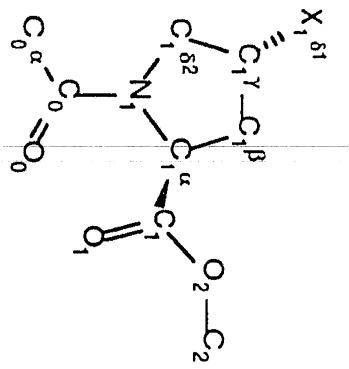

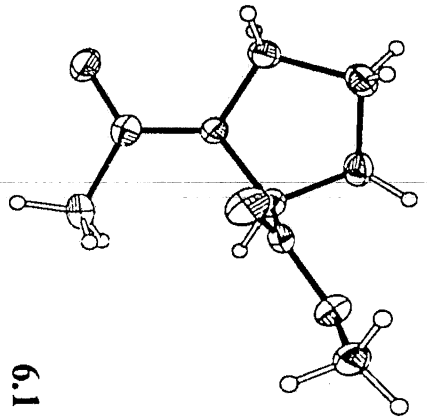

6.1

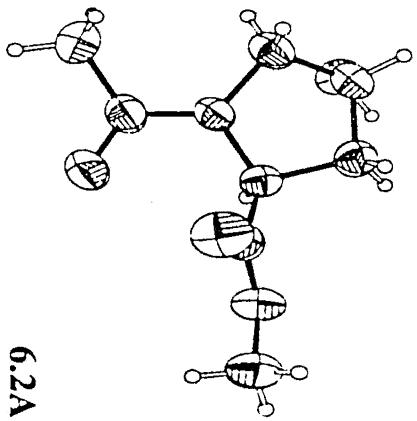

6.2A

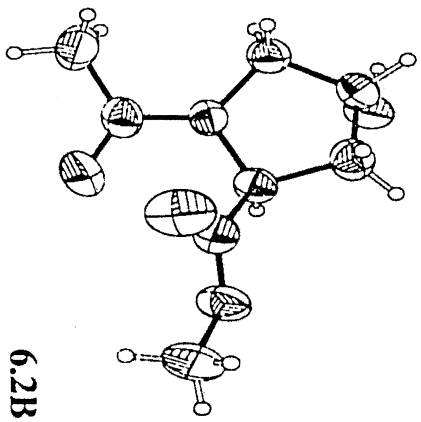

6.2B

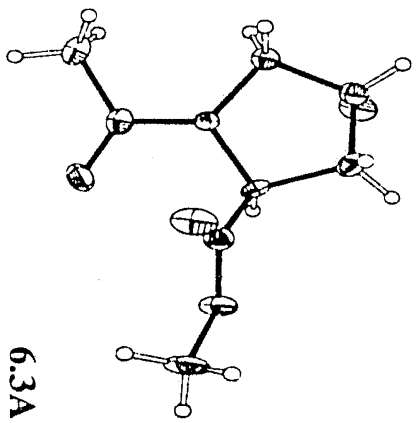

6.3A

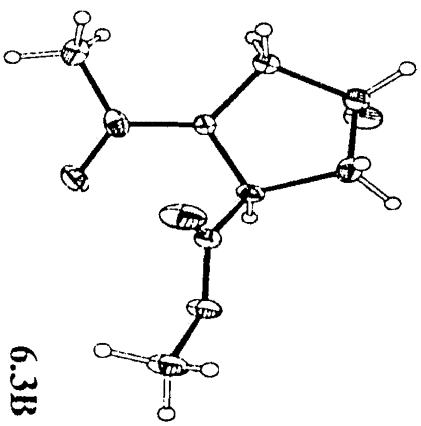

6.3B

Figure 6.3 View showing pyrrolidine ring pucker in crystalline **6.1**, **6.2** (molecules A and B), and **6.3** (molecules A and B).

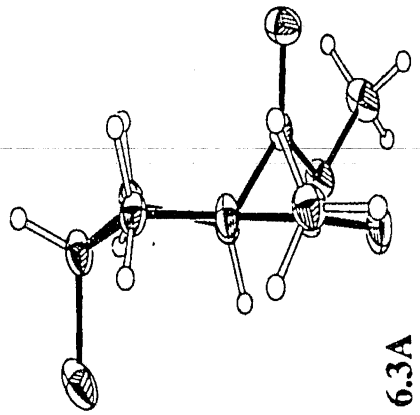

6.3A

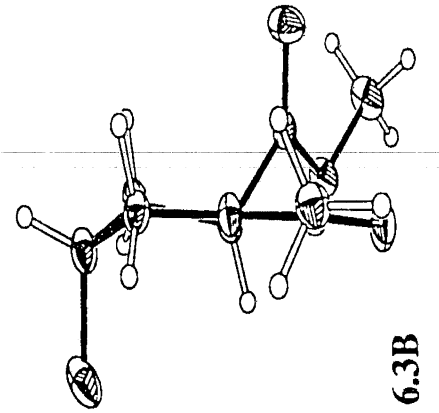

6.3B

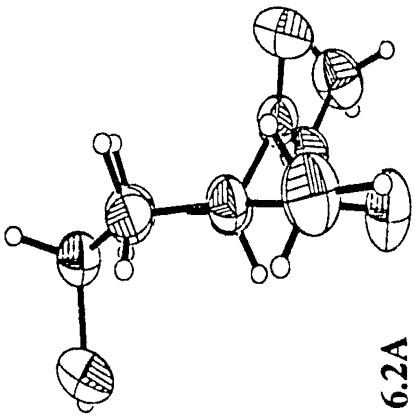

6.2A

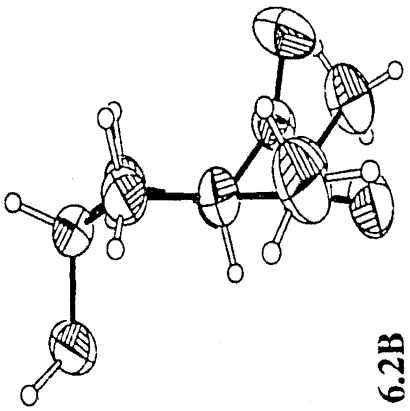

6.2B

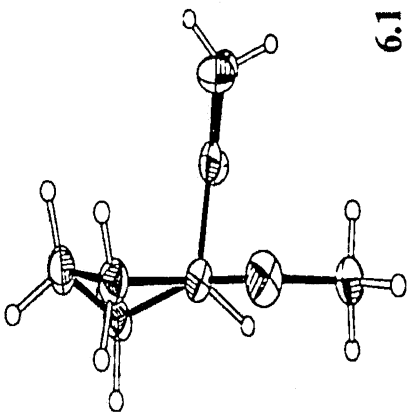

6.1

Figure 6.4 Difference in calculated and observed $C_1^{\delta 2} - C_1^{\gamma}$ (black), $C_1^{\gamma} - C_1^{\beta}$ (dark gray), and $C_1^{\beta} - C_1^{\alpha}$ (light gray) bond lengths between **6.1** and **6.2**A (□), **6.2**B (◇), **6.3**A (△), or **6.3**B (▽). Values on the ordinate were observed in crystalline structures; values on the abscissa were calculated *ab initio*. The dashed line (slope=1) is for reference.

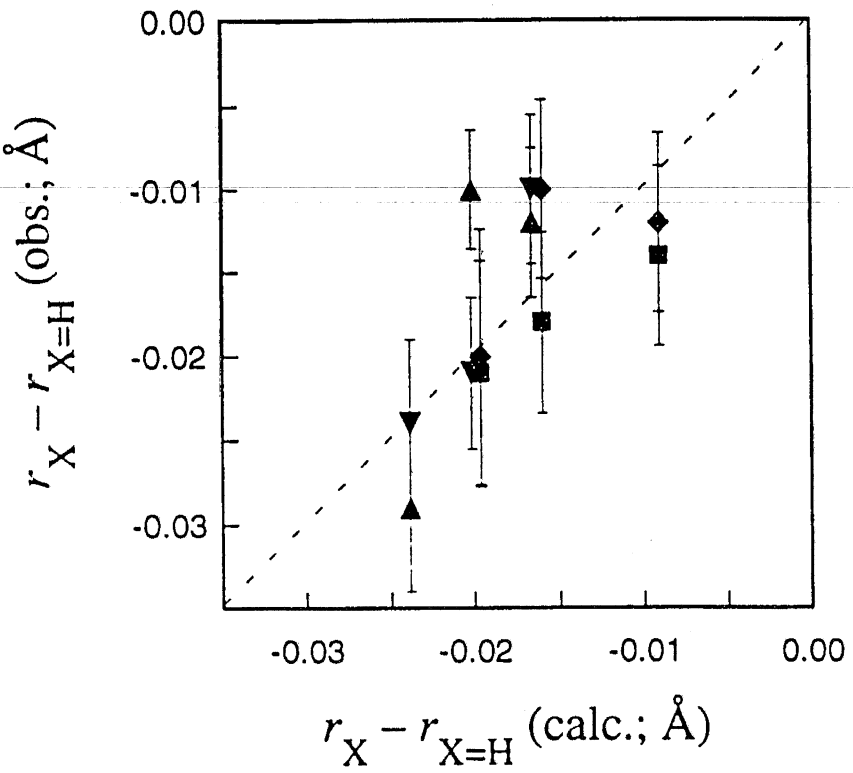
0.00
-0.01
-0.02
-0.03
-0.03
-0.02
-0.01
0.00
$r_X - r_{X=H}$ (obs.; Å)
$r_X - r_{X=H}$ (calc.; Å)

Table 6.1 Crystallographic Parameters for **6.1 – 6.3**

Parameter	**6.1**	**6.2**	**6.3**
Empirical Formula	$C_8H_{13}NO_3$	$C_8H_{13}NO_4$	$C_8H_{12}NO_3F$
Molecular Weight	171.2	187.2	189.2
Crystal System	orthorhombic	monoclinic	orthorhombic
Crystal Size (mm)	0.3 x 0.4 x 0.6	0.2 x 0.4 x 0.4	0.1 x 0.3 x 0.5
Space Group	$P2_12_12_1$	$P2_1$	$P2_12_12_1$
Z, molecule/unit cell	4	4	8
a, Å	7.328(3)	6.5077(9)	6.6060(9)
b, Å	10.052(3)	12.1992(16)	6.6603(7)
c, Å	11.643(3)	12.0478(14)	41.076(3)
β, °		98.881(10)	
V, $Å^3$	857.6(5)	945.0(2)	1807.2(2)
d(calc), g/cm^3	1.326	1.316	1.391
peaks to determine cell	25	25	26
reflections collected	2444	1463	2132
indep. reflections	1146	1334	1901
R(int)	3.06%	2.69%	2.26%
observed reflections {$F > 4.0\sigma(F)$}	1135	1273	1800
R(F)(obs data), %	3.08	3.53	3.68
wR(F)(obs data), %	4.29	4.67	5.06
s	1.59	1.31	1.06
ΔP(max), $Å^{-3}$	0.23	0.17	0.25
ΔP(min), $Å^{-3}$	–0.29	–0.15	–0.36

Table 6.2 Atomic Coordinates (x 10^5) and Equivalent Isotropic Temperature Factors (Å^2 x 10^4) for Nonhydrogen Atoms of **6.1**

Atom	*X*	*Y*	*Z*	U_{eq}[a]
C_0^{α}	6048(24)	87507(17)	33780(16)	277(6)
C_0	-3483(22)	80827(16)	23945(15)	221(5)
O_0	3793(17)	71793(12)	18445(10)	291(4)
N_1	-20241(18)	85182(13)	21035(12)	202(4)
C_1^{δ}	-30267(22)	79450(18)	11331(15)	246(5)
C_1^{γ}	-48892(23)	86148(18)	11791(16)	282(6)
C_1^{β}	-45003(24)	99412(19)	17841(15)	272(6)
C_1^{α}	-30627(21)	95542(17)	26956(14)	221(5)
C_1	-39464(23)	90069(17)	37783(15)	216(5)
O_1	-39030(16)	78674(12)	40978(11)	308(4)
O_2	-48147(15)	99782(11)	43494(10)	251(4)
C_2	-57066(24)	95785(18)	54060(15)	261(5)

[a] $U_{eq} = (1/3)\sum_i \sum_j U_{ij} a_i a_j (\mathbf{a}_i \cdot \mathbf{a}_j)$

Table 6.3 Atomic Coordinates (x 10^5) and Equivalent Isotropic Temperature Factors ($Å^2$ x 10^4) for Nonhydrogen Atoms of **6.2**

Atom	*X*	*Y*	*Z*	U_{eq}[a]
C_0^{α}(A)	4227(8)	7116(5)	11707(3)	68(2)
C_0(A)	5135(6)	6330(5)	11076(3)	52(1)
O_0(A)	5753(5)	5366(5)	11527(2)	72(1)
N_1(A)	5283(5)	6412(4)	9984(3)	44(1)
$C_1^{\delta 2}$(A)	4307(6)	7302(4)	9277(3)	50(1)
C_1^{γ}(A)	4137(6)	6841(4)	8104(3)	49(1)
$O_1^{\delta 1}$(A)	2198(4)	6277(4)	7867(2)	55(1)
C_1^{β}(A)	5978(6)	6072(4)	8173(3)	50(1)
C_1^{α}(A)	6154(5)	5570(4)	9345(3)	41(1)
C_1(A)	8416(6)	5325(4)	9809(3)	45(1)
O_1(A)	9617(4)	5950(4)	10315(3)	65(1)
O_2(A)	8869(4)	4316(4)	9498(2)	55(1)
C_2(A)	11005(6)	3992(5)	9772(4)	67(2)
C_0^{α}(B)	1017(7)	8943(5)	3665(3)	72(2)
C_0(B)	-855(6)	9297(4)	4171(3)	51(1)
O_0(B)	-2512(5)	9534(4)	3578(2)	67(1)
N_1(B)	-695(4)	9340(4)	5284(2)	45(1)
$C_1^{\delta 2}$(B)	1110(6)	9008(4)	6125(3)	48(1)
C_1^{γ}(B)	181(6)	8932(4)	7197(3)	45(1)
$O_1^{\delta 1}$(B)	-834(4)	7914(4)	7299(2)	55(1)
C_1^{β}(B)	-1467(6)	9812(5)	7052(3)	54(1)
C_1^{α}(B)	-2440(5)	9715(4)	5811(3)	44(1)
C_1(B)	-3323(6)	10788(4)	5358(3)	41(1)
O_1(B)	-2329(4)	11538(4)	5071(3)	73(1)
O_2(B)	-5354(4)	10814(4)	5338(2)	59(1)
C_2(B)	-6402(7)	11836(5)	4997(4)	77(2)

[a] $U_{eq} = (1/3)\sum_i \sum_j U_{ij} a_i a_j (\mathbf{a}_i \cdot \mathbf{a}_j)$

Table 6.4 Atomic Coordinates (x 10^5) and Equivalent Isotropic Temperature Factors ($Å^2$ x 10^4) for Nonhydrogen Atom of **6.3**

Atom	*X*	*Y*	*Z*	U_{eq}[a]
C_0^{α}(A)	21664(47)	53590(46)	25263(6)	245(9)
C_0(A)	34356(44)	50186(42)	22283(6)	195(8)
O_0(A)	41468(34)	33685(30)	21578(4)	265(7)
N_1(A)	37908(36)	66171(33)	20372(5)	163(6)
$C_1^{\delta 2}$(A)	29143(44)	86328(38)	20698(6)	186(8)
C_1^{γ}(A)	32553(46)	95483(43)	17370(6)	223(8)
$F_1^{\delta 1}$(A)	16273(27)	89927(26)	15329(4)	330(6)
C_1^{β}(A)	51542(48)	85550(48)	16137(6)	239(9)
C_1^{α}(A)	49625(45)	63882(45)	17358(6)	175(8)
C_1(A)	70106(45)	54599(42)	17968(6)	194(8)
O_1(A)	81310(31)	58832(32)	20199(5)	288(6)
O_2(A)	74827(30)	41629(31)	15607(4)	244(6)
C_2(A)	94687(48)	32699(56)	15884(7)	319(10)
C_0^{α}(B)	67097(47)	53240(42)	-200(6)	225(8)
C_0(B)	71000(42)	40544(43)	2759(6)	205(8)
O_0(B)	87641(29)	33281(33)	3407(4)	265(6)
N_1(B)	55071(34)	37171(36)	4756(5)	172(7)
$C_1^{\delta 2}$(B)	34682(39)	45675(43)	4479(6)	180(8)
C_1^{γ}(B)	25886(44)	42092(43)	7801(6)	213(8)
$F_1^{\delta 1}$(B)	31966(28)	57760(27)	9889(4)	314(5)
C_1^{β}(B)	36080(48)	23063(44)	8950(6)	236(9)
C_1^{α}(B)	57822(43)	25006(43)	7672(6)	174(8)
C_1(B)	66760(40)	4643(41)	6876(6)	166(8)
O_1(B)	61622(32)	-5881(30)	4677(5)	279(6)
O_2(B)	80498(30)	-733(28)	9154(4)	213(6)
C_2(B)	88789(52)	-20582(45)	8734(7)	274(9)

[a] $U_{eq} = (1/3)\sum_i \sum_j U_{ij} a_i a_j (\mathbf{a}_i \cdot \mathbf{a}_j)$

Table 6.5 Length (Å) of Bonds between Nonhydrogen Atoms of **6.1 – 6.3**

Bond	**6.1**	**6.2A**	**6.2B**	**6.3A**	**6.3B**
$C_0^{\alpha} - C_0$	1.500(3)	1.495(7)	1.507(7)	1.501(4)	1.503(4)
$C_0 - O_0$	1.232(2)	1.225(5)	1.232(5)	1.230(3)	1.230(3)
$C_0 - N_1$	1.347(2)	1.352(5)	1.329(5)	1.343(3)	1.353(3)
$N_1 - C_1^{\delta 2}$	1.466(2)	1.463(6)	1.484(4)	1.468(3)	1.466(3)
$N_1 - C_1^{\alpha}$	1.463(2)	1.450(6)	1.458(5)	1.468(3)	1.457(3)
$C_1^{\delta 2} - C_1^{\gamma}$	1.523(2)	1.509(5)	1.511(5)	1.513(3)	1.502(4)
$C_1^{\gamma} - X_1^{\delta 1}$	—	1.427(5)	1.421(6)	1.413(3)	1.409(3)
$C_1^{\gamma} - C_1^{\beta}$	1.535(3)	1.514(6)	1.509(7)	1.506(4)	1.511(4)
$C_1^{\beta} - C_1^{\alpha}$	1.545(2)	1.527(5)	1.535(5)	1.533(4)	1.535(4)
$C_1^{\alpha} - C_1$	1.520(2)	1.521(5)	1.499(7)	1.509(4)	1.515(4)
$C_1 - O_1$	1.205(2)	1.190(6)	1.201(6)	1.211(3)	1.193(3)
$C_1 - O_2$	1.342(2)	1.334(7)	1.319(5)	1.336(3)	1.352(3)
$O_2 - C_2$	1.450(2)	1.433(5)	1.450(7)	1.445(4)	1.441(4)

Chapter 7

Inductive Effects and the Gauche Effect on the Energetics of Prolyl Peptide Bond Isomerization: Implications for Collagen Folding and Stability

Prepared as a publication for the *Journal of the American Chemical Society*.

7.1 Introduction

Collagen is the principal structural protein in vertebrates.[162,179] *In vivo*, structural collagen consists of three polypeptide chains that form an extended right-handed triple helix.[180] Each polypeptide chain contains approximately three hundred repeats of the sequence: Gly–Xaa–Yaa, in which Xaa and Yaa are often proline (Pro) and 4(*S*)-hydroxyproline (Hyp), respectively. The hydroxylation of proline residues is a post-translational modification catalyzed by the enzyme prolyl 4-hydroxylase. Defects in prolyl 4-hydroxylase activity have been associated with the aging process as well as a variety of diseases including arthritis and rheumatism.[181,182]

The biosynthesis of collagen has been studied extensively.[183,184] Collagen strands are synthesized as a prepropeptides in which the pre sequence targets the polypeptide to the golgi complex and is then removed by a protease. Three procollagen polypeptides then become covalently crosslinked through interstrand disulfide bonds within the pro region. Before cleavage of the propeptide region and secretion into the extracellular matrix, the polypeptide chains of collagen are subjected to variety of post-translational modifications before folding into the a triple helix.[182] Of these modifications, the hydroxylation of proline residues by prolyl hydroxylase is the most prevalent, as Hyp constitutes approximately 10% of all collagen residues.

Numerous *in vitro* studies with procollagen and model peptides have explored the role of Hyp in the folding and stability of collagen.[182] Procollagen collagen polypeptides that are deficient in Hyp can form triple helices, but these triple helices are unstable at room temperature.[167,185] Thermal denaturation studies have demonstrated that triple helix stability can be correlated to overall Hyp content[166] and Hyp position within the polypeptide. Further, studies on model peptides suggest that peptide conformation is significantly affected by the hydroxylation of proline resides.[186,187] Several models have proposed that Hyp mediates collagen stability by to orienting water molecules to form interstrand hydrogen bonds.[188,189]

These models have proposed that interstrand hydrogen bonds cannot be formed directly between the hydroxyl group of Hyp residues and any mainchain heteroatoms in the adjacent polypeptide chains of the triple helix.[190] Recently, a high-resolution X–ray diffraction analysis of collagen like peptides has revealed that water molecules can form bridges between hydroxyl groups of Hyp residues and mainchain carbonyl groups.[190] These bridges consist of 1, 2, or 3 water molecules.

Since 25% of the residues in a typical collagen molecule are Pro or Hyp, the properties of these residues are likely to contribute greatly to collagen stability. In most peptide bonds, the *trans* (*Z*) isomer is greatly favored over the *cis* (*E*) isomer. In contrast, the *trans* isomer of an X-Pro peptide bond is only slightly favored over the *cis* isomer. The traditional picture of amide resonance suggests that *cis-trans* prolyl peptide bond isomerization is regulated by the bond orders of the peptide bond (Figure 7.1). The interconversion between *cis* and *trans* isomers about X-Pro peptides bonds has been identified as the slow kinetic phase in protein folding pathways[1] including that of collagen.[191,192] For proper assembly of the collagen molecule, all prolyl peptide bonds must reside in the *trans* configuration. The addition of the enzyme peptidyl–prolyl *cis–trans* isomerase (PPIase), which catalyzes the *cis–trans* interconversion of the prolyl peptide bond, accelerates the proper assembly of collagen molecules.[193] However, how the hydroxylation of proline residues affects the rate of *cis-trans* proline isomerization and collagen folding is unclear. To date, no study has addressed the inductive effect on the kinetics and thermodynamics of amide bond isomerization.

The objective of this study is to determine the energetic consequences for the prolyl peptide bond of having electron withdrawing groups on the pyrrolidine ring. Accordingly, we synthesized the hydroxylated and fluoronated derivatives of proline and we determined the effect of electron withdrawal on (i) the first pK_a of the prolyl nitrogen, (ii) the amide I

vibrational mode, and (iii) the kinetics and thermodynamics of prolyl peptide bond isomerization.

7.2 Results

Three proline derivatives were synthesized for this study: *N*-acetyl-[β,γ-^{13}C]*D*,*L*-proline methylester (**7.1**); *N*-acetyl-4(*S*)-hydroxy-*L*-proline [^{13}C]methylester (**7.2**); and *N*-acetyl-4(*S*)-fluoro-*L*-proline methylester (**7.3**) (Figure 7.2).[194] These derivatives of proline are the natural isomers found in collagen. Their synthesis as the methylester avoids intramolecular hydrogen bonding, as has been observed in *N*-acetyl-*L*-proline[82] and *N*-acetyl-*L*-proline *N*-methylamide.[83,84] Peptides **7.1** and **7.2** were enriched with ^{13}C to improve the precision of data from ^{13}C NMR spectroscopy.[43,98] Peptide **7.3** was synthesized because the nucleus of ^{19}F has spin $^{1}/_{2}$, the fluorine is small in size, and it is more electronegative than is the oxygen of the hydroxyl group. Hence, any consequences of electron-withdrawal by a hydroxyl group should be further enhanced by the presence of a fluorine atom.

Previously, we used X-ray diffraction analysis to determine the structure of unlabeled derivatives of **7.1**, **7.2** and **7.3** (Table 7.1).[195] These structures suggested that the presence of electron-withdrawing substituents has significant structural consequences on the pyrrolidine ring. First, the Cγ carbon of the pyrrolidine ring changes from an endo pucker in **7.1** to an exo pucker in compounds **7.2** and **7.3**. Second, the nitrogen become increasingly pyramidylized as the electron-withdrawing ability of the substituent was stronger. This increase in pyramidylization suggests an increase in the sp^3 character of the prolyl nitrogen. Finally, while no significant difference was detected in prolyl peptide bond length, the bonds adjacent to the electron-withdrawing substituent were shortened significantly. These structural changes imply that there may be significant energetic consequences for the prolyl peptide bond when the pyrrolidine ring of proline is hydroxylated during collagen biosynthesis.

Inductive Effects on pK_a. Values of pK_a can signify an inductive effect. Such effects on the nitrogen of a proline ring are evident in the previously determined pK_a's of L-proline (10.64) and 4(*S*)-hydroxy-L-proline (9.66) (Figure 7.3). The low pK_a of Hyp suggests that the hydroxyl group on the pyrrolidine ring is withdrawing electron density from the secondary amino group. Here, the pK_a's of L-proline, 4(*S*)-hydroxy-L-proline and 4(*S*)-fluoro-L-proline were determined to be 10.60, 9.65, and 9.20, respectively. This trend is similar to that observed for the primary amines ethylamine (10.63), ethanolamine (9.50), and 2-fluoroethylamine (8.79),[Hall, 1957 #48] and is consistent with the manifestation of an inductive effect.

Inductive effect on the amide I vibrational mode. The frequency of vibrational modes can provide evidence of an inductive effect. The frequency of the amide I vibrational mode, which is principally composed of the carbonyl stretch, is related to carbonyl bond length.[94] In D_2O, the amide I vibrational mode was maximal at 1608.10 cm^{-1}, 1613.08 cm^{-1}, and 1616.02 cm^{-1} for **7.1**, **7.2**, and **7.3**, respectively (Figure 7.4a). In dioxane, the amide I vibrational mode was maximal at 1658.99 cm^{-1}, 1660.92 cm^{-1}, and 1664.78 cm^{-1} for **7.1**, **7.2**, and **7.3**, respectively (Figure 7.4b). In both solvents, the relative frequency of **7.1**, **7.2**, and **7.3** indicates that the double-bond character of the amide group increases in the order: **7.1** > **7.2** > **7.3**. The solvent effect of approximately 50 cm^{-1} for the 3 proline derivatives is consistent with those observed previously.[196] Again, these results are consistent with the manifestation of an inductive effect. This apparent inductive effect on the amide I vibrational mode is consistent with that observed in the carbonyl stretching frequency in 4-substituted camphors.[197]

Inductive Effect on k_{EZ} and k_{ZE}. To assess the inductive effects on the rate of *cis–trans* proline isomerization, the rates of isomerization where measured for **7.1**, **7.2** and **7.3**. The *cis* to *trans* ($k_{E/Z}$) proline isomerization rate of **7.1** and **7.3** in water are illustrated as Arrhenius plots by the top two sets of data in Figure 7.5a. The *cis* to *trans* isomerization rate

was observed to be 30% faster for **7.3** than **7.1**, in dioxane, when the Arrhenius plots are interpolated at 60 °C. If the $k_{E/Z}$ isomerization rate was extrapolated to 25 °C, an increase of 8% would be predicted for the fluoroproline derivative **7.3** over **7.1** (0.20 sec^{-1} and 0.36 sec^{-1} for the $k_{E/Z}$ **7.1** and **7.3**, respectively). The slower *trans* to *cis* isomerization rates ($k_{Z/E}$), the lower two data sets in the Arrhenius plot Figure 7.5a, indicate that the $k_{Z/E}$ of **7.1** is 17% faster than **7.3**. Figure 7.5a also illustrates that the linear regressions for **7.1** and **7.3** are not parallel, which indicates that the equilibrium constants ($K_{E/Z}$) are temperature dependent. In general, the effect of electron withdrawing substituents on the kinetics of proline isomerization is consistent with electron density being pulled towards the nitrogen of the prolyl peptide bond, thereby allowing for free rotation about the prolyl peptide bond.

A kinetic analysis of the hydroxyproline derivative **7.2** in dioxane was complicated by aggregation. A 15% increase was observed in both $k_{E/Z}$ and $k_{Z/E}$ isomerization rates when the sample concentration was lowered from 100 mM to 1 mM for **7.2** (Data not shown). This concentration dependence is consistent with the aggregation observed in the FTIR experiments. However, due to a substantial increases in signal to noise, the errors for **7.2** increased from 10% at 100 mM concentration to 60% at 1 mM.

The solvent effect on proline *cis–trans* isomerization rates are significant.[43] The Arrhenius plots for compounds **7.1** and **7.2** are shown in Figure 7.5b. Because the $k_{E/Z}$ and $k_{Z/E}$ isomerization rates are lowered in aqueous solution due to hydrogen bond formation to the oxygen of the prolyl peptide bond, elevated temperatures were required to detect isomerization. Here, no detectable difference was observed in the ($k_{E/Z}$) isomerization, the upper two data sets, of proline derivatives **7.1** and **7.2**. However, the Arrhenius plots do reveal that the equilibrium constant is temperature dependent. Due to overlap of the ^{19}F resonances of the *cis* and *trans* isomers, the *cis–trans* isomerization rates of **7.3** were not determined in aqueous solution. For the slower rate of isomerization ($k_{Z/E}$) in aqueous

solution, the hydroxyproline derivative **7.2** was found to be slower than **7.1**. This relationship is similar to what was observed for **7.3** and **7.1** in dioxane.

The activation parameters derived from the inversion transfer experiments are presented in Table 7.2. These results indicate that the barrier to isomerization is enthalpic in origin and that the entropic contribution, while significant, is extremely small. In considering proline derivatives **7.1** and **7.3** in dioxane, the enthalpic contribution to the proline *cis–trans* isomerization barrier is reduced by 1.8 and 3.7 kcal/mol for $k_{E/Z}$ and $k_{Z/E}$ respectively. Since $\Delta H^{\ddagger}$ reflects the amount of bond breaking required for isomerization to occur, these parameters illustrate that the presence of an electron withdrawing substituent, fluorine, on the pyrrolidine ring reduces the amount of double bond character present within the prolyl peptide bond by pulling electron density towards the proline nitrogen. Furthermore, since the double bond character is reduced within the prolyl peptide bond, the barrier to isomerization is lower and, consequently, the rate is faster.

Inductive Effects on $K_{Z/E}$. Many factors can influence the *cis-trans* equilibrium constant ($K_{Z/E}$) about an X-Pro peptide bond. How the inductive effect, solvent effect, and temperature alter the $K_{Z/E}$ of these proline derivatives is illustrated in Table 7.3a and Table 7.3b. First, the *trans* isomer becomes increasingly preferred as the electron withdrawing ability of the substituent increases. Second, a solvent effect is observed for each proline derivative. The relative amount of *cis* isomer is greater in dioxane than in water by 5%, 6%, and 6% for **7.1**, **7.2** and **7.3**, respectively. Since the magnitude of the solvent effect is similar for each proline derivative, the solvent effect may be independent of the electron withdrawing ability of the substituent. Finally, all the proline derivative show a significant temperature dependency whereby the *cis* isomer becomes increasingly favored as the temperature increases.

The effect of temperature on $K_{Z/E}$ is illustrated by a van't Hoff analysis (assuming $\Delta C_p^{\circ} = 0$) in Figure 7.6a and Figure 7.6b. For the three proline derivatives, the enthalpic and

entropic forces that differentiate the *cis* and *trans* isomers appear to be related to the nature of the substituent. Proline derivatives **7.1**, **7.2** and **7.3** have very different thermodynamic signatures in dioxane (Table 7.5). While proline derivative **7.1** and **7.2** have different thermodynamic signatures from each other in aqueous solution, the thermodynamic signatures are strikingly similar to the respective thermodynamic parameters in dioxane. These results suggest that the presence of an electron withdrawing group on the pyrrolidine ring alters the equilibrium constant and this shift in equilibrium is independent of solvent.

7.3 Discussion

Gauche Effect and its Implications for Pyrrolidine Ring Conformation. A wealth of structural information on Pro and Hyp afforded the opportunity to provide a molecular interpretation of how the inductive effect influences the energetics of the prolyl peptide bond. One of the most prominent structural changes observed in our X-ray crystallographic studies of these proline derivatives was the different conformations observed in the pyrrolidine ring.[195] Surveys of the Brookhaven Protein Data Bank and the Cambridge Crystallographic Data Bank have identified a relationship between prolyl peptide bond conformation and pyrrolidine ring conformation of proline residues.[176,198] In proteins in which the proline residues were in the *trans* configuration, ring pucker is observed to correlate with the type of secondary structure in which the proline residue is participating: the C$^{\gamma}$-exo pucker is common for proline residues in α–helices, whereas proline residues in extended conformations prefer the C$^{\gamma}$–endo conformation. In peptides, proline residues having *cis* prolyl peptide bonds strongly prefer the C$^{\gamma}$–endo pucker. Whereas, the *trans* isomer exhibits only a slight preference for the C$^{\gamma}$–exo pucker. Although the C$^{\gamma}$-endo and C$^{\gamma}$–exo ring puckers are to some extent associated with *cis* or *trans* conformations of the prolyl peptide bond, these studies, and studies of polypeptides, clearly show that the pyrrolidine ring of Pro is very flexible and that either pucker is available.[82,199] Molecular modeling studies have

predicted a low energy of activation between the Cγ-exo pucker and the Cγ-endo pucker.[82] NMR solution studies of proline-containing peptides have indicated that the pyrrolidine ring explores a variety of puckering conformations with the Cγ-exo and the Cγ-endo puckers being the predominate puckers observed.[200]

In contrast, the Cγ-exo pyrrolidine ring pucker is the only conformation observed in X-ray crystallographic studies of Hyp and hydroxyproline containing peptides.[201] Studies of ^{1}H coupling constants of Hyp indicate that there is a strong conformational preference for the Cγ-exo pucker in solution.[200] However, the unnatural *cis*-Hyp isomer, 4-(*R*)-hydroxyproline, does not exhibit the same conformational rigidity in solution indicating that there is a stereoelectronic dependency to the ring pucker.[202,203] Similarly, conformational analysis from ^{1}H NMR coupling constants of F-pro indicate that the Cγ-exo ring pucker is preferred.[204,205]

How does the presence of a hydroxyl or fluoro group on the pyrrolidine ring confer stability to the Cγ-endo ring pucker? For substituted furanose rings like those in DNA and RNA, ring puckering is governed by the gauche effect.[206,207] The gauche effect, which describes the tendency of vicinal heteroatoms to adopt a gauche rather anti conformation about a single bond, is mediated by a favorable overlap between a σ C-H bonding orbital and σ* C-X anti-bonding orbital. The gauche effect is enhanced by the presence of stronger electron-withdrawing groups, and manifests itself by shortening bond lengths and distorting expected bond geometries. For the five-membered pyrrolidine ring, strain dictates that the atoms are in the partially eclipsed conformation. While ring stain does not allow for the optimal overlap for the Cδ–H σ bonding orbital and the Cγ–X σ* anti-bonding orbital, enough overlap of these orbitals occurs such that changes in the Cδ–Cγ bond length are observed (Table 7.4).[31,32] As the strength of the electron withdrawing substituent increases from **7.1>7.2>7.3**, the Cδ–Cγ bond length shortens in a similar fashion, **7.1>7.2>7.3**. For the pyrrolidine ring, the gauche effect manifests itself in two ways. First, an entropic component

would be anticipated through the stabilization of the C^{γ}-exo pyrrolidine ring pucker. Second, by shortening the C^{δ}–C^{γ} bond, steric hindrance between the C^{δ} of pyrrolidine ring and C^{α} of the adjacent residue would shift the equilibrium constant towards the *trans* isomer.

Inductive Effect on the Energetics of *cis–trans* Prolyl Peptide Bond Isomerization. The presence of electron withdrawing substituents on the pyrrolidine ring can influence the energetics of prolyl peptide bond isomerization by lowering the barrier to isomerization and altering the equilibrium constant. The qualitative free energy profiles presented in Figure 7.7a and Figure 7.7b illustrate how this inductive effect appears to manifest itself on the energetics of the prolyl peptide bond. In dioxane at 60 °C (Figure 7.7a), the isomerization barrier from *cis* to *trans* ($k_{E/Z}$) is 0.2 kcal/mol lower for **7.3** than **7.1**. The faster rate of isomerization indicates the prolyl peptide bond has more single bond character when fluorine is attached to the pyrrolidine ring as a consequence of electron density being localized on the nitrogen of the prolyl peptide bond. In contrast, due to the difference in the $K_{Z/E}$, the *trans* to *cis* isomerization rate was faster for **7.1** than **7.3**.

In water (Figure 7.7b), the barrier to isomerization for **7.1** is increased by 1.2 kcal/mole as a consequence of hydrogen bond formation to the oxygen of the prolyl peptide bond. This increase in the barrier to isomerization is consistent with the solvent effects observed previously.[43,58] The measured *cis* to *trans* ($k_{E/Z}$) barrier for prolyl peptide bond isomerization of **7.2** in water does not differ significantly from that of **7.1** (Figure 7.7b). In water, the *trans* to *cis* isomerization rate was found to be faster for **7.1** than **7.2**. This result is a consequence of the difference in equilibrium constants between **7.1** and **7.2** (a $K_{E/Z}$ of 3.9 and 4.9 for **7.1** and **7.2** , respectively).

While a significant difference in the *cis* to *trans* barrier for peptide bond isomerization is not observed for **7.1** and **7.2**, X-ray crystallographic, pK_a, and IR spectroscopic analyses reflect the same inductive effect observed for the fluoroproline derivative, **7.3**. These results indicate that the hydroxyproline derivative has more electron

density residing on the nitrogen of the prolyl peptide bond than does proline. Figure 7.7b reflects this data by illustrating the inductive effect of the hydroxyl group as a subtle lowering the barrier to prolyl peptide isomerization. Since the preponderance of data is consistent with this interpretation, these results suggest that the folding of the collagen triple helix should be accelerated by hydroxylation of the pyrrolidine ring. Further, these result predict that the incorporation of fluoroproline into collagen polypeptides, or proteins which have proline isomerization as the rate-limiting step in folding, should accelerate the rate of folding.

The inductive effect on the prolyl peptide bond equilibrium constant may have a significant impact on collagen stability. The equilibrium differences are temperature dependent, and, at the temperatures the *cis–trans* proline isomerization experiments were conducted, the equilibrium constants are nearly equivalent. This result suggests that thermal energy has overwhelmed the contribution of the gauche effect. At 27 °C, however, the equilibrium constants are observed to be 4.6, 5.8, and 6.2 in water for derivatives **7.1**, **7.2**, and **7.3**, respectively. Calculations of the gauche effect in furanose rings predicts 0.20 kcal/mol of stabilization when the proper orbital orientation occurs. Despite the pyrrolidine ring restricting an ideal orientation about the C^{δ}–C^{γ} bond, a $\Delta\Delta G^{\circ}$= 0.14 kcal/mol is observed at 27 °C between Pro and Hyp derivatives for the *trans* isomer. The origin for this difference is found in the shortening of the C^{δ}–C^{γ} bond which reduces steric hindrance between the C^{δ} of pyrrolidine ring and C^{α} of the adjacent residue by 0.1 Å. (Data not shown.) This structural manifestation of the gauche effect drives the equilibrium towards the *trans* isomer. For a large proline containing protein like collagen, the gauche effect has the potential to provide 14 kcal/mol [= (0.14 kcal/mol x proline residue) x 100 residues] of stability towards the desired *trans* isomer. Clearly, the packing restrictions of the collagen triple helix, which restrict Hyp to the Y position of the collagen motif, may limit the contribution of the gauche effect.[208] Thus, our studies do not exclude a role for solvent water in stabilizing the collagen

triple helix. Still these experiments suggest that presence of Hyp *alone* has the potential to contribute greatly to the stability of the collagen triple helix .

7.4 Conclusion

The combination of structural and energetic studies has provided insight into the origins of collagen assembly and stability. The placement of electron withdrawing substituents on the proline ring results in significant structural and energetic consequences. The inductive effect pyramidylizes the prolyl nitrogen, lowers the nitrogen pK_a, shifts the amide I vibrational mode downfield, and redistributes electron density about the prolyl peptide bond. Furthermore, the presence of a hydroxyl group has the ability to alter the prolyl peptide bond equilibrium constant.

Figure 7.1 Resonance structures of the prolyl peptide bond.

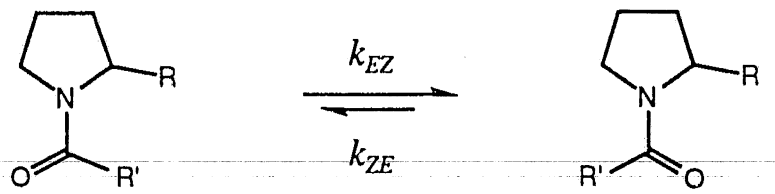

***cis* (*E*) isomer** ***trans* (*Z*) isomer**

Figure 7.2 Proline derivatives studied.

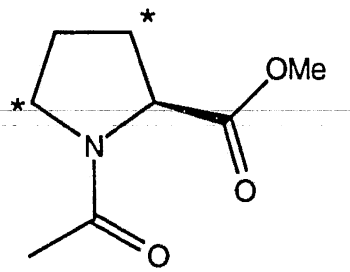

7.1

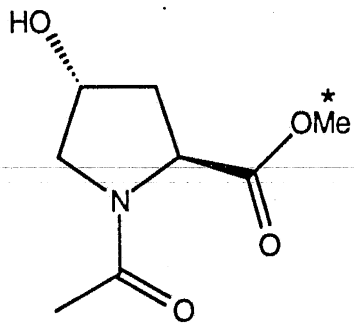

7.2

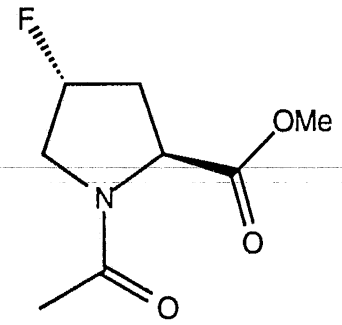

7.3

* Denotes ^{13}C enrichment

Figure 7.3 Determination secondary amino group p*K*a's of the amino acids proline, ▲; 4–(*S*)–hydroxyproline, o; and 4-(*S*)-fluoroproline, ◆. The p*K*a's were determined to be 10.60 ± 0.1, 9.65 ± 0.1, and 9.2 ± 0.1, respectively.

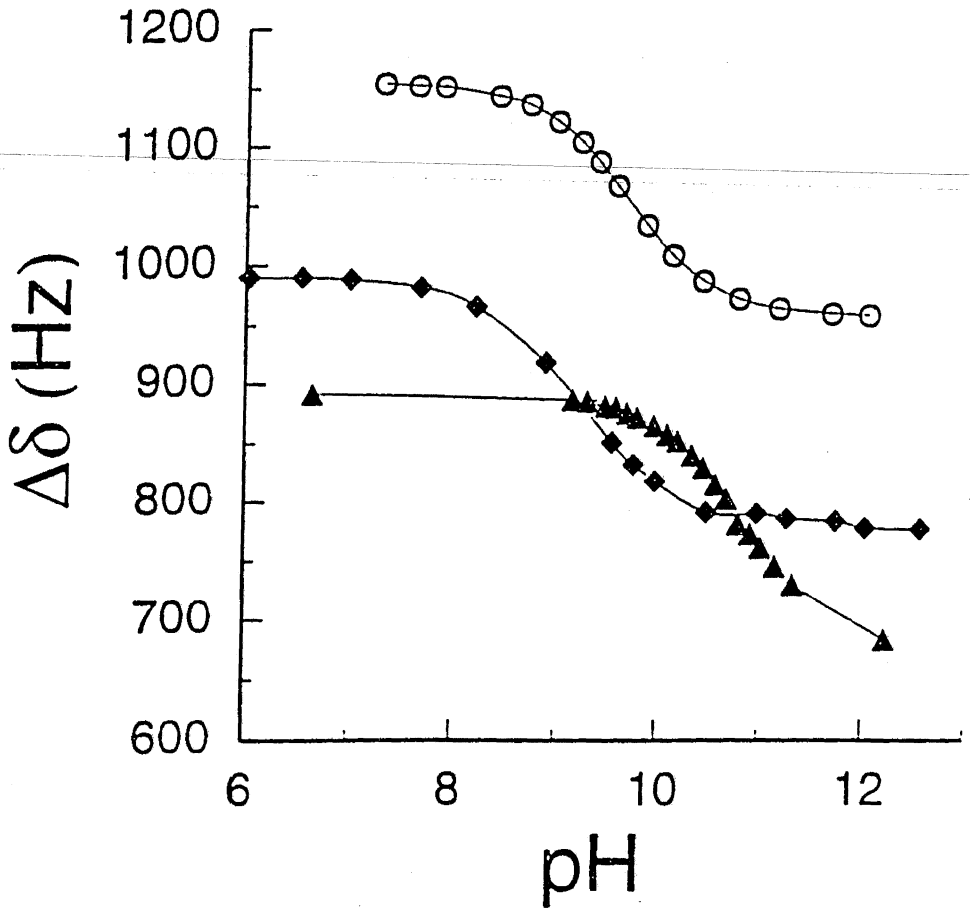
1200
1100
1000
900
800
700
600
Δδ (Hz)
6
8
10
12
pH

Figure 7.4a Amide I vibrational mode of **7.1**, **7.2**, and **7.3** in D_2O. The frequencies observed to be 1608.10 cm^{-1}, 1613.08 cm^{-1}, and 1616.02 cm^{-1} for **7.1**, **7.2**, and **7.3**, respectively.

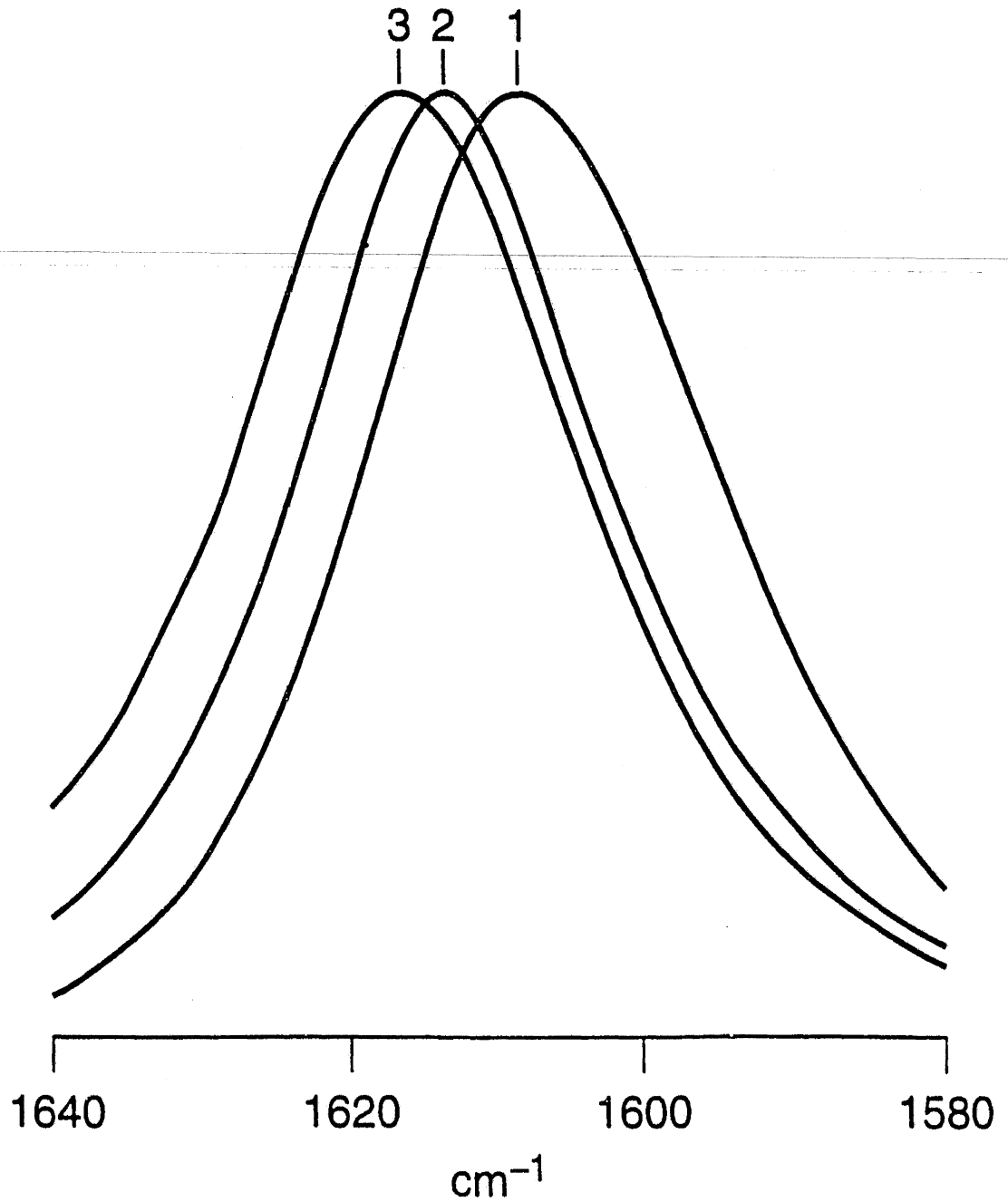
3
2
1
1640
1620
1600
1580
cm−1

Figure 7.4b Amide I vibrational mode of **7.1**, **7.2,** and **7.3** in dioxane. The frequencies observed to be 1658.99 cm^{-1}, 1660.92 cm^{-1}, and 1664.78 cm^{-1} for **7.1**, **7.2**, and **7.3**, respectively.

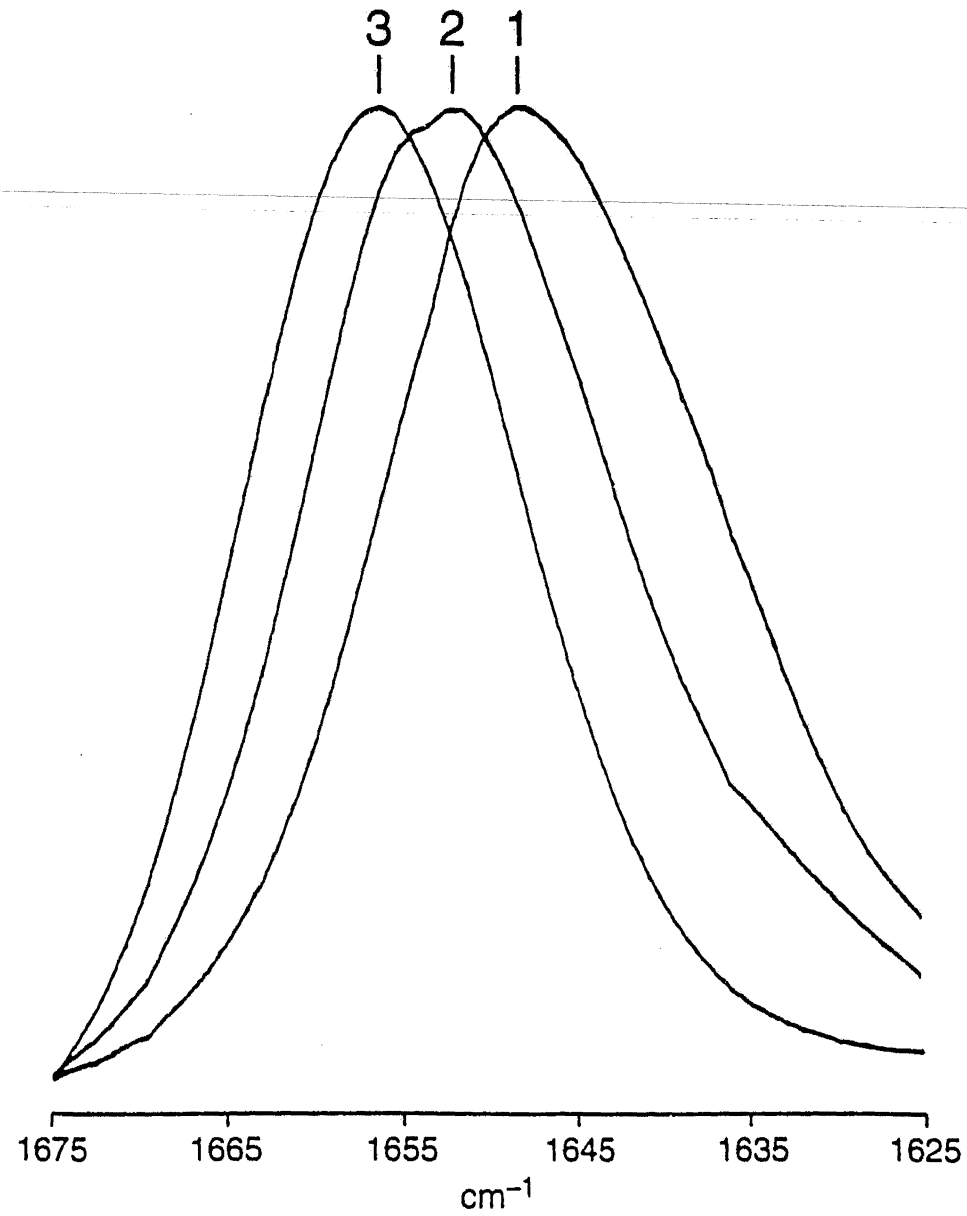
3
2
1
1675
1665
1655
1645
1635
1625
cm⁻¹

Figure 7.5a Arrhenius plots of $k_{E/Z}$ **7.1**, ▲; **7.2**, ○; and $k_{Z/E}$ **7.1**, ▼; and **7.2**, ●; in 100 mM sodium phosphate buffer, pH 7.2. Slopes were $k_{E/Z}$ = -13.14 ± 1.362, $k_{Z/E}$ = -12.07 ± 1.288 for **7.1**; $k_{E/Z}$= -14.31 ± 1.15, $k_{Z/E}$ = -11.50 ± 0.84 for **7.2.**

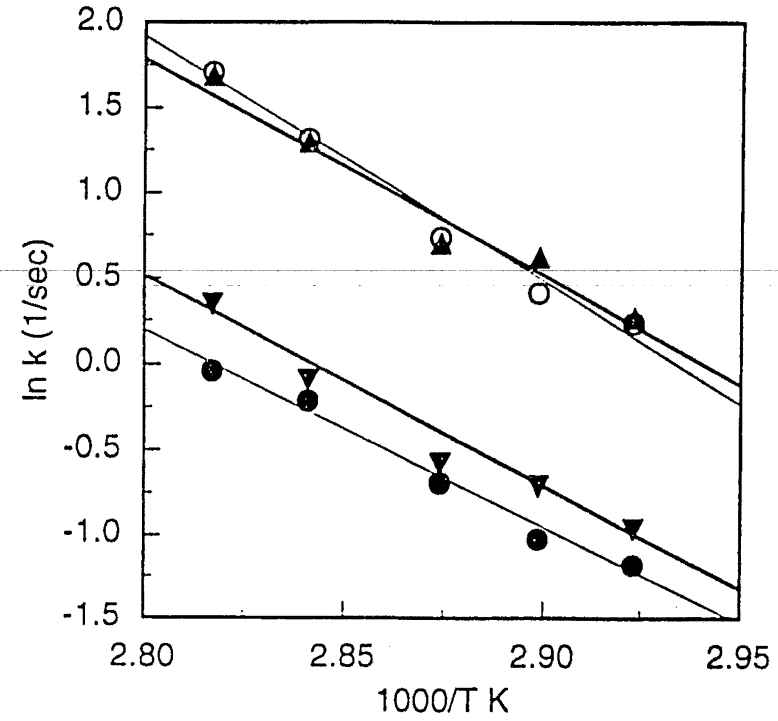
2.0
1.5
1.0
0.5
0.0
-0.5
-1.0
-1.5
ln k (1/sec)
2.80
2.85
2.90
2.95
1000/T K

Figure 7.5b Arrhenius plots of $k_{E/Z}$ **7.1**, ▲; **7.3**, ◆; and $k_{Z/E}$ **7.1**, ▼; **7.3**, ◆; in dioxane-d8. Slopes were $k_{E/Z}$ = -10.51 ± 1.044, $k_{Z/E}$ = -12.22 ± 0.315 for **7.1**; $k_{E/Z}$ = -11.002 ± 0.64, $k_{E/Z}$ = -9.613 ± 0.35, $k_{Z/E}$ = -10.63 ± 0.40 for **7.3**, respectively.

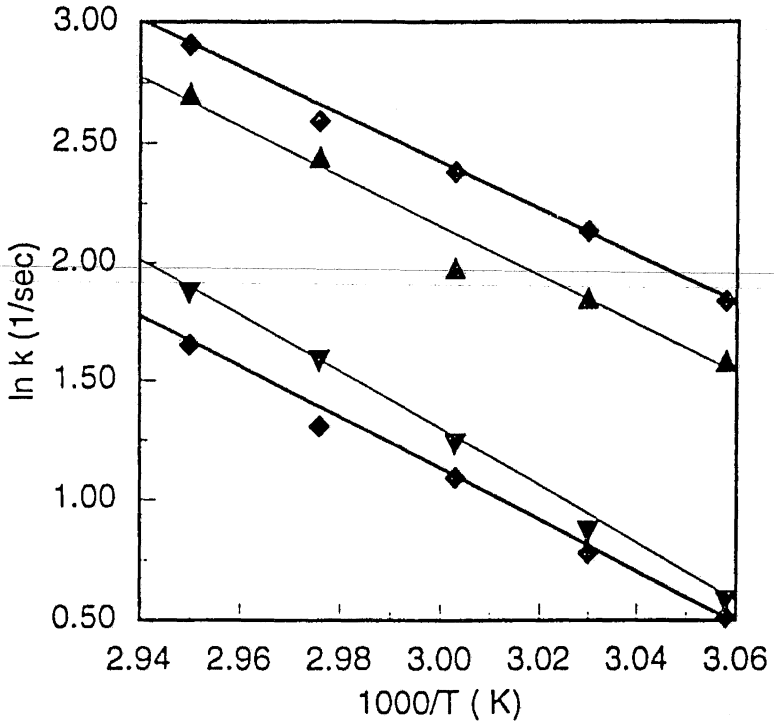
3.00
2.50
2.00
1.50
1.00
0.50
ln k (1/sec)
2.94
2.96
2.98
3.00
3.02
3.04
3.06
1000/T (K)

Figure 7.6a Van't Hoff analysis of **7.1**, ▲; **7.2**, ○ ; **7.3**, ◆; with 1 mm peptide in dioxane-d_8. Slopes were 521.5 ± 11.3 for **7.1**, 830 ± 11.7 for **7.2**, and 1150 ± 72.7 for **7.3**.

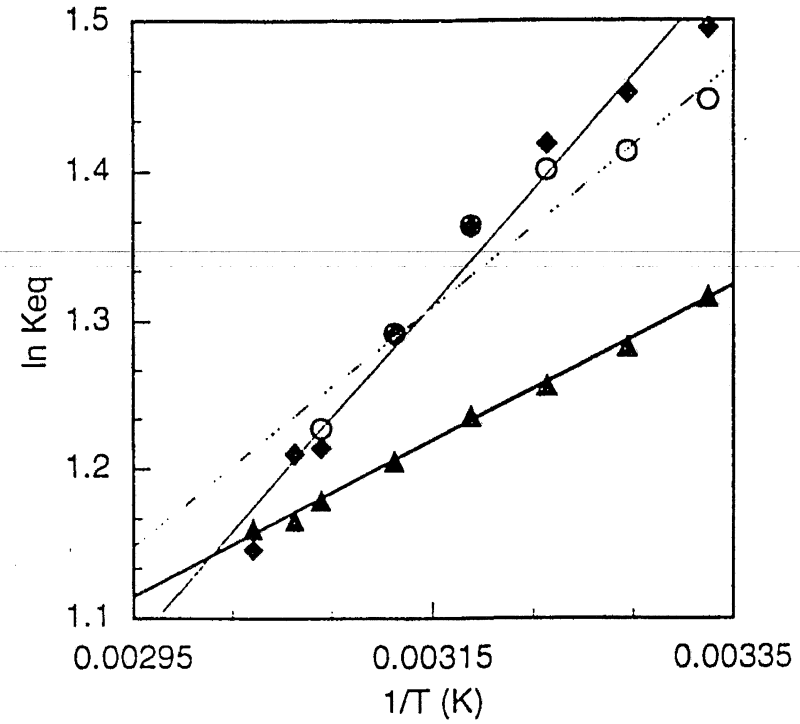
1.5
1.4
1.3
1.2
1.1
ln Keq
0.00295
0.00315
0.00335
1/T (K)

Figure 7.6b Van't Hoff analysis of **7.1,** ▲ and **7.2,** ○ ; in 100 mM sodium phosphate buffer pH 7.2. Slopes were 525.5 ± 17.1 for **7.1** and 941.0 ± 31.2 for **7.2.**

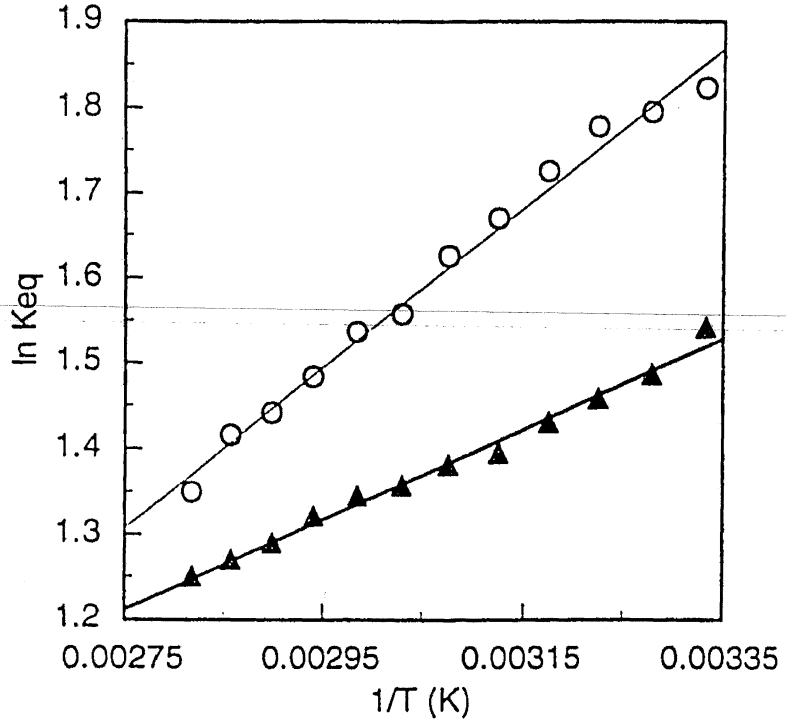
1.9
1.8
1.7
1.6
1.5
1.4
1.3
1.2
ln Keq
0.00275
0.00295
0.00315
0.00335
1/T (K)

Figure 7.7a Qualitative free energy profile for the isomerization of proline derivatives **7.1** and **7.3** in dioxane at 60 °C. For clarity, the *cis* isomers of **7.1** and **7.3** are assumed to have the same free energy.

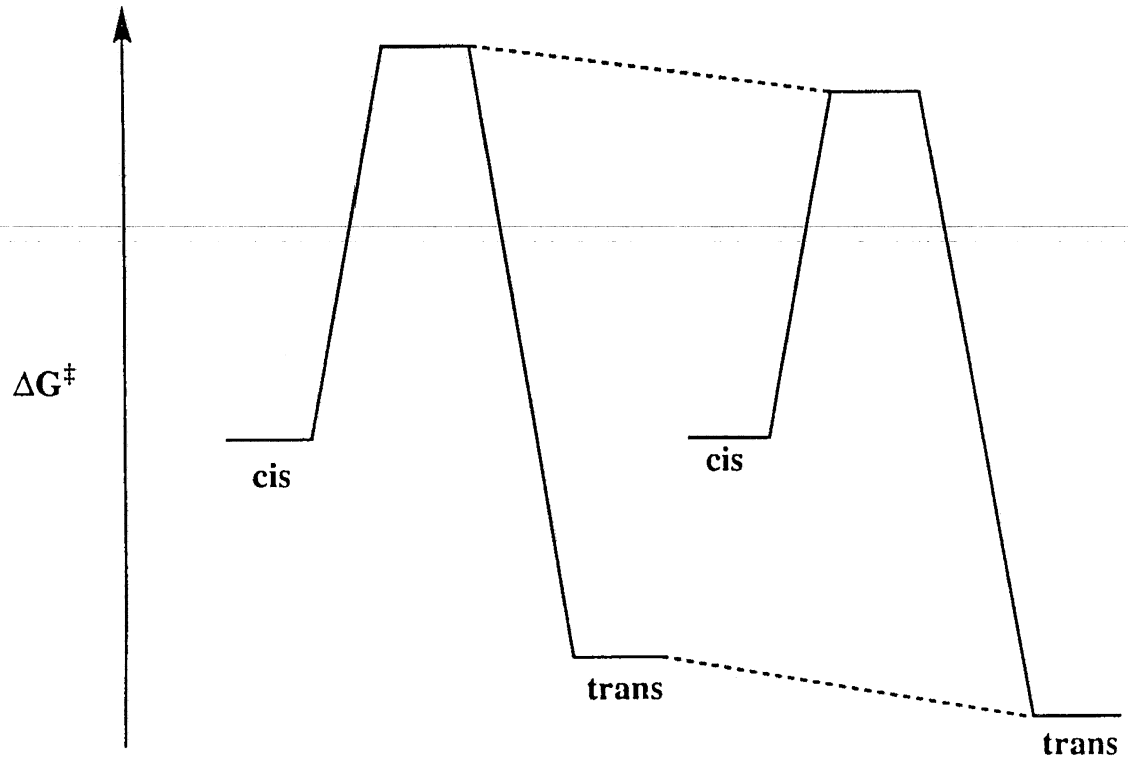

7.1 **7.3**

Figure 7.7b Qualitative free energy profile for the isomerization of proline derivatives **7.1** and **7.2** at 75 °C. For clarity, the *cis* isomers of **7.1** and **7.2** are assumed to have the same free energy.

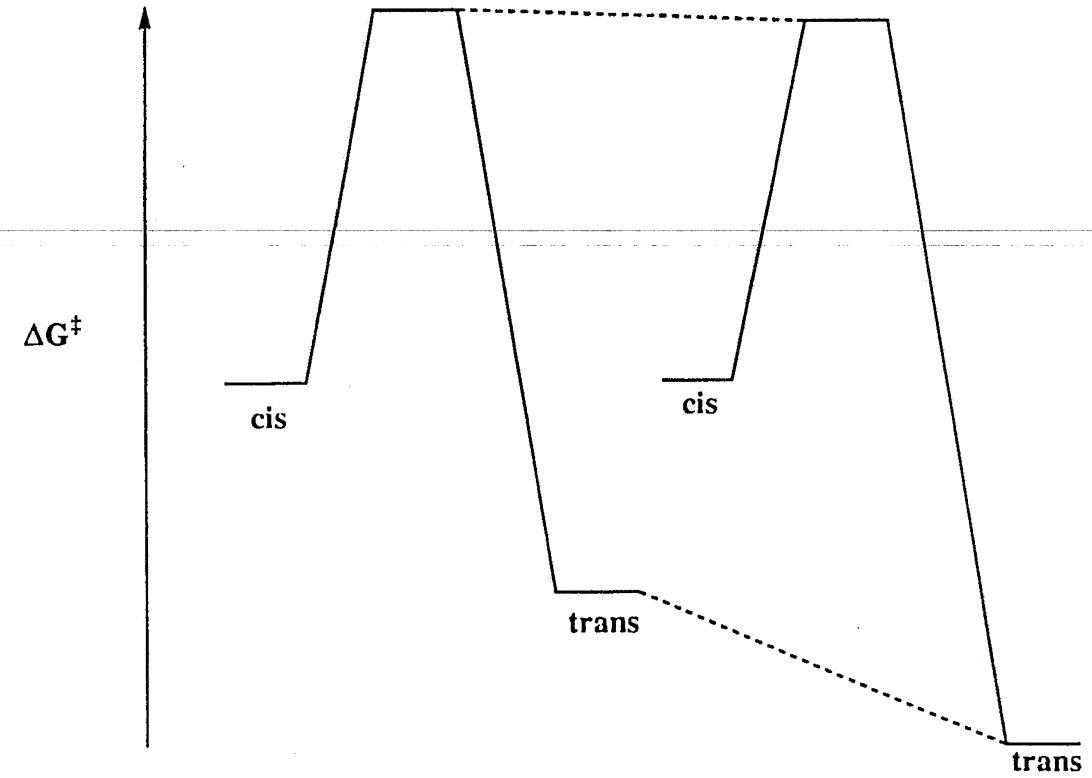

7.1 **7.2**

Table 7.1 Summary of X-Ray Diffraction Analyses[a]

Compound[b]	Pyrrolidine Ring Pucker	Pyrmidalization(δ)[c]
7.1	Cγ-endo	1.05
7.2a	Cγ-exo	-9.24
7.2b	Cγ-exo	-1.52
7.3a	Cγ-exo	-16.31
7.3b	Cγ-exo	-3.54

[a] From ref. X. [b] Two structures were observed in the unit cell of crystalline **7.2** and **7.3**. In crystalline **7.2**, the hydroxyl group of **7.2a** donates a hydrogen bond to the amide oxygen of **7.2b**. [c] The parameter δ refers to the angle which the N_1-C_O peptide bond makes with the plane defined by N_1, C^{α} and C^{δ} atoms of the pyrrolidine ring.[195]

Table 7.2 Activation Energies of Proline Derivatives

	$\Delta H^{\ddagger}$ (kcal/mol)	$\Delta S^{\ddagger}$(cal/mol °K)
Dioxane		
7.1[a] $k_{E/Z}$	20.9 ± 1.0	46.4 ± 3.1
$k_{Z/E}$	24.3 ± 0.3	53.7 ± 1.0
7.2[b] $k_{E/Z}$	21.8 ± 1.3	28.9 ± 8.9
$k_{Z/E}$	21.3 ± 1.4	18.2 ± 7.3
7.3[c] $k_{E/Z}$	19.1 ± 0.4	41.6 ± 1.0
$k_{Z/E}$	20.6 ± 0.4	43.4 ± 1.2
H_2O		
7.1[c] $k_{E/Z}$	26.1 ± 1.4	56.3 ± 3.9
$k_{Z/E}$	24.0 ± 1.3	47.6 ± 3.7
7.2[c] $k_{E/Z}$	28.4 ± 1.2	62.9 ± 3.3
$k_{Z/E}$	22.9 ± 0.8	47.8 ± 2.4
7.3 $k_{E/Z}$	nd	nd
$k_{Z/E}$	nd	nd

[a] Error where determined from an unweighted linear least squared analysis of Figure **7.3**. [b] Isomerization rates were determined at concentrations of 1 mM. [c] Isomerization rates were determined at concentration of 100 mM.

Table 7.3a Equilibrium Constants ($K_{Z/E}$) At 300 K (27 °C).

	7.1	**7.2**	**7.3**
H_2O	4.6	5.8	6.2
Dioxane	3.6	4.3	4.5

All experiments were conducted on 100 mM peptide using an external deuterium lock. Errors were observed to be less than 0.2 for all samples studied.

Table 7.3b Equilibrium Constants ($K_{Z/E}$) At 333 K (60°C)

	7.1	**7.2**	**7.3**
H_2O	3.9	4.9	nd
Dioxane	3.2	3.3	3.3

All experiments were conducted on 100 mM peptide using an external deuterium lock. Errors were observed to be less than 0.2 for all samples studied.

Table 7.4 Selected X-ray Crystallographic Bond Lengths and Bond Angles

	7.1	Ac-Pro-$NHCH_3$[84]	**7.2a**	**7.2b**	**7.3a**	**7.3b**
C^{δ}–C^{γ} (Å)	1.523	1.530	1.509	1.511	1.513	1.502
C^{γ}–C^{β} (Å)	1.535	1.503	1.514	1.509	1.506	1.511
N–C^{δ} (Å)	1.466	1.476	1.463	1.484	1.468	1.466
X–C^{δ}–C^{γ} (°)	NA	NA	107.6	112.3	108.5	109.0
N–C^{γ}–C^{δ} (°)	104.4	102.8	103.3	102.8	103.1	102.9
C^{β}-C^{γ}-C^{δ} (°)	102.9	104.2	103.7	103.2	104.5	104.2

Table 7.5 Influence of Solvent on the Thermodynamic Parameters for Proline Derivatives 7.1, 7.2 and 7.3

	ΔH° (kcal/mol)	ΔS° cal·mol/K
Aqueous		
7.1	1.04 ± 0.02	-0.46 ± 0.05
7.2	1.87 ± 0.03	-2.55 ± 0.03
Dioxane		
7.1	1.04 ± 0.01	-0.84 ± 0.04
7.2	1.65 ± 0.12	-2.58 ± 0.38
7.3	2.29 ± 0.07	-4.60 ± 0.23

Van't Hoff plots (Figure 7a and Figure 7b) were used to determine ΔH° and ΔS° from the slope and y-intercept respectively for the $K_{E/Z}$.

Chapter 8

Materials and Experimental Methods

8.1 General Experimentals

Determination of *cis-trans* isomerization rates.[46,85] The *cis-trans* isomerization rate of proline-containing peptides were determined by ^{13}C and ^{19}F NMR inversion transfer experiments. Experiments were performed on a Brüker AM500 instrument (^{1}H 498.68 MHz, ^{13}C 125.68 MHz) using a 5 mm broadband probe, a ^{1}H bandpass filter, and a ^{13}C lowpass filter; or, a Brüker AM400 instrument (^{19}F 376.48 MHz) using a 5 mm ^{19}F probe, a ^{1}H bandpass filter, ^{19}F bandstop, and a ^{19}F bandpass filter. Samples of each proline-containing peptide studied were prepared at concentrations of 100 mM unless otherwise indicated in the highest quality solvents available. Since the rate of prolyl peptide bond isomerization cannot be detected at room temperature, experiments must be performed at elevated temperatures (310–360 K). Temperature settings of the spectrometer were calibrated to within 1 °C by reference to a glycol standard. The inversion transfer pulse sequence (1) yields the spectra of a typical experiment shown in Figure 8.1.

$$(\pi/2)x - 1/2\Delta\delta - (\pi/2)x - \tau - (\pi/2)x - \text{acquire} \qquad (1)$$

The peak height for each resonance was plotted against τ (sec) (Figure 8.2) and Sigma Plot 4.16 was used to fit the inversion transfer data to the equations:

$$M_a(t) = C_1 e^{\lambda_1 t} + C_2 e^{\lambda_2 t} + M_a^{\infty} \qquad (2)$$

$$M_b(t) = C_3 e^{\lambda_1 t} + C_4 e^{\lambda_2 t} + M_b^{\infty} \qquad (3)$$

The "a" subscript refers to the *cis* resonance and the "b" subscript refers to the *trans* resonance. The complementary experiments were performed at each temperature, in which the *cis* and then the *trans* peak were each placed on resonance. Both experiments were fitted to the same equations except that the *trans* constants were denoted as C_1^*, C_2^*, C_3^*, C_4^*, and

λ_{1a}, λ_{2a}. The values of k_{ia} and k_{ib} are extracted from equations (4) and (5) and the rate constants, k_a and k_b are determined using equations (6) and (7) where α is the ratio of the *cis* and *trans* line width's.

$$k_{ia} = \frac{(C_1^*\lambda_{1a} + C_2^*\lambda_{2a})(C_3 + C_4) - (C_3^* + C_4^*)(C_1\lambda_1 + C_2\lambda_2)}{(C_3^* + C_4^*)(C_1 + C_2) - (C_1^* + C_2^*)(C_3 + C_4)} \quad (4)$$

$$k_{ib} = \frac{(C_3^*\lambda_{1a} + C_4^*\lambda_{2a})(C_1 + C_2) - (C_3\lambda_1 + C_4\lambda_2)(C_1^* + C_2^*)}{(C_3 + C_4)(C_1^* + C_2^*) - (C_3^* + C_4^*)(C_1 + C_2)} \quad (5)$$

$$k_a = \frac{(C_3\lambda_1 + C_4\lambda_2) + k_{ib}(C_3 + C_4)}{\alpha(C_1 + C_2)} \quad (6)$$

$$k_b = \frac{\alpha(C_1\lambda_1 + C_2\lambda_2) + k_{ia}(C_1 + C_2)}{C_3 + C_4} \quad (7)$$

The isomerization rate constant at room temperature was calculated by extrapolation from Arrhenius plots. Error analysis was undertaken by performing an unweighted linear least squares fit of the Arrhenius plots (See Section 8.2, 8.3 and 8.7 for specific experimental details).

Determination of the amide I vibrational mode. IR experiments were conducted on a Nicolet 5PC spectrometer unless otherwise indicated. Experiments were conducted at 25 °C using NaCl, CaF_2 plates or, a ZnSe crystal in a Spectra Tech circle cell. The frequency of the amide I vibrational mode was determined to within 2 cm^{-1}. Samples of **2.2** were prepared to a concentration of 100 mM peptide using the highest quality solvents available. (See Section 8.2, 8.3 and 8.7 for specific experimental details.)

Determination of the equilibrium constants for *cis–trans* isomers. The equilibrium constants were determined by using NMR spectroscopy to measure the peak areas of *cis* and *trans* isomers. Experiments were performed using the same instruments described above. Temperature setting of the spectrometer were calibrated to within 1 °C by reference to a glycol standard. Peak areas were determined for each isomer using Felix 2.3

software. Equilibrium constants ($K_{Z/E}$) were ascertained by calculating the *trans/cis* isomer ratio. Van't Hoff analyses was performed over a temperature range of 300 – 355 K. Error analyses were performed by doing an unweighted linear least squares fit to the van't Hoff plots. (See Section 8.2 and 8.7 for experimental details).

8.2 Solvent Effects on the Energetics of Prolyl Peptide Bond Isomerization (Chapter 2).

Materials

K^{13}CN was purchased from Cambridge Isotope Laboratories (Woburn, MA). [1-^{13}C] sodium acetate was from Merck Stable Isotopes (Montreal, Canada). Ethyl acetamidocyanoacetate Aldrich (Milwaukee, WI) was recrystallized from ethanol before use. AG3-X4A anion exchange resin was from BioRad (Richmond, CA). All other chemicals were of reagent grade or better and were used without further purification. Flash chromatography[209] was carried out on silica gel 60 (230 – 400 mm) from Fisher (Pittsburgh, PA). Analytical chromatography was carried out on pre-coated plates of silica 60 F-254 (0.25 mm) from EM Science (Gibbstown, NJ). ^{1}H, ^{13}C, and ^{19}F NMR spectra were recorded on a Brüker AM400, AM500, or AM600 spectrometer at the Nuclear Magnetic Resonance Facility at Madison. Chemical shifts for ^{1}H and ^{13}C spectra are reported relative to $CDCl_3$ (7.26, 77.0 ppm). Chemical shifts for the ^{19}F spectrum are reported relative to trifluoroacetic acid (0 ppm). Samples contained approximately 0.1 M solute in $CDCl_3$

Methods

NMR experimental. NMR experiments were conducted as described in Section 8.1. Samples contained 0.1 M of **2.1** in dry solvents that were fully deuterated (except trifluoroethanol: external deuterium lock) and neat (except water: 100 mM sodium phosphate buffer, pH 7.2, containing 80% (v/v) $H_2O/^2H_2O$). Isomerization rates were not altered by

spiking the organic solvents with 0.2 M H_2O or by halving the concentration of **2.1**. Equilibrium constants were determined as described above in Section 8.1. The same aqueous and toluene samples were used for both the determination of isomerization rates and the van't Hoff analysis.

IR experimental. IR experiments were performed as described above in Section 8.1. Samples contained 0.01 M of **2.2** except for those in water and *N*, *N*-dimethylformamide, which contained 2 M of **2.2**. The frequency of the amide I vibrational mode was not altered by doubling the concentration of **2.2** or by raising the temperature to 60 °C.

Synthesis

Synthesis of *N*-acetyl-glycine-[β, δ-^{13}C]-*D,L*-proline methylester (2.1).

***N*-Acetyl-2-cyano-[3, 5-^{13}C]-proline ethylester.**[194,210,211] Synthesis of *N*-acetyl-glycine-[β, δ-^{13}C]-*D,L*-proline methylester (**2.1**) is shown in Figure 8.3. [1, 3-^{13}C]-1, 3-dibromopropane was synthesized from [1-^{13}C] sodium acetate and K^{13}CN. (For detailed synthetic experimental; see Hinck, Ph.D. Thesis (1993).)[212] *N*-Acetyl-2-cyano-[3, 5-^{13}C]-proline ethylester was prepared by dissolving solid Na (1.28 g, 55.6 mmol) in anhydrous ethanol in a flame-dried three-neck flask. Ethyl acetamidocyanoacetate (8.43 g, 49.5 mmol) dissolved in ethanol (50 mL) was added dropwise over a 20 min to the reaction, and the resulting mixture was stirred for 30 min at 25 °C. [1, 3-^{13}C]-1, 3 Dibromopropane (5.0 g, 24.5 mmol) dissolved in ethanol (50 mL) was added dropwise over 30 min. This mixture was stirred at 25 °C for 2 h and then refluxed vigorously for 22 h. The reaction was cooled, concentrated, and dissolved in aqueous CH_2Cl_2 (50% (v/v), 100 mL). The aqueous layer was washed with CH_2Cl_2 (3 x 50 mL), and the organic extract was combined and dried over saturated Na_2SO_4, and then concentrated to yield a brown oil. The crude product was loaded on a 100 g silica column and eluted with a 1:5 to 1:2 gradient of ethyl acetate:hexanes to yield product as a white solid (4.77 g, 91%). R_f (ethyl acetate)=0.54. ^{1}H NMR($CDCl_3$) 4.12

(m, 2H, O-CH_2-), 3.56 (m, 2H, H-5,5'), 2.47 (m, 1H, H-3'), 2.21 (m, 1H, H-3), 2.09 (m, 2H, H-4,4'), 1.98 (s, 3H, acetyl-CH_3), 1.16 (t, 3H, ester -CH_3).

[β, δ-^{13}C]-*D, L*-Proline. *N*-Acetyl-2-cyano-[3,5-^{13}C]-proline ethylester (4.65 g, 21.9 mmol) was dissolved in 50 mL concentrated HCl (50 mL) and the resulting solution was refluxed for 2 h. The reaction was concentrated and dried. The resulting white solid was dissolved in H_2O and passed through a column of AG-X4A anion exchange resin. The product was eluted with H_2O. The solvent was removed from the collected product under reduced pressure to an 85 % yield of [β, δ-^{13}C]-*D,L* proline (2.14 g, 18.6 mmol). Isotopic enrichment at the β and δ positions was determined to be greater than 99% on the basis of ^{13}C coupled and uncoupled $^{\beta}$H, $^{\beta}$H', $^{\delta}$H, and $^{\delta}$H' signal intensities in the ^{1}H NMR spectrum. R_f (3:1 (v/v) ethanol:H_2O)= 0.40. ^{1}H NMR (^2H_2O) 4.14 (t, 1H C$^{\alpha}$H), 3.44 (dm, 1H, C$^{\delta}$H'), 3.38 (dm, 1H, C$^{\delta}$H), 2.39 (dm, 1H, C$^{\gamma}$H'), 2.12 (dm, 1H, C$^{\gamma}$H), 2.05 (m, 2H, C$^{\gamma}$H-H'). ^{13}C NMR (^2H_2O) 47.6 ($^{\delta}$C), 30.4 ($^{\beta}$C).

***tert*-Butoxy-[β, δ-^{13}C]-*D,L*-proline.** To a solution containing Boc-ON (1.58 g, 6.41 mmol), triethylamine (0.60 mL, 6.41 mmol) and 1:1 (v:v) H_2O: dioxane (10 mL total volume), [β, δ ^{13}C]-proline (0.5 g, 4.27 mmol) was added and the reaction was stirred for 16 h at 25 °C. The reaction was concentrated to a viscous oil, taken up in $CHCl_3$ and extracted 1N HCl (3 x 50 mL). The organic layer was extracted 1 N NaOH (3 x 50 mL), aqueous fractions were combined, and, in the presence of $CHCl_3$ (25 mL), the pH was adjusted to 1.0. The aqueous layer was extracted with $CHCl_3$ (3 x 50 mL), concentrated, and loaded on a 20 g silica column in ethyl acetate and eluted (3:1(v/v) ethyl acetate:hexanes) to yield product as a white solid (0.72 g, 77.9%). R_f (1:3 (v/v) H_2O:ethanol)= 0.68. MH^+(FAB) $C_8{}^{13}C_2H_{17}N_1O_4$= 218. ^{1}H NMR ($CDCl_3$) 4.33 (br m, 1H, $C_1{}^{\alpha}H_1$; minor isomer at 4.19), 4.30 (m, 1H, $C_1{}^{\delta}H_1$ minor isomer at 3.51), 3.67 (m, 1H, $C_1{}^{\delta}H_1$'; minor isomer at 3.28), 2.33 (m, 1H, $C_1{}^{\beta}H_1$; minor isomer at 2.31), 2.07 (m, 1H, $C_1{}^{\beta}H_1$'), 1.91 (br s, 1H, $C_1{}^{\gamma}H_1$; minor isomer at 1.90), 1.82 (m 1H, $C_1{}^{\gamma}H_1$'), 1.43 (s br, 9H, t-butoxy-3, CH_3; minor isomer at 1.37).

***tert*–Butoxy-[β, δ-^{13}C]--*D,L*–proline methylester.** *N*-methyl-nitroso urea (3.0 g, mmol) in Et_2O (25 mL) was treated with KOH (0.75 g, mmol) and allowed to stir for 10 min at 25 °C. The resulting bright yellow supernatant was added to a solution (25 mL) of *tert*-butoxy-[β, γ-^{13}C]-proline (0.72 g, 3.30 mmol) in Et_2O. The reaction was stirred at 25 °C for 30 min. The reaction was concentrated, and then taken up in ethyl acetate and washed with 1N HCl (3 x 50 mL), 1N NaOH (3 x 50 mL), saturated NaCl (1 x 50 mL), and dried over $MgSO_4$. The solution was filtered and concentrated to yield 1.2 g of viscous oil. The crude product was loaded on to a 10 g silica column and eluted(2:1(v/v) ethyl acetate:hexanes) to yield a yellow oil. The oil was passed over methanol-washed celite and activated carbon to yield product as a white solid (0.72 g, 95%). R_f (18:2:1 (v/v/v) $CHCl_3$:MeOH:AcOH) = 0.64. ^{1}H NMR ($CDCl_3$) 4.33 (m br, 1H, $C_1{}^{\alpha}H$; minor isomer at 4.19), 4.30 (m, 1H, $C_1{}^{\delta}H$; minor isomer at 3.51), 3.67 (m, 1H, $C_1{}^{\delta}H'$; minor isomer at 3.28) 3.60 (s, 3H, OCH_3; minor isomer at 3.57) , 2.33 (m, 1H, $C_1{}^{\beta}H$; minor isomer at 2.31), 2.07 (m, 1H, $C_1{}^{\beta}H'$), 1.91 (br s, 1H, $C_1{}^{\gamma}H_1$; minor isomer at 1.90), 1.82 (m, 1H, $C_1{}^{\gamma}H_1'$), 1.43 (s br, 9H, t-butoxy 3-C_0H_3; minor isomer at 1.37).

***N*-Acetyl-glycine-[β, δ-^{13}C]-*D,L*–proline methylester (2.1).** *tert*-Butoxy-[β, δ-^{13}C]–*D, L*–proline methylester (0.72 g, 3.13 mmol) was added to a solution (10 mL) containing HCL(4N). The resulting solution was stirred at 25 °C for 30 min. The reaction was then concentrated, dried to yield [β, δ–^{13}C]–*D, L*–proline methylester hydrochloride (100% yield assumed). To CH_2Cl_2 solution (50 mL) containing [β, δ–^{13}C]–*D, L*–proline methylester hydrochloride at 0 °C, triethylamine (1.2 mL, 9.70 mmol), acetamidoacetic acid (1.0 g, 8.55 mmol), 1-hydroxybenzotriazole hydrate (1.3 g, 8.55 mmol), and dicyclohexylcarbodiimide (1.76 g, 8.55 mmol) were added, respectively. The reaction was allowed to warm to 25 °C, and then stirred for 18 h. The reaction was filtered, and the filtrate was washed with 1N HCl (3 x 50 mL), 1N NaOH (3 x 50 mL), saturated NaCl (1 x 50 mL), and dried over $MgSO_4$. The organic layer was concentrated, and loaded on to a 100 g silica column in $CHCl_3$ and

eluted with a methanol gradient (1%-5% (v/v) methanol/$CHCl_3$) to yield product as a white solid (0.54 g, 75%). R_f (5% methanol/$CHCl_3$) = 0.25. ^1H NMR ($CDCl_3$) 6.58 (s, N_1H; minor isomer at 6.80), 4.83 (m br, 1H, $C_2{}^{\alpha}H$; minor isomer at 4.65), 4.02 (dd, 1H, $C_1{}^{\alpha}H$; minor isomer at 4.09), 3.86 (dd, 1H, $C_1{}^{\alpha}H'$; minor isomer at 3.80), 3.62 (s, 3H, OCH_3; minor isomer at 3.59), 3.55 (m, 1H, $C_2{}^{\delta}H$; minor isomer at 3.61), 3.40 (m, 1H, $C_2{}^{\delta}H'$; minor isomer at 3.33), 2.33 (m, 1H, $C_2{}^{\beta}H$; minor isomer at 2.31), 2.10 (s, 3H acetyl-C_0H), 2.07 (m, 1H, $C_2{}^{\beta}H'$), 1.91 (m, 2H, $C_2{}^{\gamma}H_1$). NMR ^{13}C ($CDCl_3$): 47.52 ($^{\delta}C_2$; minor isomer 46.04), 28.09 ($^{\beta}C_2$; minor isomer 32.15).

8.3 Relative Strength of Amide–Amide and Amide-Water Hydrogen Bonds (Chapter 3).

Materials

Amide solvents (Aldrich Chemical; Milwaukee, WI) were distilled from either 4Å molecular sieves (formamides) or CaH_2 (secondary amides). *Note:* Acetamide, the simplest primary amide, was not studied due to its high melting point (82.3 °C).

Methods

NMR experimental. Experiments were carried out as described in Section 8.1. All samples contained 0.1 M of **3.1** in neat solvent and used an external deuterium lock.

IR experimental. Experiments were performed as described in Section 8.1. Samples contained 0.01 M **3.2** in neat solvent and were not altered significantly by raising the temperature to 60 °C. The presence of ^{13}C in **3.2** decreased the frequency of its amide I vibrational mode (by 41 cm^{-1} in dioxane; by 50 cm^{-1} in water), and thereby avoided overlap with amide solvents.

8.4 Mechanism and Thermodynamics of Amide Hydrogen Bond Formation in Aqueous and Organic Solvents: Dimerization of δ-Valerolactam (Chapter 4).

Materials

δ-Valerolactam, CCl_4, tetramethyl silane and trimethylsilyl propanoic acid were purchased from the Aldrich Chemical (Milwaukee, WI). Using flame dried glassware, CCl_4 and δ-Valerolactam were twice fractionally distilled from CaH_2 under N_2.

Methods

NMR experimental. ^1H NMR data were collected on a Brüker AM500 spectrometer at the National Magnetic Resonance Facility at Madison. Chemical shifts were referenced to internal tetramethyl silane (CCl_4 samples) and trimethylsilyl propanoic acid (aqueous samples).

IR experimental. CCl_4 samples were prepared under N_2 in a glove bag. Experiments in CCl_4 were performed on a Nicolet 740 FTIR spectrometer with a 0.1 mm path length, CaF_2 plates, and a spectral resolution of 2 cm^{-1}. Experiments in H_2O were performed on a Nicolet 5PC FTIR Spectrometer equipped with a ZnSe crystal in a Spectra Tech circle cell, and a spectral resolution of 2 cm^{-1}.

8.5 Contribution of a Phenolic Hydrogen Bond to Ribonuclease A Stability and Catalysis (Chapter 5).

Materials

E. coli strain BL21(DE3) (F- ompT r_B-m_B-) and plasmid pET22B(+) were from Novagen (Madison, WI). All enzymes for the manipulation of recombinant DNA were from Promega (Madison, WI). Reagents for DNA synthesis were from Applied Biosystems

(Foster City, CA), except for acetonitrile, which was from Baxter Healthcare (McGaw, IL). Oligonucleotides were synthesized on an Applied Biosystems 392 DNA/RNA synthesizer, and purified using Oligo Purification Cartridges (Applied Biosystems). DNA was sequenced with a Sequenase 2.0 kit from United States Biochemicals (Cleveland, OH). DE52 diethylaminoethyl cellulose anion exchange resin was from Whatman (Maidstone, England), and S-Sepharose cation exchange resin was from Pharmacia LKB (Piscataway, NJ). Poly(C) was purchased from Sigma Chemical (St. Louis, MO) or from Midland Certified Reagent (Midland, TX) and was precipitated from aqueous ethanol (70% v/v) before use. Wild-type RNase A was purchased from Sigma (St. Louis, MO). Bacto yeast extract, Bacto tryptone, Bacto peptone, and Bacto agar, were from Difco (Detroit, MI). Bacterial terrific broth (TB)[19] contained (in 1 L) Bacto tryptone (12 g), Bacto yeast extract (24 g), glycerol (4 mL), KH_2PO_4 (2.31 g), and K_2HPO_4 (12.54 g). All media were prepared in distilled, deionized water and autoclaved. Ultraviolet and visible absorbance measurements were made with a Cary 3 spectrophotometer equipped with a Cary temperature controller. All other chemicals reagents were of commercial reagent grade or better and were used without purification unless otherwise indicated.

Methods

Preparation of Tyr97 mutants. Single-stranded DNA from pBXR, which contains the cDNA of RNase A and the plasmid pET22B, was a generous gift from Steve delCardayré. This single-stranded DNA had been isolated from *E. coli* strain CJ236, which occasionally incorporates uridine residues instead of thymidine. Oligonucleotide-mediated site-directed mutagensis was performed on this DNA by using the method of Kunkel.[213] The TAC codon for Tyr97 of RNase A was changed to TTT (phenylalanine), GCC (alanine), or GGC (glycine) by oligonucleotide-mediated site-directed mutagenesis. mutagenesis reactions were transformed into BL21(DE3) cells.

Production and purification of RNase A from *E. coli*. [7,45] A freezer stock was prepared of *E. coli* strain BL21(DE3) harboring plasmid wild-type or mutated plasmid pBXR from a mid-log phase culture grown in LB medium containing ampicillin (400 μg/mL). This freezer stock was used to inoculate a starter culture (15 mL) of TB medium containing ampicillin (400 μg/mL). This culture was grown to mid-log phase (A_{600} = 0.5 O.D.) and used to inoculate a larger culture (1 L) of the same medium containing ampicillin (400 μg/mL). The inoculated culture was shaken (250 rpm) at 37 °C until it reached late log phase (A_{600} = 1.9 O.D.), and was then induced to express the cDNA that codes for RNase A by the addition of IPTG (to 2 mM). Shaking at 37 °C was continued for 4 h, before the cells were harvested by centrifugation for 10 min at 5000 x *g*.

The cell pellet was resuspended in cell lysis buffer (250 mL), which was 20 mM Tris•HCl buffer, pH 7.8, containing urea (6 M) and EDTA (1 mM), and the suspension was shaken for 20 min at 37 °C. This suspension was then centrifuged for 15 min at 30,000 x *g*, and the resulting pellet was resuspended in solubilization buffer (250 mL), which was 20 mM Tris•HCl buffer, pH 7.8, containing urea (6 M), NaCl (0.4 M), DTT (20 mM), and EDTA (1 mM), and the suspension was shaken for 20 min at 37 °C. This suspension was then centrifuged for 15 min at 30,000 x *g*. The supernatant was collected and to it was added reduced DTT (0.22 g). The resulting solution was stirred at room temperature for 10 min. Glacial acetic acid was added to lower the pH to 5.0, and the resulting solution was dialyzed exhaustively against 20 mM Tris•AcOH buffer, pH 5.0, containing NaCl (0.1 M). The insoluble material that accumulated during dialysis was removed by centrifugation. The soluble fraction was then reoxidized by exhaustive dialysis (>24 h) against refolding buffer, which was 50 mM Tris•AcOH buffer, pH 7.8, containing NaCl (0.1 M), reduced glutathione (1 mM), and oxidized glutathione (0.2 mM). The refolded sample was then dialyzed exhaustively against 20 mM Tris•AcOH buffer, pH 8.0.

The dialyzed sample was passed through a column (15 cm x 4.9 cm^2) of SE-52 anion exchange resin equilibrated with the same buffer. The flow-through was loaded onto a column (15 cm x 1.8 cm^2) of mono-S cation exchange resin equilibrated with Tris•AcOH buffer (20 mM), pH 8.0, and the loaded column was washed with the same buffer (100 mL). RNase A was eluted with a linear gradient of NaCl (0.0 – 0.35M), in Tris•AcOH buffer, pH 8.0. Fractions were collected and assayed for ribonuclease activity. The purity of active fractions was assessed by SDS-PAGE. Fractions containing RNase A of >95% purity were pooled and characterized.

T_m determination. As RNase A is denatured, its 6 tyrosine residues become exposed to solvent and its extinction coefficient at 287 nm decreases significantly.[214] The thermal stability of RNase A proteins was assessed by monitoring by the change of absorbance at A_{286} with temperature.[161] Solutions of protein (1.0 – 3.0 mg/mL) in 100 mM sodium acetate buffer (100 mM NaCl, at pH 6.0) was prepared to a total sample volume of 0.8 mL. The unfolding absorbance A_{286} was recorded at 1 °C increments between 10 and 95 °C after a five minute equilibration at each temperature. Thermal renaturation of the mutant proteins, from 95 – 10 °C, were observed to have the same midpoint (T_m) as thermal denaturation. The T_m value and error was determined by a nonlinear regression analysis of the unfolding curves using Sigma Plot 4.16.

Steady-state kinetics. The cleavage of poly(C) was monitored by the change in ultraviolet hyperchromicity. The $\Delta\varepsilon$ for this reaction, calculated from the difference in molar absorptivity of the polymeric substrate and the mononucleotide cyclic phosphate product was 2380 $M^{-1}cm^{-1}$ at 250 nm.[7] RNase A concentrations were determined by using a Bradford assay (Bio Rad) where a standard curve was determined for wild-type RNase A by assuming that $A_{277.5}^{0.1\%} = 0.72$.[215] All assays were performed at 25 °C in 0.1 M MES buffer, pH 6.0, containing NaCl (0.1 M), with substrate poly(C) concentrations between 10 μM – 0.4 mM.

The total reaction volume was 0.8 mL. The values and errors for k_{cat} and K_m were determined from the initial velocity data using the program HYPERO.[216]

8.6 Inductive Effect on the Structure of Proline Residues (Chapter 6).

Materials

N-Acetyl-proline methylester (**6.1**), 4(*S*)-hydroxyproline methylester hydrochloride, and 4(*R*)-hydroxyproline methylester hydrochloride were from Bachem Biosciences (Philadelphia, PA), and were used without further purification. All other reagents and all solvents were from Aldrich Chemical (Milwaukee, WI), and were used without further purification.

Methods

X-Ray diffraction analysis. Single crystals suitable for x-ray diffraction analysis were obtained by evaporation at ambient temperature of solutions of **6.1** or **6.3** in 2-propanol, or of **6.2** in ethyl acetate. Cell parameter data and intensity data were collected using a Siemens P4 diffractometer with CuKα radiation (λ = 1.54178 Å). The unit cell parameters and their ESDs were derived from a least squares treatment based on 25 (**6.1** and **6.2**) or 26 (**6.3**) high-angle reflections in the range 48°>θ>50° (**6.1**), 45°>θ>50° (**6.2**), or 53°>θ >56°(**6.3**). Integrated relative intensities for the independent reflections with 2θ<114° were measured in the Wyckoff (**6.1** and **6.2**) or the 2θ–θ (**6.3**) scan mode. The intensity of three standard reflections, checked after each 100 (**6.1**), 50 (**6.2**), or 50 (**6.3**) reflections, varied by less than 5% (**6.1**), 4% (**6.2**), or 6% (**6.3**). Data were corrected for Lorentz and polarization effects but not for absorption. The structures were solved by direct methods using the program SHELXTL PLUS,[217] and refined anisotropically with the full-matrix least squares procedure. Hydrogen atom positions were calculated and refined by using a riding model.

***Ab initio* calculations.** *Ab initio* calculations were performed on an FPS-522 computer by using the electronic structure packages GAMESS[218] and Spartan[219] by A. S. Edison. Geometries were first optimized at the STO-3G level of theory, and then fully optimized at the 3-21G level of theory. For each molecule (**6.1 – 6.3**), bond distances were calculated for the form of the particular peptide bond isomer (*cis* or *trans*) and ring pucker (C$^{\gamma}$-endo or C$^{\gamma}$-exo) observed in the crystalline state.

Synthesis

***N*-Acetyl-4(*S*)-acetoxyproline methylester.** 4(*S*)-Hydroxyproline methylester hydrochloride (4.0 g, 22 mmol) was dissolved in acetic anhydride (40 mL), and the resulting solution was stirred for 12 h at room temperature. The mixture was then concentrated under reduced pressure, and the resulting residue was subjected to flash chromatography (1:1 (v/v) ethyl acetate:hexanes) to yield product as a white solid (3.6 g, 75%). R_f (ethyl acetate)=0.40. ^{1}H NMR ($CDCl_3$) 5.16 (br s, 1H, $C_1{}^{\gamma}H_1$; minor isomer at 5.10), 4.33 (t, J=2 Hz, 1H, $C_1{}^{\alpha}H$), 3.74 (dd, J=12Hz, J=4.5Hz, 1H, $C_1{}^{\delta 2}H$), 3.55 (s, 3H, C_2H_3; minor isomer at 3.61), 3.43 (br d, J=11Hz, 1H, $C_1{}^{\delta 2}H'$; minor isomer at 3.42), 2.21 (m, 1H, $C_1{}^{\beta}H$; minor isomer at 2.34), 2.03 (m, 1H, $C_1{}^{\beta}H'$), 1.90 [s, 3H, $C_0{}^{\alpha}H_3$; minor isomer at 1.80], 1.89 [s, 3H, $O_1{}^{\delta 1}C(O)CH_3$; minor isomer at 1.87]; ^{13}C NMR ($CDCl_3$, ppm) 171.85 (C_0), 169.91 [$O_1{}^{\delta 1}C(O)$], 168.90 (C_1), 72.40 ($C_1{}^{\gamma}$; minor isomer at 70.80), 56.82 ($C_1{}^{\alpha}$; minor isomer at 58.02), 52.75 ($C_1{}^{\delta 2}$; minor isomer at 51.15), 51.92 (C_2; minor isomer at 52.42), 34.54 ($C_1{}^{\beta}$; minor isomer at 36.54), 21.85 ($C_0{}^{\alpha}$), 20.45 [$O_1{}^{\delta 1}C(O)CH_3$].

***N*-Acetyl-4(*S*)-hydroxyproline methylester (6.2).** Anhydrous potassium carbonate[220] (0.151 g, 1.09 mmol) was added to a solution of *N*-acetyl-4-(*S*)-acetoxyproline methylester (2.5 g, 11 mmol) in methanol (12 mL), and the resulting slurry was stirred for 30 min at room temperature. The mixture was then filtered, the filtrate was concentrated under reduced pressure, and the resulting residue was subjected to flash chromatography (1:2 (v/v)

ethyl acetate-hexane) to yield product as a white solid (1.50 g, 74%). R_f (ethyl acetate)=0.17. MS (EI, *m/e*): 187.25. ^{1}H NMR ($CDCl_3$) 4.62 (d, *J*=2.5Hz, 1H, $C_1\gamma H$; minor isomer at 4.49), 4.33 (t, *J*=8Hz, 1H; $C_1\alpha H$; minor isomer at 4.40), 3.59(d, *J*=9Hz, 1H, $C_1\delta^2 H$), 3.55 (s, 3H, C_2H_3; minor isomer at 3.57), 3.35 (d, *J*=5.5Hz, 1H, $C_1\delta^2 H'$), 2.91 (br s, 1H, $O_1\delta^1 H$), 2.14–2.09 (m, 1H, $C_1\beta H$; minor isomer at 2.28–2.23), 1.92 (s, 3H, $C_0\alpha H_3$; minor isomer at 1.78), 1.88–1.83 (m, 1H, $C_1\beta H'$; minor isomer at 2.04–2.00); ^{13}C NMR ($CDCl_3$) 172.55 (C_0; minor isomer at 172.38), 170.46 (C_1; minor isomer at 169.90), 69.28 ($C_1\gamma$; minor isomer at 67.70), 57.24 ($C_1\alpha$, minor isomer at 518.40), 55.54 ($C_1\delta$; minor isomer at 54.01), 51.90 (C_2; minor isomer at 52.36), 37.45 ($C_1\beta$; minor isomer at 39.27), 21.80 ($C_0\alpha$, minor isomer at 21.20).

***N*-Acetyl-4(*R*)-acetoxyproline methylester.** 4(*R*)-Hydroxyproline methylester hydrochloride (0.25 g, 1.4 mmol) was dissolved in acetic anhydride (4 mL), and the resulting solution was stirred for 24 h at room temperature. The mixture was concentrated under reduced pressure, and the resulting residues was subjected to flash chromatography (ethyl acetate) to yield product as a white solid (0.295 g, 93%). R_f (18:2:1 (v/v/v) $CHCl_3$:methanol:acetic acid)=0.75. ^{1}H NMR ($CDCl_3$) 5.20 (br s, 1H, $C_1\gamma H$), 4.61 (d, *J*=4.5Hz, 1H, $C_1\alpha H$; minor isomer at 4.41), 3.78 (dd, *J*=6Hz, 1H, $C_1\delta^2 H$), 3.65 (s, 3H, C_2H_3; minor isomer at 3.70), 3.602 (br d, *J*=5.5Hz, 1H, $C_1\delta^2 H'$), 2.42 –2.32 (m, 1H, $C_1\beta H$), 2.22 (br d, *J*=7Hz, 1H, $C_1\beta H'$; minor isomer at 2.36), 2.01 (s, 3H, $C_0\alpha H_3$; minor isomer at 1.96), 1.94 [s, 3H, $O_1\delta^1 C(O)CH_3$; minor isomer at 1.89]; ^{13}C NMR ($CDCl_3$) 171.60 (C_0), 170.36 [$O_1\delta^1 C(O)$; minor isomer at 169.98], 169.72 (C_1; minor isomer at 169.88), 72.81 ($C_1\gamma$; minor isomer at 71.48), 52.35 (C_2), 56.97 ($C_1\alpha$; minor isomer at 58.87), 53.16 ($C_1\delta$; minor isomer at 52.68), 34.84 ($C_1\beta$; minor isomer at 37.08), 22.23 ($C_0\alpha$; minor isomer at 22.09), 20.90 [$O_1\delta^1 C(O)CH_3$].

***N*-Acetyl-4(*R*)-hydroxyproline methylester.** Anhydrous potassium carbonate (0.015 g, 0.11 mmol) was added to a solution of *N*-acetyl-4(*R*)-acetoxyproline methylester (0.251 g, 1.10 mmol) in methanol (12 mL), and the resulting slurry was stirred for 10 min at room

temperature. The mixture was then filtered, concentrated under reduced pressure, and subjected to flash chromatography (ethyl acetate) to yield product as a white solid (0.145 g, 75%). R_f (18:2:1 (v/v/v) $CHCl_3$/methanol/acetic acid)=0.34. ^1H NMR ($CDCl_3$) 4.48 (d, J=5Hz, 1H, $C_1{}^{\gamma}H$), 4.41 (m, 1H, $C_1{}^{\alpha}H$), 3.77–3.72 (m, 1H, $C_1{}^{\delta 2}H$), 3.68–3.61 (m, 1H, $C_1{}^{\delta 2}H'$), 3.66 (s, 3H, C_2H_3), 2.80 (s, 1H, $O_1{}^{\delta 1}H$), 2.34–2.25 (m, 2H, $C_1{}^{\beta}H_2$), 2.06 (s, 3H, $C_0{}^{\alpha}H_3$; minor isomer at 2.00); ^{13}C NMR ($CDCl_3$) 174.4 (C_0), 169.6 (C_1), 71.2 ($C_1{}^{\gamma}$; minor isomer at 68.8), 57.2 ($C_1{}^{\alpha}$; minor isomer at 59.0), 56.2 ($C_1{}^{\delta}$; minor isomer at 55.2), 52.8 (C_2) 37.0 ($C_1{}^{\beta}$; minor isomer at 39.4), 22.0 ($C_0{}^{\alpha}$).

***N*-Acetyl-4(*S*)-fluoroproline methylester (6.3).** The hydroxyl group in *N*-acetyl-4(*R*)-hydroxyproline methylester was converted to a fluoro group by using the morpholino analogue of diethylaminosulfur trifluoride.[221] Morpholinosulfur trifluoride (0.564 g, 3.22 mmol) was added dropwise over 10 min and with stirring over 10 min to a solution (5 mL) at –80 °C under nitrogen of dichloromethane containing *N*-acetyl-4(*R*)-hydroxyproline methylester (0.120 g, 0.645 mmol). The reaction was allowed to warm to room temperature, and was then stirred for 48 h. The mixture was concentrated under reduced pressure, quenched with water (2 mL), concentrated again under reduced pressure, and subjected to flash chromatography (1:4 (v/v) ethyl acetate-hexanes) to yield product as a colorless oil (0.060 g, 50%). R_f (ethyl acetate)= 0.36. MS (FAB): 190.2535. ^1H NMR ($CDCl_3$) 5.23 (dt, J=26.5Hz, J=3Hz, 1 H, $C_1{}^{\gamma}H$; minor isomer at 5.17), 4.70 (d, J=5Hz, 1H, $C_1{}^{\alpha}H$; minor isomer at 4.45), 3.87–3.62 (m, 2H, $C_1{}^{\delta 2}H_2$), 3.67 (s, 3H, C_2H_3; minor isomer at 3.71), 2.43 (t, J=15Hz, broad, 1H, $C_1{}^{\beta}H$; minor isomer at 3.64), 2.32 (m, 1H, $C_1{}^{\beta}H'$; minor isomer at 3.45); 2.05 (s, 3H, C_2H_3; minor isomer at 1.98); ^{13}C NMR ($CDCl_3$) 172.30 (C_0), 169.20 (C_1), 91.80 (d, J_F=180Hz, $C_1{}^{\gamma}$), 54.18 ($C_1{}^{\delta}$; minor isomer at 53.98), 52.31 (C_2; minor isomer at 52.72), 52.11 ($C_1{}^{\alpha}$; minor isomer at 58.11), 35.89 ($C_1{}^{\beta}$; minor isomer at 36.06), 22.15 ($C_0{}^{\alpha}$; minor isomer at 22.10); ^{19}F NMR ($CDCl_3$) δ –114.302 (minor isomer at –114.943).

8.7 Inductive Effects and the Gauche Effect on the Energetics Prolyl Peptide Bond Isomerization: Implications for Collagen Folding and Stability (Chapter 7).

Materials

tert-Butoxy-*L*-proline and 4(*R*)-*L*-hydroxyproline and were purchased from Bachem Bioscience Inc (Philadelphia, PA). *N*-methyl-*N*-nitroso-urea was purchased from Sigma Chemical (St. Louis, MO.). All other reagents were purchased from Aldrich Chemical (Milwaukee, WI.) and used without further purification unless otherwise indicated. NMR solvents were purchased from Aldrich Chemical in pre-packaged ampules and used without further purification.

Methods

pK_a determination. The secondary amine pK_a's of the parent amino acids of **7.1**, **7.2**, and **7.3** were determined by ^{1}H NMR spectroscopy. Experiments were performed on a Brücker AM500 instrument (498.68 MHz) using a 5 mm ^{1}H probe, and ^{1}H bandpass filter. Solvent suppression was applied to the water signal and a deuterium oxide insert was used to provide an external lock. A 50 mL stock solution, 400 mM for each amino acid, were prepared in a 100 mM sodium phosphate buffer, pH 7.0. A 400 µL aliquot was removed from the stock solution and the chemical shift difference between the α and β protons **7.1** and **7.2**, or the α and δ, **7.3**, were measured at 25 °C. The aliquot was returned to the stock solution and the pH was decreased by approximately 0.1 units by the addition of a 100 µL aliquot of 1N KOH. Values of pK_a were determined by plotting log $(\Delta\delta-\Delta_B/\Delta_{BH^+}-\Delta\delta)$ vs pH where the x-intercept is the pK_a. Errors were determined by linear least squares analysis.

NMR experimental. Samples of **7.1**, **7.2**, and **7.3** were prepared at concentrations of 100 mM and 1 mM in dioxane-d_8. Aqueous samples were prepared in contained 80% (v/v)

$H_2O/^2H_2O$ in 100 mM sodium phosphate buffer, pH 7.2. See Section 8.1 experimental details.

IR experimental. Samples of **7.1**, **7.2**, and **7.3** were prepared at concentrations of 100 mM and 1 mM in dioxane, distilled from CaH_2, and D_2O. No concentration effects were observed for **7.1** and **7.3** in either solvent. A second vibrational mode was present in the amide I region in a 100 mM solution of **7.2**. This mode was absent in a 1 mM solution of **7.2**. This second vibrational mode was likely the result of a hydrogen bond from the hydroxyl group of one molecule of **7.2** to the amide carbonyl group of another molecule of **7.2**, as was observed in crystalline **7.2**. To minimize such aggregation, experiments of all proline derivatives were performed at 1 mM concentrations in dioxane. Of course, solute – solvent interactions may also be significant for **7.2** because dioxane may accept a hydrogen bond from the hydroxyl group of **7.2**.

Synthesis

***N*–Acetyl-[β, γ-^{13}C]-*D, L*–proline methylester (7.1).** *tert*-Butoxy-[β, γ-^{13}C]–*D, L*–proline methylester (0.5 g, 2.16 mmol) was added to a solution (10 mL) of dioxane containing HCl (4N). The resulting solution was stirred at 25 °C for 30 min. The reaction was then concentrated, dried and then stirred with acetic anhydride (25 mL) at 25 °C for 16 h. The reaction was concentrated, taken up in ethyl acetate and washed 1N HCl (3 x 50 mL), 1N NaOH (3 x 50 mL), and saturated NaCl. The organic layer was dried over $MgSO_4$, filtered, and concentrated to yield a yellow oil. The crude product was loaded on a 10 g silica column in $CHCl_3$ and eluted with 1-5% methanol:$CHCl_3$ gradent to yield product as a white solid (0.37 g, 85%). R_f (ethylacetate)= 0.17. MH^+(FAB)= ^{1}H NMR ($CDCl_3$) 4.55 (d br, 1H, $C_1{}^{\alpha}H$; minor isomer at 4.46), 3.76 (m, 1H, $C_1{}^{\delta}H$; minor isomer at 3.61), 3.62 (s, 3H, ester-C_2H_3; minor isomer at 3.69), 3.47 (m, 1H, $C_1{}^{\delta}H'$; minor isomer at 3.33), 2.28 (m, 1H, $C_1{}^{\beta}H$; minor isomer at 2.09), 2.03 (s, 3H, acetyl-C_0H_3; minor isomer at 1.95) 2.01 (m, 2H, $C_1{}^{\gamma}H$;

minor isomer at 1.82), 1.98 (m, 1H, $C_1{}^{\beta}H'$; minor isomer at 1.83). NMR ^{13}C ($CDCl_3$) 47.52 ($^{\delta}C_1$; minor isomer 46.04), 29.19 ($^{\beta}C_1$; minor isomer 31.23).

***N*-Acetyl-4(*S*)-hydroxy proline [^{13}C]methylester (7.2).** Anhydrous potassium carbonate (0.01g, 0.08 mmol) was added to a solution of *N*-acetyl-4 -(*S*)–acetoxyproline methylester (0.15 g, 0.66 mmol) in 5 g of ^{13}C 99.98 % enriched methanol. The resulting slurry was stirred at 25 °C for 30 min. The mixture was filtered, and the filtrate was concentrated. The crude product was loaded on a 10 g silica column and eluted (1:2 (v/v) ethyl acetate:hexanes) to yield a product as a clear oil (0.079 g, 64 %). R_f (ethyl acetate)= 0.17. MH^+(FAB)=189.14. ^1H NMR ($CDCl_3$) 4.62 (s, 1H, $C_1{}^{\gamma}H$; minor conformational isomer at 4.49), 4.33 (t, 1H; $C_1{}^{\alpha}H$; minor isomer at 4.25), 3.80 (s, 1H, $C_1{}^{\delta 2}H$), 3.55 (s, 3H, OCH_3; minor isomer at 3.70), 3.35 (d, *J*=11Hz, 1H, $C_1{}^{\delta 2}H$; minor isomer at 3.42), 2.91 (s, broad, 1H, OH), 2.12 (m, $C_1{}^{\beta}H$; minor isomer at 2.26), 1.90 (s, 3H, $COCH_3$; minor isomer at 1.78), 1.86 (m, 1H, $C_1{}^{\beta}H$); ^{13}C NMR ($CDCl_3$) 58.40 (C_2; minor isomer at 57.24).

Figure 8.1 Shown are ^{13}C spectra of **2.1** in 20 % D_2O: 80% H_2O; 100 mM sodium phosphate buffer, pH 7.2, (348 K) at different τ (sec) delay times. **1**, 0.001 sec; **5**, 0.15 (sec); **10**, 0.40 (sec); **15**, 0.80 (sec); **20**, 2.0 (sec); **25**, 4.0 (sec).

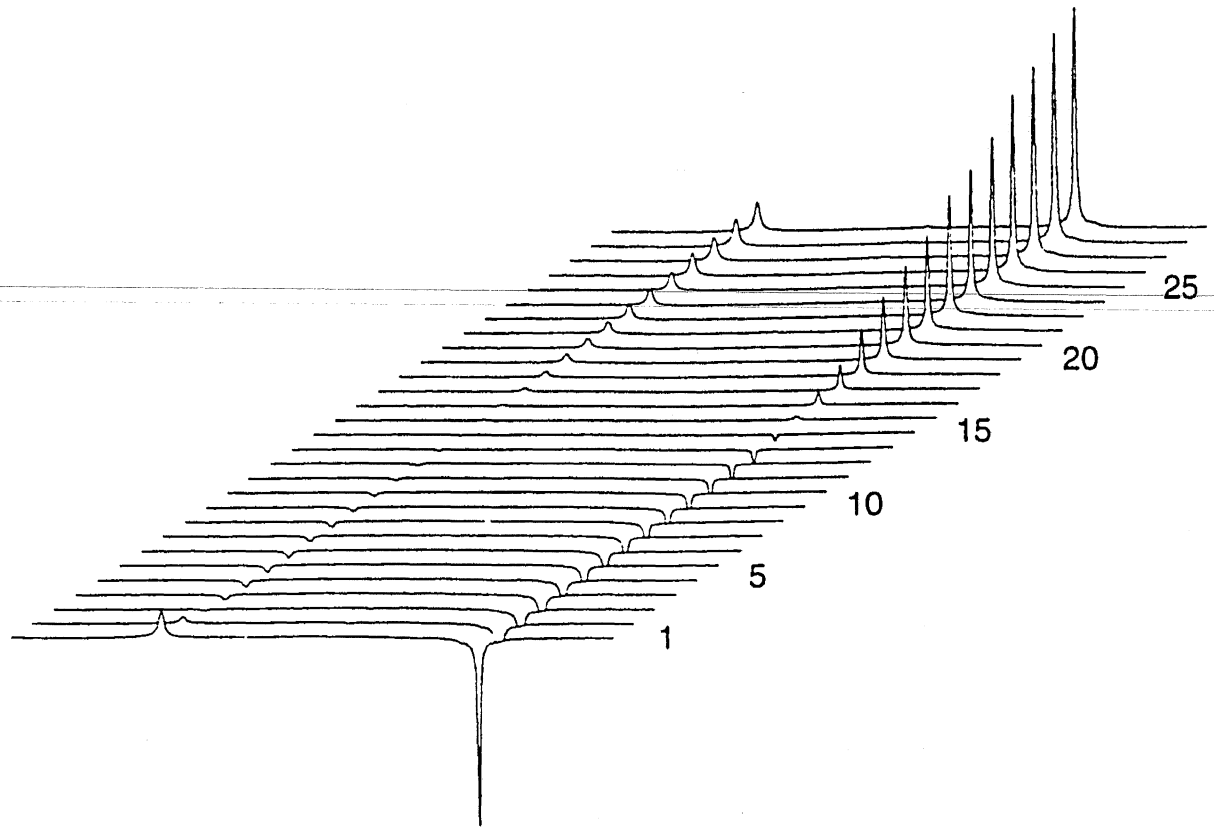
25
20
15
10
5
1

Figure 8.2 Magnetization transfer curves of **2.1** in 20 % D_2O: 80% H_2O 100 mM sodium phosphate buffer, pH 7.2, (348 K). The *cis* (▲) and *trans* (●) resonances of a typical experiment where individual peak heights are plotted against τ (sec) delay times.

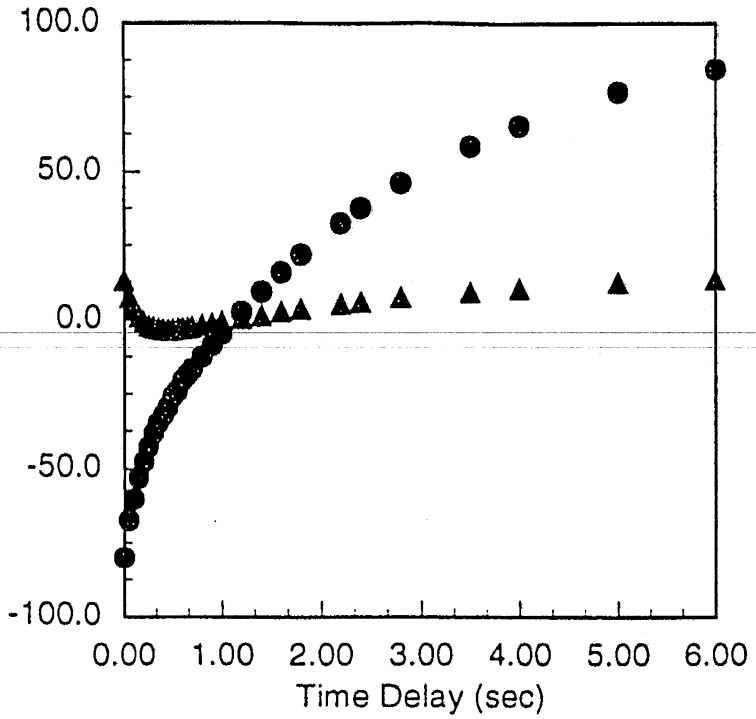
100.0
50.0
0.0
-50.0
-100.0
0.00
1.00
2.00
3.00
4.00
5.00
6.00
Time Delay (sec)

Figure 8.3 Synthesis of *N*-acetyl-glycine-[β,γ-^{13}C]-*D, L*-proline-methylester.

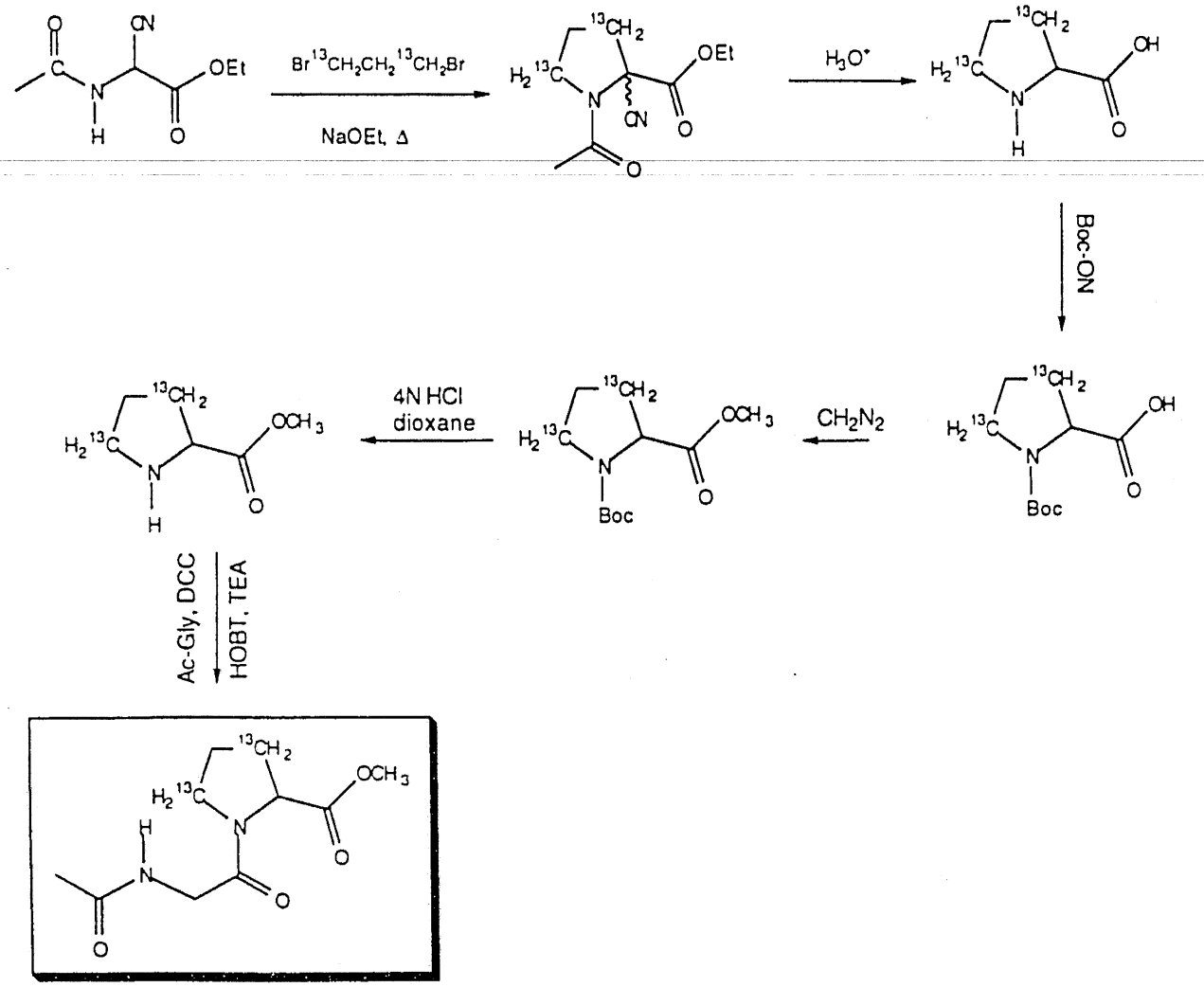
Br13CH2CH213CH2Br
NaOEt, Δ
H3O+
Boc-ON
CH2N2
4N HCl
dioxane
Ac-Gly, DCC
HOBT, TEA
Boc

2.1

References

(1) Brandts, J. F.; Halvorson, H. R.; Brennan, M. Consideration of the Possibility That the Slow Step in Protein Denaturation Reactions Is Due to *Cis–Trans* Isomerization of Proline Residues. *Biochemistry* **1975**, *14*, 4853-4963.

(2) Jeffrey, G. A.; Saenger, W. *Hydrogen Bonding in Biological Structures*; Springer-Verlag: New York, 1991.

(3) Blackburn, P.; Moore, S. Pancreatic ribonucleases. *The Enzymes* **1982**, *XV*, 317-433.

(4) Richards, F. M.; Wyckoff, H. W. In *The Enzymes*; P. D. Boyer, Ed.; Academic Press: New York, 1971; pp 647-806.

(5) Fankuchen, I. An X-ray and Crystallographic Study of Ribonuclease. *J. Gen. Physiol.* **1941**, *24*, 315-316.

(6) Gutte, B.; Merrifield, R. B. The Total Synthesis of an Enzyme with Ribonuclease A Activity. *J. Am. Chem. Soc* **1969**, *91*, 501.

(7) delCardayré, S. B.; Ribó, M.; Yokel, E. M.; Rutter, W. J.; Raines, R. T. Catalysis by ribonuclease A: Production, purification, and characterization of wild-type enzyme and mutants at position Gln11. *Protein Engineering* **1995**, In Press.

(8) Anfinsen, C. B.; Haber, E.; Sela, M.; White, F. H. The Kinetics of Formation of native Ribonuclease During Oxidation of the Reduced Polypeptide Chain. *Proc. Natl. Acad. Sci.* **1961**, *47*, 1309-1314.

(9) Rose, G. D.; Wolfenden, R. Hydrogen bonding, Hydrophobicity, Packing, and Protein Folding. *Annu. Rev. Biophys. Biomol. Struct.* **1993**, *22*, 381-415.

(10) Dill, K. A. Dominate Forces in Protein Folding. *Biochemistry* **1990**, *29*, 7733-7755.

(11) Kim, P. S.; Baldwin, R. L. Folding Reaction Intermediates. *Annu. Rev. Biochem.* **1990**, *59*, 631-660.

(12) Anfinsin, C. B. Principles that Govern the Folding of Protein Chains. *Science* **1973**, *181*, 223-230.

(13) Fersht, A. R.; Dill, K. A. Folding and Binding. *Curr. Opin. Stuc. Biol.* **1994**, *4*, 67-68.

(14) Tanford, C. *The Hydrophobic Effect*; Wiley: New York, 1980.

(15) Cleland, W. W.; Kreevoy, M. M. Low-Barrier Hydrogen Bonds and Enzymic Catalysis. *Science* **1994**, *264*, 1887-1890.

(16) Klotz, I. M.; Frazen, J. S. Hydrogen Bonds between Model Peptide Groups in Solution. *J. Am. Chem. Soc.* **1962**, *84*, 3461-3466.

(17) Tsuboi, M. On the Molecular Assocation in Amides as Revealed by Their Near-Inrared Absorption Spectra. *Bull. Chem. Soc. Jpn.* **1954**, *24*, 75-77.

(18) Susi, H.; Timasheff, S. N.; Ard, J. S. Near Infrared Investigation of Interamide Hydrogening in Aqueous Solution. *J. Biol. Chem.* **1964**, *239*, 3051-3054.

(19) Jorgensen, W. L. Interactions between Amides in Solution and the Thermodynamics of Weak Binding. *J. Am. Chem. Soc.* **1989**, *111*, 3770-3771.

(20) Dado, G.; Gellman, S. H. Structural and Thermodynamic Characterization of Temperature-Dependent Changes in the Pattern of of a Synthetic Triamide. *J. Am. Chem. Soc.* **1993**, *115*, 4228-4245.

(21) *Physical Chemical Analysis of Biopolymer Self-Assembly Interactions*; Record, M. T.; Richey, B., Ed.; ACS: New York, 1988, pp 145-159.

(22) Radzicka, A.; Wolfenden, R. Comparing the Polarities of the Amino-Acid - Side-Chain Distribution Coefficients Between the Vapor-Phase, Cyclohexane, 1-Octanol, and Neutral Aqueous Solution. *Biochemistry* **1988**, *27*, 1664-1670.

(23) Privalov, P. L.; Gill, S. J. Stability of Protein Structure and Hydrophobic Interactions. *Adv. Prot. Chem.* **1988**, *39*, 193-234.

(24) Zimm, B. H.; Bragg, J. K. Theory of the Phase Transition between Helix and Random Coil in Polypeptide Chains. *J. Chem. Phys.* **1959**, *31*, 526-535.

(25) Scholtz, J. M.; Baldwin, R. L. The Mechanism of a-helix Formation by Peptides. *Annu. Rev. Biophys. Biomol. Struc.* **1992**, *21*, 95-118.

(26) Epand, R. M.; Scheraga, H. A. The Influence of Long-Range Interactions on the Structure of Myoglobin. *Biochemistry* **1968**, *7*, 2864-2872.

(27) Taniuchi, H.; Anfinsen, C. B. An Experimental Approach to the Study of the Folding of Staphylococcal Nuclease. *J. Biol. Chem.* **1969**, *244*, 3864-3875.

(28) Marqusee, S.; Baldwin, R. L. Helix Stabilization by Glu-...Lys+ salt bridges in short peptides of de novo Design. *Proc. Natl. Acad. Sci.* **1987**, *84*, 8898-8902.

(29) Armstrong, K.; Baldwin, B. L. In *Protein Society Symposium*; San Diego, 1992; pp 21.

(30) Karlström, G.; Linse, P.; Wallqvist, A.; Jonsson, B. J. Intermolecular Potentials for the H_2O-C_6H_6 and the C_6H_6-C_6H_6 Systems Calculated in an Ab Initio SCF CI Approximation. *J. Am. Chem. Soc.* **1983**, *105*, 3777-3782.

(31) Ben-Naim, A. The Role of Hydrogen Bonds in Protein Folding and Protein Association. *J. Phys. Chem.* **1991**, *95*, 1427-1444.

(32) Weissman, J. S.; Kim, P. S. Reexamination of the Folding of BPTI: Predominance of Native Intermediates. *Science* **1991**, *253*, 1386-1393.

(33) Markley, J. L.; Hinck, A. P.; Loh, S. N.; Prehoda, K.; Truckses, D.; Walkenhorst, W. F.; Wang, J. In *Protein Structure-Fuction Relationship*; Z. H. Zaidi; A. Abbasi and D. L. Smith, Ed.; TWEL Publishers: Karachi, 1993; pp 193-202.

(34) Markley, J. L.; Hinck, A. P.; Loh, S. T.; Prehoda, K.; Truckses, D.; Walkenhorst, W. F.; Wang, J. Case Study of Protein Structure, Stability and Function: NMR Investigations of the Proline Residues in Staphyloccal Nuclease. *Pure & Appl. Chem.* **1994**, *66*, 65-69.

(35) Matthews, B. W. Mutational Analysis of Protein Stability. *Curr. Opin. Struct. Biol.* **1991**, *1*, 17-21.

(36) Matthews, B. W. Structural and Genetic Analysis of Protein Stability. *Annu. Rev. Biochem.* **1993**, *62*, 139-160.

(37) Sauer, R. T.; Jordan, S. R.; Pabo, C. O. l 1990 Repressor: A Model System for Understanding Protein-DNA Interactions and Protein Stability. *Adv. Prot. Chem.* **1990**, *40*, 1-61.

(38) Fersht, A. R.; Matouschek, A.; Serrano, L. The Folding of an Enzyme. I. Theory of Protein Engineering Analysis of Stability and Pathway of Protein Folding. *J. Mol. Biol.* **1992**, *224*, 771-782.

(39) Sosnick, T. R.; Mayne, L.; Hiller, R.; Englander, S. W. Bariers in Protein Folding. *Struct. Biol.* **1994**, *1*, 149-156.

(40) Pauling, L. *The Nature of the Chemical Bond*; New York, 1948, pp 450.

(41) Wiberg, K. B.; Laidig, K. E. Barriers to Rotation Adjacent to Double Bonds. 3. The C-O Barrier in Formic Acid, Methyl Formate, Acetic Acid, and Methyl Acetate. The Origin of Ester and Amide "Resonance". *J. Am. Chem. Soc.* **1987**, *109*, 5935-5943.

(42) Bennet, A. J.; Somayaji, V.; Brown, R. S.; Santariero, B. D. The Influence of Altered Amidic Resonance on the Infrared and ^{13}C and ^{15}N NMR Spectroscopic Characteristics and Barriers to Rotation about the N-C(O) bond in Some Anilides and Toluamides. *J. Am. Chem. Soc.* **1991**, *113*, 7563-7571.

(43) Eberhardt, E. S.; Loh, S. N.; Hinck, A. P.; Raines, R. T. Solvent Effects on the Energetis of Prolyl Peptide Bond Isomerization. *J. Am. Chem. Soc.* **1992**, *114*, 5437-5439.

(44) Beintema, J. J. Structure, Properties, and Molecular Evolution of Pancreatic-Type Ribonucleases. *Life Chem. Rep.* **1987**, *4*, 333-389.

(45) delCardayré, S. B. Phd Thesis, University of Wisconsin-Madison, 1994.

(46) Grathwohl, C.; Wuthrich, K. NMR Studies of the Rates of Proline *Cis-Trans* Isomerization in Oligopeptides. *Biopolymers* **1981**, *20*, 2623-2633.

(47) Schmid, F. X.; Baldwin, R. L. Acid catalysis of the formation of the slow-folding species of RNase A: Evidence that the reaction is proline isomerization. *Proc. Natl. Acad. Sci. U.S.A.* **1978**, *75*, 4764-4768.

(48) Kelley, R. F.; Richards, F. M. Replacement of Proline-76 with Alanine Eliminates the Slowest Kinetic Phase in Thioredoxin Folding. *Biochemistry* **1987**, *26*, 6765-6774.

(49) Kiefhaber, T.; Quass, R.; Hahn, U.; Schmid, F. X. Folding of Ribonuclease T_1. 2. Kinetic Models for the Folding and Unfolding Reactions. *Biochemistry* **1990**, *29*, 3053-3061.

(50) Hurle, M. R.; Marks, C. B.; Kosen, P. A.; Anderson, S.; Kuntz, I. D. Denaturant-Dependent Folding of Bovine Pancreatic Trypsin Inhibitor Mutants with Two Intact Disulfide Bonds. *Biochemistry* **1990**, *29*, 4410-4419.

(51) Kiefhaber, T.; Schmid, F. X. Kinetic Coupling between Protein Folding and Prolyl Isomerization. II. Folding of Ribonuclease A and Ribonuclease T_1. *J. Mol. Biol.* **1992**, *224*, 231-240.

(52) Kim, P. S.; Baldwin, R. L. Specific Intermediates in the Folding Reactions of Small Proteins and the Mechanism of Protein Folding. *Annu. Rev. Biochem.* **1982**, *51*, 458-489.

(53) Nall, B. T. Proline Isomerization and Protein Folding. *Comm. Mol. Cell. Biophys.* **1985**, *3*, 123-143.

(54) Jaenicke, R. Folding and the Association of Proteins. *Prog. Biophys. Mol. Biol.* **1987**, *49*, 117-237.

(55) Fischer, G.; Bang, H.; Berger, E.; Schellenberger, A. Conformational Specificty of Chymotrypsin Toward Proline-Containing Substrates. *Biochim. Biophys. Acta* **1984**, *791*, 87-97.

(56) Harrison, R. K.; Stein, R. L. Substrate Specificities of the Peptidyl Prolyl *Cis-Trans* Isomerase Activities of Cyclophilin and FK-506 Binding Protein: Evidence for the Existence of a Family of Distict Enzymes. *Biochemistry* **1990**, *29*, 3813-3816.

(57) Harrison, R. K.; Stein, R. L. Mechanistic Studies of Peptidyl Prolyl *Cis-Trans* Isomerase: Evidence for Catalysis by Distortion. *Biochemistry* **1990**, *29*, 1684-1689.

(58) Kofron, J. L.; Kuzmic, P.; Kishore, V.; Colón-Bonilla, E.; Rich, D. H. Determination of Kinetic Cinstants for Peptidyl Prolyl *Cis-Trans* Isomerases by an Improved Spectrophotometric Assay. *Biochemistry* **1991**, *30*, 6127-6134, 10818.

(59) Fischer, G.; Schmid, F. X. The Mechanism of Protein Folding. Implications of in Vitro Refolding Models for de Novo Protein Folding and Translocation in the Cell. *Biochemistry* **1990**, *29*, 2205-2212.

(60) Schreiber, S. L. Chemistry and Biology of the Immunophilins and their Immunosuppressive Ligands. *Science* **1991**, *251*, 283-287.

(61) Gething, M.; Sambrook, J. Protein Folding in the Cell. *Nature* **1992**, *355*, 33-45.

(62) Cyert, M. S. Imminosuppression: Immunosuppressants Hit the Target. *Current Biology* **1992**, *2*, 18-20.

(63) Harrison, R. K.; Caldwell, C. G.; Rosegay, A.; Melillo, D.; Stein, R. L. Confirmation of the Secondary Deuterium Isotope Effect for the Peptidyl Prolyl *Cis-Trans* Isomerase Activity by a Competative, Double-label Technique. *J. Am. Chem. Soc.* **1990**, 7063-7064.

(64) Liu, J.; Albers, M. W.; Chen, C.-M.; Schreiber, S. L.; Walsh, C. T. Cloning, Expression, and Purification of Human Cyclophilin in Escherichia Coli and Assessment of the Catalytic Role of Cysteines by Site-Directed Mutagenesis. *Proc. Natl. Acad. Sci. U.S.A.* **1990**, *87*, 2304-2308.

(65) Park, S. T.; Aldape, R. A.; Futer, O.; DeCenzo, M. T.; Livingston, D. J. PPIase Catalysis by Human FK506-Binding Protein Proceeds Through a Conformational Twist Mechanism. *J. Biol. Chem.* **1992**, *267*, 3316-3324.

(66) Connelly, P. R. Thermodynamics of Interaction of FK506-Binding Protein and its Ligands. *Transplantation Proceedings* **1991**, *23*, 2883-2885.

(67) Kallen, J.; Spitzfaden, C.; Zurini, M. G. M.; Wider, G.; Widmer, H.; Wüthrich, K.; Walkinshaw, M. D. Structure of Human Cyclophilin and its Binding Site for Cyclosporin A Determined by X-ray Crystallography and NMR Spectroscopy. *Nature* **1991**, *353*, 276-279.

(68) Wüthrich, K.; Spitzfaden, C.; Memert, K.; Widmer, H.; Wider, G. Protein Secondary Structure Determination by NMR - Application with Recombinant Human Cyclophilin. *FEBS Lett.* **1991**, *285*, 237-247.

(69) Fesik, S. W.; Gampe, R. T.; Eaton, H. L.; Gemmecker, G.; Olejniczak, E. T.; Neri, P.; Holzman, T. F.; Egan, D. A.; Edalji, R.; Simmer, R.; Helfrich, R.; Hochlowski, J.; Jackson, M. NMR studies of [U^{13}C]Cyclosporin A: Bound Conformation and Portions of Cyclosporin Involved in Binding. *Biochemistry* **1991**, *30*, 6574-6583.

(70) Neri, P.; Meadows, R.; Gemmecker, G.; Olejniczak, E.; Nettesheim, D.; Logan, T.; Simmer, R.; Helfrich, R.; Holzman, T.; Severin, J.; Fesik, S. 1H, 13C, and 15N Backbone Assignments of Cyclophilin When Bound to Cyclosporin A (CsA) and Peliminary Structural Characterization of the CsA Binding Site. *FEBS Lett.* **1991**, *294*, 81-88.

(71) Fesik, S. W.; Neri, P.; Meadows, R.; Olejniczak, E. T.; Gemmecker, G. A Model of the Cyclophilin/Cyclosporin A (CSA) Complex from NMR X-ray Data Suggests that CSA Binds as a Transition State Analogue. *J. Am. Chem. Soc.* **1992**, *114*, 3165-3166.

(72) Moore, J. M.; Peattie, D. A.; Fitzgibbon, M. J.; Thompson, J. A. Solution Structure of the Major Binding Protein for the Immunosuppressant FK506. *Nature* **1991**, *351*, 248-250.

(73) Michnick, S. W.; Rosen, M. K.; Wandless, T. J.; Karplus, M.; Schreiber, S. L. Solution Structure of FKBP, a Rotomase Enzyme and Receptor for FK506 and Rapamycin. *Science* **1991**, *252*, 836-839.

(74) Van Duyne, G. D.; Standaert, R. F.; Karplus, P. A.; Schreiber, S. L.; Clardy, J. Atomic Structure of FKBP-FK506, an Immunophilin-Immunosuppressant Complex. *Science* **1991**, *252*, 839-842.

(75) Van Duyne, G. D.; Standaert, R. F.; Schreiber, S. L.; Clardy, J. Atomic Structure of the Rapamycin Human Immunophilin FKBP-12 Complex. *J. Am. Chem. Soc.* **1991**, *113*, 7433-7434.

(76) Stein, R. L. Protein Structure: Exploring the Catalytic Activity of Immunophilins. *Curr. Biol.* **1991**, *1*, 234-236.

(77) Stein, R. L. Mechanism of Enzymatic and Nonenzymatic Prolyl *Cis-Trans* Isomerization. *Adv. Prot. Chem.* **1993**, *44*, 1-24.

(78) Radzicka, A.; Pedersen, L.; Wolfenden, R. Influences of Solvent Water on Protein Folding: Free Energies of Solvation of *Cis* and *Trans* Peptides are Nearly Identical. *Biochemistry* **1988**, *27*, 4538-4541.

(79) Wolfenden, R.; Radzicka, A. Purification of Human Cyclophilin in Escherichia Coli and Assessment of the Catalytic Role of Cysteins by Site-Directed Mutagenesis. *Chemtracts-Biochemistry and Molecular Biology* **1991**, *2*, 52-54.

(80) Higashijima, T.; Tasumi, M.; Miyazawa, T. ^{1}H Nuclear Magnetic Resonance Studies of N-Acetyl-L-Proline N-Methylamide. Molecular Conformations, Hydrogen Bondings, and Thermodynamics Quantities in Various Solvent. *Biopolymers* **1977**, *16*, 1259-1270.

(81) Novoa, J. J.; Whangbo, M.-H. The Nature of Intramolecular Hydrogen-Bonded and Non-Hydrogen-Bonded Conformations of Simple Di- and Triamides. *J. Am. Chem. Soc.* **1991**, *113*, 9017-9026.

(82) Detar, D. F.; Luthra, N. P. Conformations of Proline. *J. Am. Chem. Soc.* **1977**, *99*, 1232-1244.

(83) Liang, G.-B.; Rito, C. J.; Gellman, S. H. Variations in the Turn-Forming Characteristics of *N*-Acyl Proline Units. *Biopolymers* **1992**, *32*, 293-301.

(84) Matsuzaki, T.; Iitaka, Y. The Crystal Structure of Actyl-L-proline-N-methylamide. *Acta Cryst.* **1971**, *B27*, 507-516.

(85) Led, J. J.; Gesmar, H. The Applicability of the Magnetization-Transfer Technique to Determine Chemical Exchange Rates in Extreme Cases. The Importance of Complementary Experiments. *Journal of Magnetic Resonacne* **1982**, *49*, 444-463.

(86) Neuman, R. C.; Woolfenden, W. R.; Jonas, V. The Effect of Hydrogen Bonding on the Barrier to Rotation about Amide Bonds. *J. Chem. Phys.* **1969**, *73*, 3177-3180.

(87) Neuman, R. C.; Jonas, V.; Anderson, K.; Barry, R. Hindered Rotation in *N*-Methylformaide. A peptide Bond Model System. *Biochem. Biophys. Res. Comm.* **1971**, *44*, 1156-1161.

(88) Drakenberg, T.; Forsén, S. The Barrier to Internal Rotation in Monosubstituted Amides. *Chem. Comm.* **1971**, *21*, 1404-1405.

(89) Drakenberg, T.; Dahlqvist, K.; Forsén, S. The Barrier to Internal Rotation in Amides. IV. *N,N*-Dimethylamides; Substituent and Solvent Effects. *J. Phys. Chem.* **1972**, *76*, 2178-2183.

(90) Mirkin, N. G.; Krimm, S. Ab Initio Vibrational Anaylsis of Hydrogen Bond *Trans*- and *Cis-N*-Methylacetamide. *J. Am. Chem. Soc.* **1991**, *113*, 9742-9747.

(91) Miyazawa, T.; Shimanouchi, T.; Mizushima, S. I. Characteristic Infrared Bonds of Monosubstituted Amides. *J. Chem. Phys.* **1956**, *24*, 408-418.

(92) Eaton, G.; Symons, M. C. R.; Rastogi, P. P. Spectroscopic Studies of the Solvation of Amides with N-H Groups. *J. Chem. Soc. Faraday Trans.* **1989**, *85*, 3257-3271.

(93) Pimental, G. C.; McClellen, A. L. *The Hydrogen Bond*; Freeman: New York, 1960.

(94) Krimm, S.; Bandekar, J. In *Advances in Protein Chemistry*Acadenic Press: New York, 1986; Vol. 38; pp 181-364.

(95) Jorgensen, W. L.; Gao, J. *Cis-Trans* Energy Differences for the Peptide bond in the Gas Phase and Aqueous Solution. *J. Am Chem. Soc.* **1988**, *110*, 4212-4216.

(96) Wolfenden, R. Free Energies of Hydration and Hydrolysis of Gaseous Acetamide. *J. Am. Chem. Soc.* **1976**, *98*, 1987-1988.

(97) Radzicka, A.; Achwson, S. A.; Wolfenden, R. *Cis/Trans* Isomerization at Proline: Desolvation and Its Consequences for Protein Folding. *Bioorganic Chemistry* **1992**, *20*, 382-386.

(98) Eberhardt, E. S.; Loh, S. N.; Raines, R. T. Thermodynamic Origin of Prolyl Peptide Bond Isomers. *Tetrahedron Lett.* **1993**, *34*, 3055-3056.

(99) Stewart, W. E.; Siddall, T. H. Nuclear Magnetic Resonance Studies of Amides. *Chem. Rev.* **1970**, *70*, 517-551.

(100) Harrison, R. K.; Stein, R. L. Mechnaistic Studies of Enzymic and Nonenzymic Prolyl *Cis-Trans* Isomerization. *J. Am. Chem. Soc.* **1992**, *114*, 3464-3471.

(101) Dunker, A. K. A Proton Motive Force Transducer and its Role in Proton Pumps, Proton Engines, Tobacco Mosaic Virus Assembly and Hemoglobin Allosterism. *J. Theor. Biol.* **1982**, *97*, 95-127.

(102) Gerwert, K.; Hess, B.; Engelhard, M. Proline Residues Undergo Structural Changes During Proton Pumping in Bacteriorhodopsin. *FEBS Lett.* **1990**, *261*, 449-454.

(103) Williams, K. A.; Deber, C. M. Proline Residues in Transmembrane Helicies: Structural or Dynamic Role? *Biochemistry* **1991**, *30*, 8919-8923.

(104) Wang, Q.-P.; Bennet, A. J.; Brown, R. S.; Santarsiero, B. D. Distorted Amides as models for Activated Peptide N-C(O) Units. Synthesis, Hydrolytic Profile, and Molecular Structure of 2,3,4,5-Tretrahydro-2-oxo-1,5-propanobenzazepine. *J. Am. Chem. Soc.* **1991**, *113*, 5757-5765.

(105) Cheng, H. N.; Bovey, F. A. *Cis-Trans* Equillibrium and Kinetic Studies of Acetyl-L-Proline and Glycyl-L-Proline. *Biopolymers* **1977**, *16*, 1465-1472.

(106) Jacobson, J.; Melander, W.; Vaisnys, G.; Horvath, C. Kinetic Study on *Cis-Trans* Proline Isomerization by High-Performance Liquid Chormatography. *J. Phys. Chem.* **1984**, *88*, 4536-4542.

(107) Galardy, R. E.; Laikopoulou-Kyriakides, M. The Rate of s-Cis/s-Trans Isomerization in Angiotensin II is at Least 70-Fold Greater than in His-Pro and is not Rate Limiting in Receptor Binding. *Int. J. Pep. Prot. Res.* **1982**, *20*, 144-148.

(108) Lin, L.-N.; Brants, J. F. Determination of *Cis-Trans* Proline Isomerization by Trypsin Proteolysis. Application to a Pentapeptide andto Oxidized Ribonuclease A. *Biochem.* **1983**, *22*, 553-559.

(109) Shirley, B. A.; Stanssens, P.; Hahn, U.; Pace, C. N. Contrabution of Hydrogen Bonding to the Conformational Stability of Ribonuclease T1. *Biochem* **1992**, *31*, 725-732.

(110) Dreyfus, M.; Maigret, B.; Pullman, A. A Non-Empirical Study of Hydrogen Bonding in the Dimer of Formamide. *Theoret. Chim. Acta.* **1970**, *17*, 109-119.

(111) Dreyfus, M.; Pullman, A. A Non-empirical Study of the Hydrogen Bond between Peptide Units. *Theor. Chim. Acta.* **1970**, *19*, 20-37.

(112) Sneddon, S. F.; Tobias, D. J.; Brooks, C. L. Thermodynamics of Amide Hydrogen Bond Formation in Polar and Apolar Solvents. *J. Mol. Biol.* **1989**, *209*, 817-820.

(113) Dado, G.; Gellman, S. H. On the Use of AMI Calculations for the Study of Intramolecular Hydrogen Bonding Phenomena in Simple Amides. *J. Am. Chem. Soc.* **1992**, *114*, 3138-3139.

(114) Spencer, J. N.; Garrett, R. C.; Mayer, F. J.; Merkle, J. E.; Powell, C. R.; Tran, M. T.; Berger, S. K. Amide Hydrogen Bonding in Organic Medium. *Can. J. Chem.* **1980**, *58*, 1372-1375.

(115) Bloemendal, M.; Somsen, G. A Study of Solute-Solute Interactions of Amides Dissolved in *N*-Methylformaide by Enthalpic Interaction Coefficients. *J. Solution Chem.* **1988**, *17*, 1067-1079.

(116) Nikolic´, A. D.; Rozsa-Tarjani, M.; Komaromi, A.; J., C.; Petrovic´, S. D. Hydrogen Bonding of N-monosubstituted Amides. IR Study of N-ethylacetamide and N-methylpropionamide. *J. Mol. Struct.* **1992**, *267*, 49-54.

(117) Gellman, S. H.; Dado, G. P.; Liang, G.-B.; Adams, B. R. Conformation Directing Effects of a Single Intramolecular Amide–Amide Hydrogen Bond: Variable-Temperature NMR and IR Studies on a Homologous Diamide Series. *J. Am. Chem. Soc.* **1991**, *113*, 1164-1173.

(118) Schellman, J. A. The Thermodynamics of Urea Solutions and the Heat of Formation of the Peptide Hydrogen Bond. *Comptes Rendus des Travravaux du Laboratoire Carlsberg Sererie Chimique* **1955**, *29*, 223-229.

(119) Williams, D. H.; Cox, J. P. L.; Doig, A. J.; Gardner, M.; Gerhard, U.; Kaye, P. T.; Lal, A. R.; Nicholls, I. A.; Salter, C. J.; Mitchell, R. C. Toward the Semiquantitative Estimation of Binding Constants. Guides for Peptide-Peptide Binding in Aqueous Solution. *J. Am. Chem. Soc.* **1991**, *113*, 7020-7030.

(120) Williams, D. H. The Molecular Basis of Biological Order. *Aldrichimia Acta* **1991**, *24*, 71-80.

(121) Doig, A. J.; Williams, D. H. Binding Energy of an Amide-amide Hydrogen Bond in Aqueous and Nonpolar Solvents. *J. Am. Chem. Soc.* **1992**, *114*, 338-343.

(122) Williams, D. H. Binding Energy of an Amide-Amide Hydrogen Bond in Aqueous and Nonpolar Solvents. *Aldrichimica Acta-An Addendum* **1992**, *25*, 9.

(123) Bodanszky, M. *Peptide Chemistry*; Springer-Verlag: New York, 1988.

(124) Forsén, S.; Hoffman, R. A. Study of Moderately Rapid Chemical Exchange Reactions by Means of Nuclear Magnetic Double Resonance. *J. Chem. Phys.* **1963**, *39*, 2892-2901.

(125) Stickle, D. F.; Preasta, L. G.; Dill, K. A.; Rose, G. D. Hydrogen Bonding in Globular Proteins. *J. Mol. Biol.* **1992**, *226*, 1143-1159.

(126) Richardson, J. S.; Richardson, D. C. Amino Acid Preferences for Specific Locations at the End of a Helicies. *Science* **1988**, *240*, 1648-1652.

(127) Dasgupta, S.; Bell, J. A. Design of Helix Ends. Amino Acid Preferences, Hydrogen Bonding and Electrostatic Interactions. *Int. J. Peptide Protein Res.* **1993**, *41*, 499-511.

(128) Serrano, L.; Heira, J.; Sancho, J.; Fersht, A. R. Effect of Alanine vs Glycine in alpha-Helicies on Protein Stability. *Nature* **1992**, *356*, 453-455.

(129) Fersht, A. R.; Serrano, L. Principles of Protein Stability Derived From Protein Engineering Experiments. *Curr. Opin. Struct. Biol.* **1993**, *3*, 75-83.

(130) Kobayashi, M.; Nishioka, K. Hydration of N-Monosubstituted Amides in the Binary Solvents Dioxane-D_2O and Dioxane-H_2O. *J. Phys. Chem.* **1987**, *91*, 1247-1251.

(131) Eaton, G.; Symons, M. C. R.; Rastogi, P. P.; O'Duinn, C.; Waghorne, W. E. Solvation of Some Amides in Mixed-Solvent Systems - Comparison of the Results of Infrared Spectroscopic and Calorimetric Measurments. *J. Chem. Soc., Faraday Trans. 1* **1992**, *88*, 1137-1142.

(132) Scholtz, J. M.; Marqusee, S.; Baldwin, R. L.; York, E. J.; Stewart, J. M.; Santoro, M.; Bolen, D. W. Calorimetric Determination of the Enthalpy Change for the Alpha-Helix to Coil Transition of an Alanine Peptide in Water. *Proc. Natl. Acad. Sci.* **1991**, *88*, 2854-2858.

(133) Schnolzer, M.; Kent, S. B. H. Constructing Proteins by Dovetailing Unpotected Synthetic Peptides: Backbone-Engineered HIV Protease. *Science* **1992**, *256*, 221-225.

(134) Chung, H. H.; Benson, D. R.; Schultz, P. G. Probing the Structure and Mechanism of Ras Protein with an Expanded Genetic Code. *Science* **1993**, *259*, 806-809.

(135) Bordwell, F. G. Equilibrium Acidities in Dimethyl Sulfoxide Solution. *Acc. Chem. Res.* **1988**, *21*, 456-463.

(136) Gill, S. J.; Noll, L. Calorimetric Study of Association of Diketopiperazine in Water. *J. Phys. Chem.* **1972**, *76*, 3065-3068.

(137) Symons, M. C. R.; Eaton, G. Solvation of Acetone in Protic and Aprotic Solvents and Binary Solvent Mixtures. *J. Chem. Soc. Faraday Trans. I* **1985**, *81*, 1963-1977.

(138) Chothia, C. Structural Invariants in Protein Folding. *Nature* **1975**, *254*, 304-308.

(139) Matthews, B. W.; Nicholson, H.; Becktel, W. J. Enhanced Protein Thermostability from Site-directed Mutations that Decrease the Entropy of Unfolding. *Proc. Natl. Acad. Sci. USA* **1987**, *84*, 6663-6667.

(140) Eriksson, A. E.; Baase, W. A.; Zhang, X.; Heinz, D. W.; Blaber, M.; Baldwin, E. P.; Mattews, B. W. Response of a Protein Structure to Cavity-Creating Mutations and Its Relation to the Hydrophobic Effect. *Science* **1992**, *255*, 178-183.

(141) Lim, W. A.; Farruggio, D. C.; Sauer, R. T. Structural and Energetic Consequences of Disruptive Mutations in a Protein Core. *Biochemistry* **1992**, *31*, 4334-4333.

(142) Pace, C. N.; Laurents, D. V.; Thompson, J. A. pH Dependence of the Urea and Guanidine Hydrochloride Denaturation of Ribnuclease A and Ribnuclease T1. *Biochemistry* **1990**, *29*, 2564-2572.

(143) Wlodawer, A.; Lennart, S. Structure of Ribonuclease A: Results of Joint Neutron and X-Ray Refinement at 2,0-Å Resolution. *Biochemistry* **1983**, *22*, 2720-2728.

(144) Thompson, J. E.; Raines, R. T. Value of Acid-Base Catalysis to Ribonuclease A. *J Am. Chem. Soc.* **1994**, *116*, 5467-5468.

(145) Usher, D. A.; Erenrich, E. S.; Eckstein, F. Geometry of the First Step in the Action of Ribonuclease A. *Proc. Natl. Acad. Sci.* **1972**, *69*, 115-118.

(146) Thompson, J. E.; Venegas, F. D.; Raines, R. T. Energetics of Catalysis by Ribonuclease A: Fate of the 2',3' Cyclic Intermediate. *Biochemistry* **1994**, *33*, 7408-7414.

(147) Usher, D.; Richardson, D.; Eckstein, F. Absolute Sterochemistry of the Second Step of Ribonuclease Action. *Nature* **1970**, *228*, 633.

(148) Witzel, H.; Bardard, E. A. Mechanism and Binding Sites in the Ribonuclease Reaction II, Kinetic Studies of the First Step of the Reaction. *Biochem. Biophys. Res. Comm.* **1962**, *7*, 295-299.

(149) Messmore, J. M.; Raines, R. T. (Unpublished Results).

(150) Murdock, A. L.; Grist, K. L.; Hirs, C. H. W. On the Dinitrophenylation of Bovine Pancreatic Ribonuclease A. Kinetics of the Reaction in Water and 8M Urea. *Arch. Biochem. Biophys.* **1966**, *114*, 375-390.

(151) Flogel, M.; Albert, A.; Biltonen, R. The Magnitude of Electrostatic Interaction in Inhibitor Binding and During Catalysis by Ribonuclease A. *Biochemistry* **1975**, *14*, 2616-2621.

(152) Deakyne, C. A.; Allen, L. C. Role of Active-Stie Residues in the Catalytic Mechanism of Ribonuclease A. *J. Am. Chem. Soc.* **1979**, *79*, 3951-3959.

(153) Anslyn, E.; Breslow, R. On the Mechanism of Catalysis by Ribonuclease: Cleavage and Isomerization of the Dinucleotide UpU Catalyzed by Imidazole Buffers. *J. Am. Chem. Soc.* **1989**, *111*, 4473-4482.

(154) Haydock, K.; Lim, C.; Brünger, A. T.; Karplus, M. Simulation Analysis of Structures on the Reaction Pathway of RNAse A. *J. Am. Chem. Soc.* **1990**, *112*, 3826-3831.

(155) Messmore, J. M.; Fuchs, D.; Raines, R. T. Revealing Structure-Function Relationship with Semisynthesis. *J. Am. Chem. Soc.* Submitted.

(156) Eftink, M.; Biltonen, R. In *Hydrolytic Enzymes*New York, 1987; pp 333-376.

(157) Kiefhaber, T.; Kohler, H.-H.; Schmid, F. X. Kinetic Coupling between Protein Folding and Prolyl Isomerization. *J. Mol. Biol.* **1992**, *224*, 217-229.

(158) Dodge, R. W.; Laity, J. H.; Rothwarf, D. M.; Shimotakahara, S.; Scheraga, H. A. Folding Pathway of Guanidine-Denatured Disulfide-Intact Wild-Type and Mutant Bovine Pancreatic Ribonuclease A. *J. Prot. Chem.* **1994**, *13*, 409-421.

(159) Kellis, J. T.; Nyberg, K.; Sali, D.; Fersht, A. R. Contribution of Hydrophobic Interactions to Protein Stability. *Nature* **1988**, *333*, 784-786.

(160) Eriksson, A. E.; Baase, W. A.; Matthews, B. W. Similar Hydrophobic Replacements of Leu99 and Phe153 within Core T4 Lysozyme Have Different Structural and Thermodynamic Consequences. *J. Mol. Biol.* **1993**, *229*, 747-769.

(161) Pace, N. C.; Shirley, B. E.; Thomson, J. A. In *Protein Structure*; T. E. Creighton, Ed.; IRL Press: New York, 1990; Vol. 1; pp 311-330.

(162) Ramachandran, G. N.; Reddi, A. H., Ed. *Biochemistry of Collagen*; Plenum Press: New York, 1976.

(163) Bornstein, P.; Traub, W. *The Proteins;* 3 ed.; Academic Press: New York, NY, 1979; Vol. 4, pp 411-632.

(164) Nemethy, G. *Collagen*; CRC: Boca Raton, FL, 1988; Vol. 1.

(165) Jones, E. Y.; Miller, A. Analysis of Structural Design - Features in Collagen. *J. Mol. Biol.* **1991**, *218*, 209-219.

(166) Sakakibara, S.; Inouye, K.; Shudo, K.; Kishida, Y.; Kobayashi, Y.; Prockop, D. J. Synthesis of (Pro-Hyp-Gly)n of Defined Molecular Weights. Evidence for the Stabiliztion Collagen Triple Helix by Hydroxyperoline. *Biochem. Biophys. Acta.* **1973**, *303*, 198-202.

(167) Berg, R. A.; Prockop, D. J. The Thermal Transition of a Non-Hydroxylated form of Collagen. Evidence for a Role for Hydroxyproline in Stabilizing the Triple Helix of Collagen. *Biochem. Biophys. Res. Comm.* **1973**, *52*, 115-120.

(168) Fraser, R. D. B.; MacRae, T. P.; Suzuki, E. Chain Conformation in the Collagen Molecule. *J. Mol. Biol.* **1979**, *129*, 463-481.

(169) Okuyama, K.; Arnott, S.; Takayanagi, M.; Kakudo, M. Crystal and Molecular Structure of a Collagen-like Polypeptide $(Pro\text{-}Pro\text{-}Gly)_{10}$. *J. Mol. Biol.* **1981**, *152*, 427-443.

(170) Fasman, G. D. *Practical Handbook of Biochemistry and Molecular Biology*; CRC Press: Boca Raton, FL, 1989, pp 35-39.

(171) Exner, O. *Correlation Analysis in Chemistry*; Plenum: London, 1978, pp 493-540.

(172) Ceppi, E.; Eckhardt, W.; Grob, C. A. 4-Substituted Quinuclidinum Perchlorates in the Determination of Polar Subtituent Effects. *Tetrahedron Lett.* **1973**, *37*, 3627-3630.

(173) IUPAC-IUB Commission on Biochemical Nomenclature. *Biochemistry* **1970**, *9*, 3471-3479.

(174) Madison, V.; Schellman, J. Location of Proline Derivatives in Conformational Space. I. Conformation Calculations; Optical Activity and NMR Experiments. *Bioploymers* **1970**, *9*, 511-567.

(175) Stewart, D. E.; Sarkar, A.; Wampler, J. E. Occurrence and Role of *Cis* Peptide-Bonds in Protein Structures. *J. Mol. Biol.* **1990**, *214*, 253-260.

(176) Milner-White, J. E.; Bell, L. H.; Maccallum, P. H. Pyrrolidine Ring Puckering in *Cis* and *Trans*-proline Residues in Proteins and Polypeptides. *J. Mol. Biol.* **1992**, *228*, 725-734.

(177) Cushley, R.; Codington, J. F.; Fox, J. J. Nucleosides. XLIX. Nuclear Magnetic Studies of 2'- and 3'-Halogeno Nucleosides. The Conformations of 2'-Fluorouridine and 3'-Deoxy-3'Fluoro-ß-Darabinofuranosyl Uracil. *Can. J. Chem.* **1968**, *46*, 1131-1140.

(178) Balaji, V. N.; Rao, M. J.; Dietrich, S. W.; Sasisekharan, V. Geometry of Proline and Hydroxyproline. 1. Analysis of X-ray Crystal-Structure Data. *Biochem. Biophys. Res. Commun.* **1986**, *140*, 895-900.

(179) Nimni, M. E. *Collagen*; CRC Press: Boca Raton, FL, 1988.

(180) Rich, A.; Crick, F. H. C. The Molecular Structure of Collagen. *J. Mol. Biol.* **1961**, *3*, 483-506.

(181) Baldwin, C. T.; Constanteu, C. D.; Dumars, K. W.; J., P. D. A Single Base Mutantion that Converts Glycine 907 of the alpha 2(I) Chain of Type I Procollagen to Aspartate in a Lethal Variant of Osteogenesis Imperfecta. The Single Amino Acid Substitution Near the Carboxyl Terminus Destabilizes the Whole Triple Helix. *J. Biol. Chem.* **1989**, *264*, 3002-3006.

(182) Kadler, K. In *Protein Profile*; 1994; pp 519-638.

(183) Prockop, D. J.; Kivirikko, K. I.; Tuderman, L.; Guzman, N. A. The Biosynthesis of Collagen and its Disorders. *New. Eng. J. Med.* **1979**, *301*, 77-85.

(184) Prockop, D. J.; Kivirikko, K. I.; Tuderman, L.; Guzman, N. A. The Biosynthesis of Collagen and its Disorders. *New. Eng. J. Med* **1979**, *301*, 13-23.

(185) Rao, N. V.; Adams, E. Collagen Triple Helix Stabilization by Hydroxyproline in (Ala-Hyp-Gly)n. *Biochem. Biophys. Res. Comm.* **1979**, *86*, 654-660.

(186) Bruckner, P.; Bachinger, P. H.; Timpl, R.; Engel, J. Three Conformationally Distinct Domains in the Amino-Terminal Segment of Type III Procollagen and its Rapid Triple Helix Leads to and Comes from Coil Transition. *Eur. J. Biochem.* **1978**, *90*, 595-603.

(187) Chopra, R. K.; Ananthanarayanan, V. S. Conformational Implications of Enzymatic Proline Hydroxylation in Collagen. *Proc. Natl. Acad. Sci. U.S. A.* **1982**, *79*, 7180-7184.

(188) Ramachandran, G. N.; Bansal, M.; Bhatnagar, R. S. A Hypothesis on the Role of Hydroxyproline in Stabilizing Collagen Structure. *Biochim. Biophys. Acta.* **1973**, *322*, 166-171.

(189) Suzuki, E.; Fraser, R. D. B.; MacRae, T. P. Role of Hydroxyproline in the Stabilization of the Collagen Molecule via Water Molecules. *Int. J. Biol. Macromol.* **1980**, *2*, 54-56.

(190) Bella, J.; M., E.; Brodsky, B.; Berman, H. M. Crystal and Molecular Structure of a Collagen–Like Peptide at 1.9 Å Resolution. *Science* **1994**, *266*, 75-81.

(191) Bächinger, H. P.; Bruckner, P.; Timpl, R.; Prockop, D. J.; J., E. Folding Mechanism of the Triple Helix in Type-III Collagen and Type-III pN-Collagen. Role of Disulfide Bridges and Peptide Bond Isomerization. *Eur.J Biochem* **1980**, *106*, 619-632.

(192) Bruckner, P.; Eikenberry, E. F.; Prockop, D. J. Formation of the Triple Helix of Type I Procollagen in cellulo. A Kinetic Model Based on *Cis-Trans* Isomerization of Peptide Bonds. *Eur. J. Biochem.* **1981**, *118*, 607-613.

(193) Bächinger, H. P. The Influence of Peptidyl-Prolyl *Cis-Trans* Isomerase on the in Vitro Folding of Type III Collagen. *J. Biol. Chem.* **1987**, *262*, 17144-17148.

(194) Hinck, A. P.; Eberhardt, E. S.; Raines, R. T. NMR Strategy for Determining Xaa-Pro Peptide Bond Configuration in Proteins: Mutants of Staphylococcal Nuclease with Altered Configuration at Proline-117. *Biochemistry* **1993**, *32*, 11810-11818.

(195) Panasik, N.; Eberhardt, E. S.; Edison, A.; Powell, D. R.; Raines, R. T. Inductive effects on the structure of proline residues. *Int. J. Pept. Protien Res.* **1994**, *44*, 262-269.

(196) Reichhardt, C. *Solvents and Solvent Effects in Organic Chemistry*; VCH: New York, 1990, pp 534.

(197) Laurence, C.; Berthelot, M.; M., L.; Helbert, M.; Morris, D. G.; J-F., G. The Influence of Solvent on the Inductive Order of Substituents from Infrared Measurements on 4-Substituted Camphors: a New Model of Inductive Effects. *J. Chem. Soc. Perkin Trans. II* **1984**, 705-710.

(198) Ashida, T.; Kakudo, M. Conformations of Prolyl Residues in Oligopeptides. *Bull. Chem. Soc. Japan* **1974**, *47*, 1129-1133.

(199) de Leeuw, F. A. A. M.; Altona, C.; Kessler, H.; Bermel, W.; Friedrich, A.; Krack, G.; Hull, W. E. Conformational Analysis of Proline Rings from Proton Spin-Spin Coupling Constants and Force-Field Calculations: Application to the Cyclic Tripeptides. *J. Am. Chem. Soc.* **1983**, *105*, 2237-2246.

(200) Anteunis, M. J. O.; Callens, R.; Asher, V.; Sleeck, J. Ring Conformational Aspects of Proline and Hydroxyproline. High Conformational Purity of Pro in DKP's and Hydantoins. *Bull. Soc. Chim. Belg.* **1978**, *87*,

(201) Garbay-Jaureguiberry, C.; Arnoux, B.; Prangé, T.; Wehri-Altenburger, S.; Pascard, C.; P., R. B. X-ray and NMR Studies of L-4-Hydroxyproline Conformation in Oligopeptides Related to Collagen. *J. Am. Chem. Soc.* **1980**, *102*, 1827-1837.

(202) Abraham, R. J.; McLauchlan, K. A. The Proton Resonance Spectra ond Conformations of the Prolines Part I. *Mol. Phys.* **1962**, *5*, 195-203.

(203) Abraham, R. J.; McLauchlan, K. A. The Proton Resonance Spectras and Conformations of the Prolines Part II. *Mol. Phys.* **1962**, *5*, 513-523.

(204) Gerig, J. T.; Macleod, R. R. Conformations of *Cis*- and *Trans*-4-fluoro-L-proline in Aqueous Solution. *J. Am. Chem. Soc.* **1973**, *95*, 5725-5729.

(205) Gerig, J. T.; Mcleod, R. R. Conformations of Glycyl-4-fluoro-L-prolyl-L-Tryptophan in Aqueous Solution. *J. Am. Chem. Soc.* **1976**, *98*, 3970-3975.

(206) Plavec, J.; Thibaudeau, C.; Chattopadhyaya, J. How Does the 2'-Hydroxyl Group Drive the Pseudorotational Equilibrium in Nucleoside and Nucleotide by the Tuning of the 3'-Gauche Effect. *J. Am. Chem. Soc.* **1994**, *116*, 6558-6560.

(207) Koole, L. H.; Buck, H. M.; Nyilas, A.; Chattopadhyaya, J. Structural Properties of modified deoxyadenosine structures in solution. Impact of the gauche and anomeric effects on the furanose conformation. *Can. J. Chem.* **1987**, *65*, 2089-2094.

(208) Nemethy, G.; Scheraga, H. A. Stabilization of Collagen Fibrils by Hydroxyproline. *Biochemistry* **1986**, *25*, 3184-3188.

(209) Still, W. C.; Kahy, M.; Mitra, A. Rapid Chromatographic Technique for Preparative Separations with Moderate Resolution. *J. Org. Chem.* **1978**, *43*, 2923-2925.

(210) Roberts, J. L.; Poulter, C. D. 2', 3', 5'-Tri-*O*-benoyl [4-13C] Uridine. An efficient, Regiospecific Synthesis of the Pyrimidine Ring. *J. Org. Chem.* **1978**, *43*, 1547-1550.

(211) Bak, B.; Led, J. J. Preparation of [1-^{13}C], [3-^{13}C], [1-D], and [3-D] Enriched Cyclobutenes. *J. Labelled. Cpd.* **1967**, *IV*, 22-27.

(212) Hinck, A. P. Thesis, University of Wisconsin-Madison, 1993.

(213) Kunkel, T. A.; Roberts, J. D.; Zakour, R. A. Rapid and Efficient Site Specific Mutagensis Without Phenotypic Selection. *Methods Enzym.* **1987**, *154*, 367-382.

(214) Hermans, J. J.; Scheraga, H. A. . *J. Am. Chem. Soc.* **1961**, *83*, 3283-3292.

(215) Sela, M.; Anfinsen, C. B.; Harrington, W. F. The Correlation of Ribonuclease Activity with Specific Aspects of Tertiary Structure. *Biochem. Biophys. Acta* **1957**, *26*, 502.

(216) Cleland, W. W. Statistical Analysis of Kinetic Data. *Methods Enzym.* **1979**, *63*, 103-138.

(217) Sheldrick, G. M. In Madison, 1990.

(218) Schmidt, M. W.; Baldridge, K. K.; Boatz, J. A.; Jensen, J. A.; Koseki, S.; Gordon, M. S.; Nguyen, K. A.; Windus, T. L.; Elbert, S. T. In QCPE Bulletin: 1990.

(219) Hehre, W. J. Spartan. *Wavefunction Inc*

(220) Ager, D. J. . *J. Chem. Res. Synop.* **1977**, *6*, 6-7.

(221) Resnati, G. Synthesis of Chiral and Bioactive Fluoroorganic Compounds. *Tetrahedron* **1993**, *49*, 9385-9445.